THE INTRAMOLECULAR VIBRATIONAL ENERGY DISTRIBUTION OF INFRARED MULTIPHOTON EXCITED MOLECULES

A thesis presented

by

Jyhpyng Wang

to

The Division of Applied Sciences

in partial fullfillment of the requirements
for the degree of
Doctor of Philosophy
in the subject of
Applied Physics

Harvard University
Cambridge, Massachusetts
August, 1988

ABSTRACT

Polyatomic molecules in the electronic ground state can absorb a large number of infrared photons from a resonant high power infrared laser. For sufficiently high laser power, most molecules will even reach the dissociation limit. When this phenomenon was discovered in 1973 it was hoped that infrared multiphoton excitation would lead to the realization of "bond-selective" laser-controlled photochemistry. Despite the selectivity of infrared excitation at low energy, however, at high excitation vibrational energy is no longer confined to the pump mode because of the interaction between vibrational modes. This thesis explores the intramolecular dynamics of infrared multiphoton excited molecules. Time-resolved spontaneous and coherent anti-Stokes Raman spectroscopy was employed to measure the energy distribution among vibrational modes immediately following infrared excitation. Both cases of intramolecular equilibrium below the dissociation threshold, as well as cases of nonequilibrium close to dissociation were found. The results are consistent with nonlinear dynamics theory.

ACKNOWLEDGEMENTS

I would like to thank all the people who have helped me in the work presented in this thesis. They have helped me not only in achieving academic goals, but also the personal growth during the past five years.

My advisor, Professor Eric Mazur, has given me a rigorous training as an experimental physicist. In addition to his knowledge of science, his cheerful disposition, patience and generosity makes him a wonderful teacher. With his broad interests in arts and nature, he has taught me not only how to work, but also how to play. His insistence on quality and efficiency has shaped my work style, as well as my ideas on being a scientist. I cherish the days I worked with him. It has been a period of hope, wonder, growth and accomplishment.

Professor Nicolaas Bloembergen has been a great inspiration to me. His wonderful lectures in modern optics have inspired me to join this research field. He is always helpful and kind. I have learned very much from his advice and his insightful ways of thinking. I wish I had not been shy and had bothered him much more for enlightenment.

Professor Isaac Silvera helped me through some hard times during my first year at Harvard. Due to my difficulties with English, I was depressed and lacked confidence. He encouraged me at that time, and has continued to give me helpful advice through these years.

I wish to express my deep gratitude to my colleagues: Kuei-Hsien Chen has gone through all the dirty work of setting up and carrying out the experiments with me, and

contributed substantially to this work; Luis Aviles and Professor Cheng-Zai Lu worked together with me on the coherent Raman spectroscopy experiment; Doo Soo Chung provided expertise in chemistry; and Peter Saeta offered advice in Macintosh programming. I also enjoyed working with the other members of our research group: Ka Yee Lee, Juen-Kai Wang and Maarten Buijs. They have all contributed in making my days at Harvard happy. The time I have been with them, especially those unforgettable precious moments like the jazzy group lunches and cheerful group days, will be missed.

I would also like to thank the many people in Gordon McKay Laboratory and the Division of Applied Sciences who have made these places wonderful. In particular, I owe my gratitude to Professor Pauline Mitchell of the academic office, Tomás Rosado of the stock room and Ralph Generazzo of the purchasing office for their help.

Finally, I would like to express my appreciation to Harvard University for supporting my first year of studies, and the Army Research Office, the Joint Service Electronics Program and Hamamatsu Photonics for their support of this work.

CONTENTS

CHAPTER 1

INTRODUCTION

1.1 Spectroscopy, lasers and laser chemistry

Spectroscopy has long been an important tool in science. Even in the early days, when prisms and photographic plates were the only available equipment for spectroscopy, scientists discovered the missing frequencies in the continuum spectrum of sunlight due to the absorption of the atoms near the surface of the sun. Early atomic spectroscopy led to the discoveries of the Pauli principle, which forms the basis for understanding atomic structure, chemical periodicity and molecular structure. Two important spectroscopic discoveries, the discrete atomic spectrum and the falling tail in the spectrum of black body radiation, led to the birth of quantum mechanics. As the technology improved, spectroscopy provided much information on the structure of matter, which, in turn, opened new frontiers of science.

Before the invention of the laser, spectroscopy was limited to the linear regime in terms of the response of matter to the probing light. The lack of pulsed light sources further limited spectroscopy to probing static properties of matter. This situation has changed dramatically since the invention of the laser. The properties of laser radiation, such as high power, short pulse duration, narrow bandwidth and coherence, have made

possible many experiments which could not be done before. For example, the transient dynamics of carriers in semiconductors, which occur on a picosecond time scale, can be studied only by experimental techniques with comparable time resolution. Therefore, picosecond and femtosecond lasers have almost become an obligatory tool in this field. In the frequency domain, the coherence of laser light makes various optical heterodyne detection techniques possible. In fact, the development of laser technology has led to a large field of research known as quantum electronics, which currently attracts as much attention as does spectroscopy.

The high intensity of laser radiation also makes it possible to study the nonlinear interaction of light and matter. Before the invention of the laser, the light sources available were too weak to study these nonlinear interactions. The radiation fields of the lasers, however, are strong enough to alter certain properties of matter, such as the index of refraction of a dielectric material or the energy levels of a molecular system. Strong interaction between light and matter has been used to develop nonlinear spectroscopy techniques and new light sources. For example, high resolution Doppler-free spectroscopy[1,2] is based on the "hole burning"[1,2] effect on the inhomogeneously broadened line profile. Nonlinear parametric amplifiers[1] have been developed which provide continuously tunable coherent light. With lasers, traditional electronics has been extended all the way to the 10^{15} Hz regime.

In chemistry, the laser has also contributed to many new research areas. Owing to the narrow bandwidth and high intensity of laser radiation, molecules can be excited to specific levels with properly chosen laser wavelengths. It is this control of molecular excitation that raised great hopes for developing laser controlled chemical reactions. Indeed, from the fast growing list of laser-induced reactions one may conclude that laser-controlled chemistry is a viable technology.

In addition to selective excitation, with short laser pulses one can study the interaction of intense light with isolated molecules under nearly collisionless condition. Many laser induced unimolecular reactions have already been discovered. With sufficiently short pulses, it even becomes possible to monitor the evolution of the population of the energy levels of isolated molecules.

1.2 Molecular energy levels

In principle the energy levels of a molecule can be solved from the Schrödinger equation. In practice, however, even for simple molecules with only a few atoms, the Hamiltonian is either unknown or too difficult to solve. Therefore accurate values for the molecular energy levels can only be obtained from spectroscopic data.

The energy levels of a typical molecule become much easier to understand with the help of the adiabatic approximation.[3] Under this approximation, the energy levels of a molecule can be classified into three categories, according to the different dynamics inside the molecule. Electronic energy levels correspond to the motion of electrons, vibrational energy levels to the motion of the atoms with respect to each other, and rotational energy levels to the rotation of the molecule in free space. Since electrons are much lighter than atoms, the steps of the electronic levels are much larger than those of vibrational energy levels. Similarly, the energy steps of vibrational energy levels are much larger than those of the rotational energy levels.

In the simplest approximation, these three categories of motion are approximately decoupled, so that the total wavefunction of the molecule can be approximated by the product of the separate wavefunctions corresponding to the three categories of motion. The total energy of the molecule is then approximately the sum of the electronic, vibrational and rotational energy. Typical values of the energy levels are 20,000–50,000 cm^{-1}, 500–

5,000 cm^{-1} and 1–10 cm^{-1} for electronic, vibrational and rotational energy, respectively. A diagram of molecular energy levels is shown in Fig. 1.1.

When the frequency of an external electromagnetic wave matches one of the energy steps of a molecule, exchange of energy between the electromagnetic wave and the molecule occurs. The efficiency of this energy exchange depends on how close the electric magnetic wave is in resonance with the molecule and the symmetry relations between the initial and final molecular energy levels. The spectrum of a molecule, determined by observing the exchange of energy between the molecule and the external electromagnetic wave as a function of frequency, provides both dynamic and structural information of the molecule.

In addition to probing the states of the molecules, high power pulsed lasers can be employed to manipulate the populations of the molecular states. Pumping molecules into states which cannot be reached by thermal excitation has enabled one to study new molecular phenomena. In the next section we shall discuss the phenomenon of infrared multiphoton excitation in polyatomic molecules and the impact of this phenomenon on the understanding of molecular vibrations.

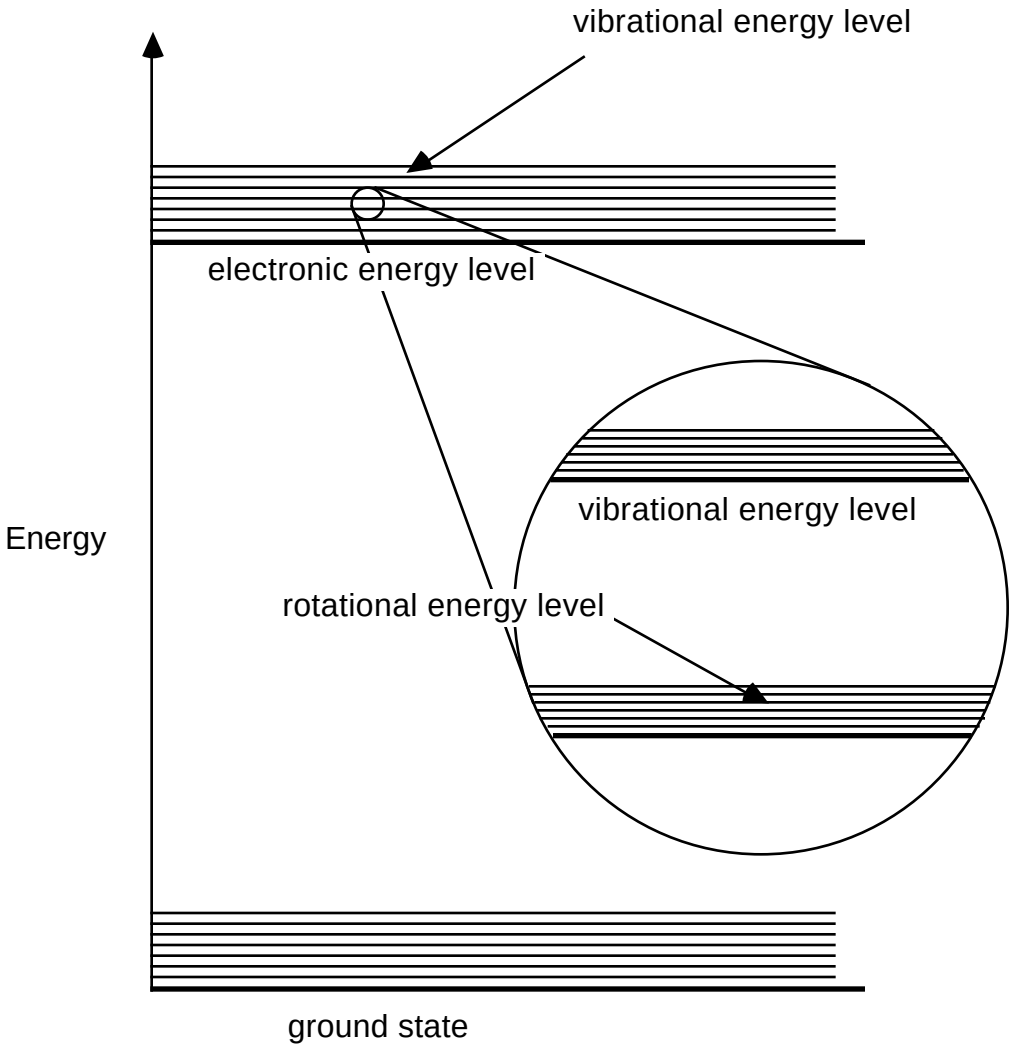

Fig. 1.1. Molecular energy diagram. Because of the large differences in energy scales, rotational energy levels form a band just above each vibrational level, while vibrational levels form a band above each electronic level.

1.3 A brief history of infrared multiphoton excitation

In 1973 it was discovered that isolated SiF_4 molecules in ground electronic state can be dissociated by a short, intense pulse from a CO_2 laser.[4] The experiment was performed at low sample gas density such that the CO_2 laser pulse duration was much shorter than the mean free time of the sample molecules. Since collisions can be ignored on the time scale of this experiment, the dissociation is solely due to the interaction of an intense infrared pulse with single, isolated molecules.

Subsequently it was discovered that when the laser is properly tuned to the vibrational frequency of $^{32}SF_6$, the dissociation rate of $^{32}SF_6$ is thirty-five times larger than that of $^{34}SF_6$ due to the small mass difference of the two sulfur isotopes.[5] This discovery provided an efficient method to separate a number of isotopes.*

Due to the anharmonicity of the vibrational potential well, the vibrational energy levels of a molecule are not equally spaced. Consequently one might think that infrared multiphoton excitation cannot occur at all, since the laser will be out of resonance after the molecule is excited up to the first few levels. Indeed, infrared multiphoton excitation has never been observed in diatomic molecules where there is only one single vibrational mode (see Fig. 1.2). For polyatomic molecules the situation becomes more complicated, because nonresonant vibrational modes can also participate in the excitation due to the coupling between modes. Many experiments have been performed to characterize this phenomenon and to understand the underlying mechanism of infrared multiphoton excitation.[6-11] The total internal energy of infrared multiphoton excited molecules as well as the dissociation

* The vibrational frequency of the molecules has to be close to those of the available lasers, and the frequency difference due to the mass difference of the isotopes must be larger than the width of the absorption profile.

yields of various infrared multiphoton dissociated molecules were measured as functions of infrared laser fluence, intensity, and frequency.[12-15] The general effects of molecular size were also studied.[13] It was discovered that the larger the molecule is, the less the excitation depends on pumping intensity, and that larger molecules are less sensitive to the detuning of the pumping laser frequency. Infrared double resonance was also employed to study the population of the ground state and the first excited state after infrared multiphoton excitation.[16]

At high infrared laser intensity, some molecules are excited above the dissociation threshold. Laser induced fluorescence,[17] mass spectroscopy, and time of flight measurements combined with molecular beam techniques were employed to study the vibrational and translational energy distributions of the dissociation fragments.[18] These energy distributions are directly related to the intramolecular vibrational energy distribution right before dissociation. The result of these experiments all pointed to an equilibrium distribution of the intramolecular vibrational energy for infrared multiphoton dissociated molecules. In other words, just before dissociation, the vibrational energy distribution of the molecule is in equilibrium. Such a conclusion raised serious doubts about the feasibility of "mode selective" laser chemistry. In addition it became clear that a detailed knowledge of the intramolecular energy transfer process was needed to understand the process of infrared multiphoton dissociation.

In 1980, Raman spectroscopy was first employed by a research group in Soviet Union to study infrared multiphoton excitation.[19] The Raman spectrum of infrared multiphoton excited SF_6 demonstrated that the sample gas was separated into two ensembles, one highly excited and one close to ground state. This confirmed the "bottleneck effect",[6] an important part of the currently accepted theoretical picture of infrared multiphoton excitation. Since these first Raman experiments on SF_6, the Soviet group and our group at Harvard University have employed Raman spectroscopy to study

the *intramolecular* (as opposed to *intermolecular*) vibrational energy distribution of infrared multiphoton excited molecules.[20-27] In 1986, for the first time a nonequilibrium intramolecular vibrational energy distribution in isolated, highly excited molecules was observed.[27] Subsequently, similar observations were made for various molecules. Currently, in our group, efforts are directed toward the improvement of both spectral and time resolution using coherent anti-Stokes Raman spectroscopy.

Owing to the rapid advances in computer technology, computer simulations of the infrared multiphoton excitation of small molecules have recently become possible. Empirical Hamiltonians fitted to data from high resolution infrared spectroscopy were used as the propagators* to calculate the evolution of the wavefunctions.[28] It was shown that, as long as the spectrum of the molecule is simple enough to interpret and the Hamiltonian can be constructed properly, intramolecular dynamics can be studied by computer simulations.

1.4 The quasicontinuum model

Although no one has yet been able to model infrared multiphoton excitation starting from the Schrödinger equation, phenomenological models of infrared multiphoton excitation can be developed.[6] First of all, it should be noted that the density of states of a constant energy shell is a fast growing function of energy. For a medium-sized molecule like SF_6, it is estimated that the density of vibrational states grows rapidly to

---

* The wavefunction at $t=\tau$ can be calculated from the Hamiltonian and the wavefunction at $t=0$. The wavefunction, or the state of the molecule, propagates according to the Schrödinger equation $|\psi(\tau)> = \exp(iH\tau)|\psi(0)>$. In other words, for small τ, $|\psi(\tau)>-|\psi(0)> = iH\tau|\psi(0)>$. By choosing τ sufficiently small, the wavefunction at $t=\tau$ can be calculated to an arbitrary accuracy.

10^6 states/cm^{-1} at high excitation. Such a high density of states results in a broad absorption profile which compensates for the anharmonicity shifts and allows the molecules to continue to absorb photons in the high excitation region. Secondly, because the coupling between vibrational modes cannot be ignored at high excitation, the energy absorbed by the pump mode is quickly distributed into the nonresonant background modes. Depending on the size of the molecule and the coupling between modes in a particular excitation region, the energy of the pump mode may or may not be evenly distributed into all modes. In the present study both equilibrium and nonequilibrium cases were found.

The high density of states also results in a fast transverse relaxation time which destroys the coherence in the excitation process. Therefore, in the high density of states region (quasicontinuum) the multiphoton absorption process breaks down into steps of single photon absorption. For large molecules the quasicontinuum starts at fairly low excitation, and thus the infrared multiphoton excitation for large molecules depends essentially only on the pump fluence, not on intensity.

Although infrared multiphoton excitation happens mainly due to the absorption of many infrared photons in the quasicontinuum, the low lying vibrational levels also play an important role. At low excitation, the density of states is low and the vibrational levels are close to those of a simple harmonic oscillator. The anharmonicity in this region is still larger than the bandwidth of a single-mode CO_2 laser, so that rotational broadening of vibrational levels and power broadening of the laser are necessary to compensate for the anharmonicity shifts. For smaller molecules, where the quasi-continuum starts only at high excitation, a strong laser intensity is needed to excite the molecules through the discrete region. Indeed, infrared multiphoton excitation of small molecules was found to depend strongly on laser intensity.

Rotational broadening of the vibrational levels in the low excitation region results in an interesting effect in infrared multiphoton excitation. In the low excitation region the infrared absorption profile is narrow and therefore only a fraction of the molecules that has the right rotational energy to compensate for the anharmonicity shifts can be excited into the quasi-continuum. The rest of the molecules are "bottlenecked" in the low excitation region. Since power broadening of the absorption profile relaxes the selection of rotational states, the higher the laser intensity, the larger the fraction of molecules that is excited into the quasi-continuum region. This "bottleneck" effect can clearly be seen in the Raman spectrum of infrared multiphoton excited SF_6[20] where the Raman peak splits into two, one for the "hot" ensemble and the other for the "cold", "bottlenecked" ensemble.

As we have seen, the quasicontinuum model, which is based on simple physical concepts, explains all the gross features of infrared multiphoton excitation. It provides a general picture of infrared multiphoton excitation without involving complicated calculations. Other models of infrared multiphoton excitation also exist. In the following section infrared multiphoton excitation will be discussed from the point of view of classical nonlinear dynamics.

1.5 Intramolecular chaos

One way of looking at infrared multiphoton excitation is to view the molecule as a collection of coupled nonlinear oscillators driven by external periodic forces.[29,30] This does not simplify the problem because even in the classical limit there are no general

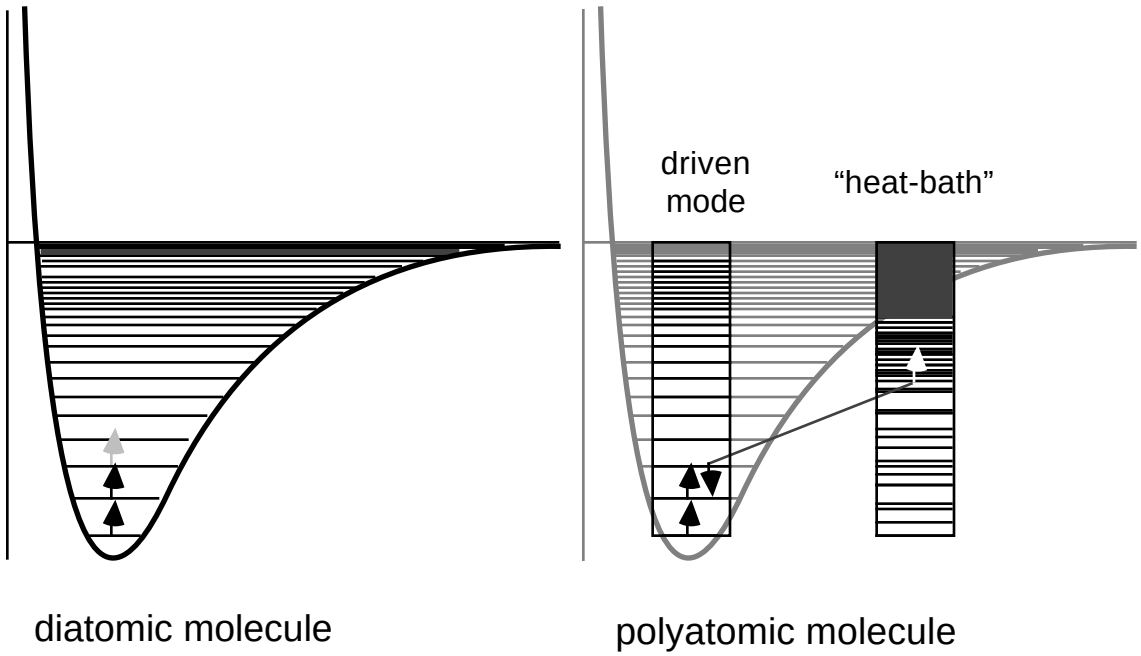

Fig. 1.2. Infrared multiphoton excitation of diatomic molecules is impossible due to anharmonicity. For polyatomic molecules, modes which are not in resonance with the CO_2 laser can also participate in the infrared multiphoton excitation process through intermode coupling.

solutions for the equations of motion for a system of coupled nonlinear oscillators. However, one can study the energy distribution of the system without knowing the solution to these equations of motion, much in the same manner as is done in statistical mechanics.

The question of interest here, for the understanding of infrared multiphoton excitation, is how the state of the molecule evolves from one with localized vibrational energy to one where energy is randomly distributed among all modes. Also, one would like to know what determines the final energy distribution.

In Boltzmann's statistical mechanics the calculation of the energy distribution and other physical quantities is based on the ergodicity assumption, which states that the time average of a physical quantity of a system is equal to its ensemble average. Although Boltzmann's statistical mechanics works well for systems that have a large number of degrees of freedom, it does not apply to small isolated systems.

It is well known from classical mechanics that for a system with an integrable Hamiltonian, the trajectory of the system in the phase space is limited by constants of motion, and therefore it is impossible for the system to become ergodic. For example, in the planetary system the angular momentum is a constant of motion. This constant of motion limits the trajectory of a planet to an ellipse, instead of the surface of an ellipsoid which is allowed by energy conservation. Since the trajectory of this system only covers a small part of the phase space and repeats itself, the system cannot become ergodic.

Similarly, the trajectory of two uncoupled harmonic oscillators is a spiral curve on the surface of a 4-dimensional torus (see Fig. 1.3). Since there is no coupling between these two modes, the energy of each oscillator is a constant of motion. This means that the radii of the two circles R_1 and R_2 are fixed. Therefore, the trajectory covers only the surface of the torus, which is a small part of the total phase space allowed by energy conservation.

For a system of many uncoupled oscillators, the trajectory lies on a multidimensional torus, which cannot easily be visualized, but again the trajectory covers only a small part of the total phase space allowed by energy conservation. None of the systems discussed above are ergodic, because the possible states of the system are not

evenly distributed in the phase space allowed by energy conservation. The fundamental question is now: how can such a system of many oscillators become ergodic? Couplings between the oscillators will induce transitions between the states of the oscillators. According to the Boltzmann *H*-theorem, one might expect that this process increases the entropy and the system eventually becomes ergodic. However, as we will see shortly, whether or not the system becomes ergodic depends on a number of conditions.

In the early fifties Fermi, Pasta and Ulam used one of the early computers to study the effects of small nonintegrable perturbations on a system of harmonic oscillators.[31] As a model system they used a string with many vibrational modes. By introducing couplings between the vibrational modes, the originally integrable Hamiltonian became nonintegrable. The whole computer experiment was intended to demonstrate that nonintegrable perturbations, no matter how small, will eventually lead the system to ergodicity. To their surprise, however, the system did not evolve into ergodicity, although intermode energy transfer did occur. The result showed that the energy was "localized" only in a few modes. Nearly at the same time Kolmogorov, Arnold and Moser proved a theorem, now referred to as the KAM theorem,[32] which states that small nonintegrable perturbations can only distort, not destroy the phase space torus* on which the trajectory of a system of nonlinear oscillators lies, except for those modes where the following resonance condition happens to be fulfilled:

$$\sum_i n_i \nu_i = 0. \tag{1.1}$$

---

* the phase space trajactory of *n* uncoupled simple harmonic oscillators lies on the surface of a torus in a 2*n* dimensional space *(*see Fig. 1.3).

Here ν_i are the frequencies of the modes and n_i are small integers.

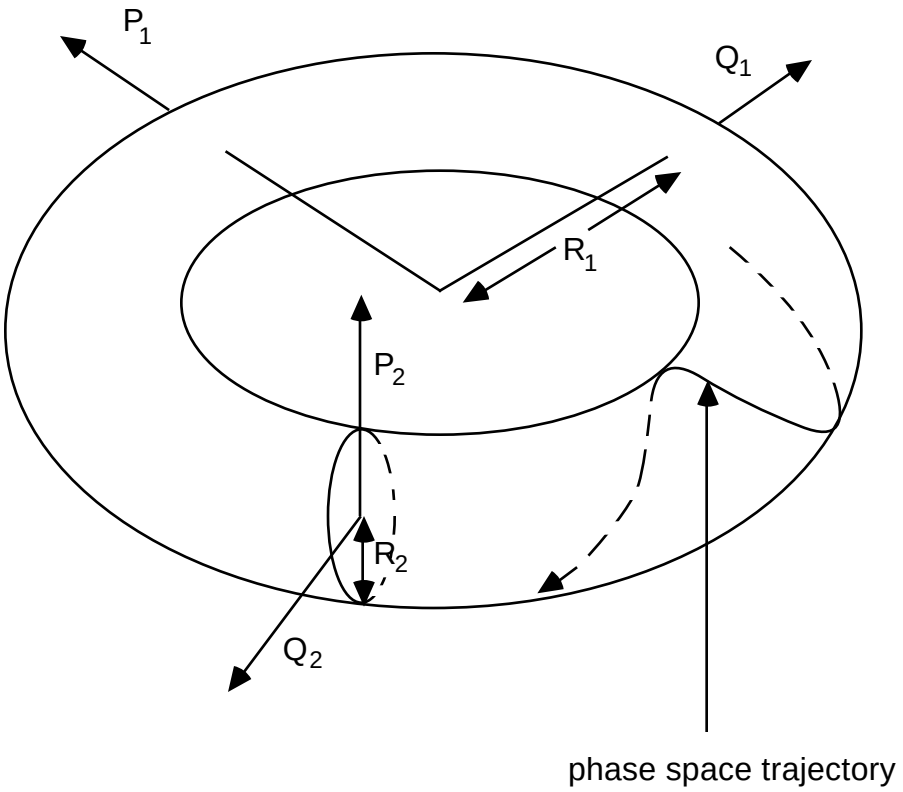

Fig. 1.3. Phase space of two uncoupled simple harmonic oscillators. The trajectory of the phase space lies on a torus in a four dimensional space. P_1, Q_1, P_2, Q_2 are the canonical variables of the two oscillators respectively. R_1, R_2 are related to the energy of the two oscillators.

Both Fermi's experiment and the KAM theorem suggest that, in general, a system of nonlinear oscillators can only become ergodic when the energy involved is large enough, or when condition (1.1) is satisfied. As we will see, this is consistent with both the infrared multiphoton dissociation data and the experimental results presented in this thesis. In the language of classical nonlinear dynamics then, infrared multiphoton excitation can be seen as the transition of regular to chaotic molecular phase space trajectories induced by an external electromagnetic field. At low excitation, the phase space tori of the various modes are only slightly distorted by the anharmonicity and the intermode coupling, while still maintaining their general shapes, and the infrared absorption profile is narrow. As the excitation increases, more and more tori are destroyed and the absorption profile broadens. Eventually, all of the tori are destroyed and the molecule reaches a chaotic state where the trajectory spreads over the entire phase space (see Fig. 1.4). If the molecule dissociates under these conditions, the state distribution of the dissociation products should agree with the RRKM (Rice-Ramsperger-Kassel-Marcus) unimolecular reaction theory,[33] which assumes intramolecular equilibrium. As we have mentioned before, this is indeed observed experimentally for many molecules.

It is interesting to compare the number of resonances that satisfy condition (1.1) for each molecule studied in this thesis with the infrared multiphoton excitation data obtained. According to the KAM theorem, the more often condition (1.1) is satisfied, the more likely the molecule will behave ergodically after infrared multiphoton excitation. For SF_6 and CF_2Cl_2, one can calculate the number of incidences where condition (1.1) is satisfied as a function of the excitation energy (see programs in Appendix A), and compare the results of the calculation with the experimental results. The comparison is shown in Fig. 1.5. The

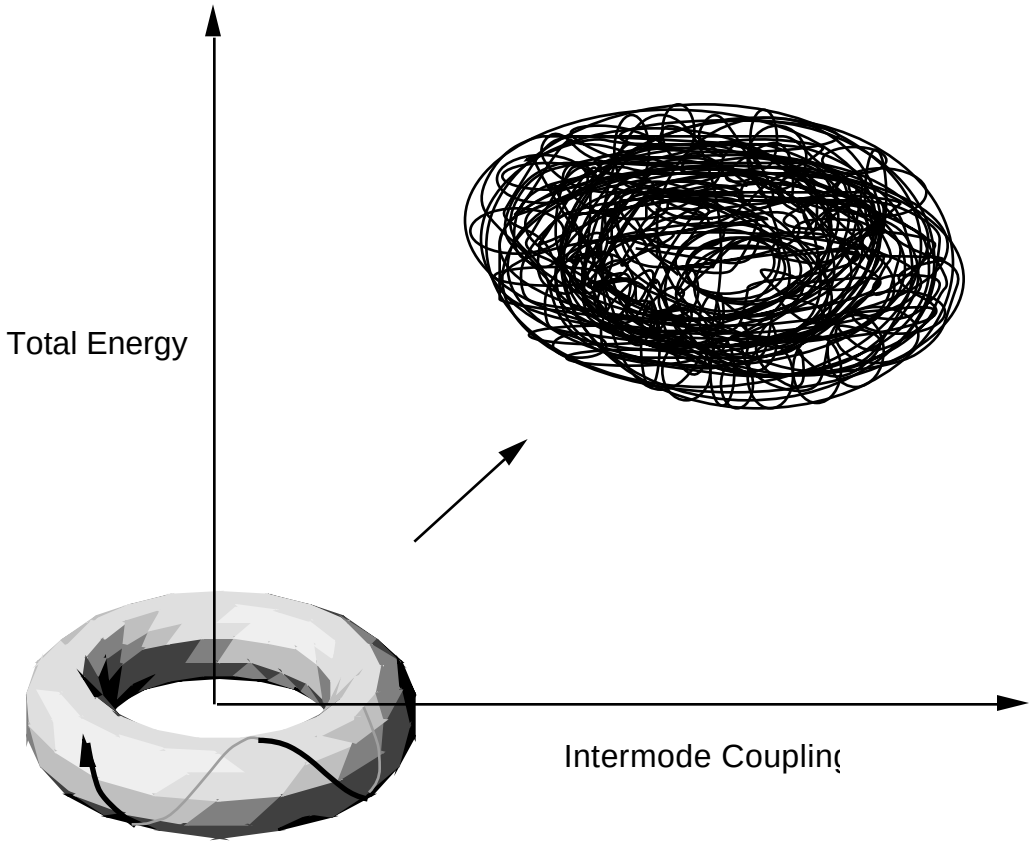

Fig. 1.4. Transition from regular periodic trajectories to chaotic ones in phase space as the total energy and the intermode coupling increase.

vertical axis shows the number of times, N, where the following condition is satisfied:

$$\sum_i n_i \nu_i \leq 20 \text{ cm}^{-1}. \tag{1.2}$$

Here n_i is the integer coefficient of the ith mode, and ν_i the frequency. Note that the n_i can be negative, otherwise Eq. (1.1) can never be satisfied. The $20\,\text{cm}^{-1}$ on the right hand side

of the equation is chosen close to the total anharmonicity of a typical vibrational mode, which can be roughly thought of as the linewidth of a typical ν_i. Since our goal is to compare the number of incidences where Eq. (1.1) is satisfied for different molecules under the same conditions, the choice of the number on the right hand side of Eq. (1.2) is not critical. In the calculation the set $\{n_i\}$ is permuted to cover all possible combinations, and the number of incidences is sorted according to the total internal energy of the molecule,

$$E = \sum_i |n_i| \nu_i \, . \tag{1.3}$$

As one can see from Fig. 1.5, for SF_6, the number of incidences where Eq. (1.2) is met, is orders of magnitude larger than for CF_2Cl_2. Also, the larger the excitation energy is, the bigger the difference between the two molecules. Note that for both molecules N increases rapidly with energy .

Figure 1.5 strongly suggests that SF_6 will behave ergodically at a much lower excitation energy than CF_2Cl_2. Indeed, the experimental results presented in chapter 4 and 5 show that the intramolecular vibrational energy distribution of SF_6 after infrared multiphoton excitation is an equilibrium one, while the one of CF_2Cl_2 is not.

1.6 Mode-selective excitation vs. intramolecular vibrational energy equilibrium

The experimentally observed intramolecular equilibrium for dissociating molecules raised serious doubts regarding the feasibility of selective chemical bond breaking by infrared lasers. Experimental studies indicate that intramolecular energy relaxation takes

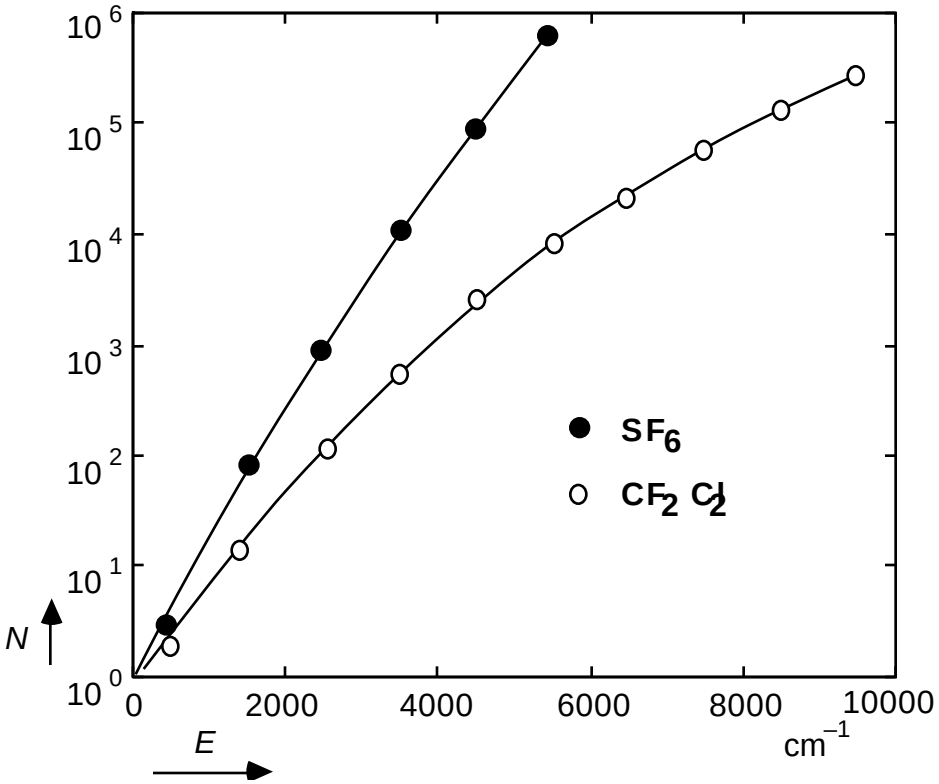

Fig. 1.5. Number of times, *N*, where Eq. (1.1) is satisfied as a function of excitation energy for SF_6 and CF_2Cl_2. For SF_6 *N* is one to two orders of magnitude larger than for CF_2Cl_2. This graph suggests that SF_6 will behave ergodically at a much lower excitation energy than CF_2Cl_2.

place on a picosecond time scale.[34,35] With today's molecular laser technology it is still hard to beat this time scale. It has been proposed that it may be possible to use laser pulses with a complicated preprogrammed coherence structure to match the evolution of the molecular states in such a way that the collective motion of the atoms leads to a selective bond breaking state.[36] However, this approach will work only when the time scale of the

coherence structure of the pumping pulse is shorter than the transverse relaxation time of the vibrational states. Practically, there is not yet a way to control the coherence structure of an infrared laser pulse on such a short time scale.

1.7 Objective of this work

Although the quasicontinuum model explains the general features of infrared multiphoton excitation, one cannot obtain a clear picture of intramolecular vibrational energy relaxation without measuring the intramolecular vibrational energy distributions. Most of the experiments done before this thesis do not supply mode-specific information other than for the pumped mode. Spectroscopic measurements on modes which do not interact directly with the infrared pumping laser are necessary for understanding how the nonresonant background modes participate in the infrared multiphoton excitation. In the first stage of this research project, time-resolved spontaneous Raman spectroscopy was employed to measure the vibrational energy of each accessible Raman active mode after infrared multiphoton excitation for molecules with different sizes and symmetries (see chapter 2–5). The intramolecular vibrational energy distributions were obtained as functions of infrared fluence, frequency and time. In the second stage, a high resolution coherent anti-Stokes Raman experiment was set up to measure the state-to-state population within each vibrational mode. In both cases, the realization of low density, high time resolution Raman spectroscopy provides direct measurements of the state of the molecules.

References

1 Y.R. Shen, *The Principles of Nonlinear Optics* (John Wiley & sons, New York, 1984)

2 M.D. Levenson, *Introduction to Nonlinear Laser Spectroscopy* (Academic Press, New York, 1982)

3 A.S. Davydov, *Quantum Mechanics*, 2nd Edition, Chapter 15 (Pergamon Press, New York, 1976)

4 N.R. Isenor, V. Merchant, R.S. Hallsworth and M.C. Richardson, Can. J. Phys. **51**, 1281 (1973)

5 R.V. Ambatzumian, N.V. Chekalin, V.S. Doljikov, V.S. Letokhov, and E.A. Ryabov, Chem. Phys. Lett. **25**, 515 (1974)

6 N. Bloembergen and E. Yablonovitch, Physics Today **5**, 23 (1978)

7 V.N. Bagratashvili, V.S. Letokhov, A.A. Makarov, E.A. Ryabov, *Multiphoton Infrared Laser Photophysics and Photochemistry* (Harwood Academic Publishers, New York, 1985)

8 D.S. King, *Dynamics of the Excited State*, Ed. K.P. Lawley (Wiley, New York, 1982)

9 W. Fuss and K.L. Kompa, Prog. Quant. Electr. **7**, 117 (1981)

10 P.A. Schulz, Aa. S Sudbø, D.J. Krajnovitch, H.S. Kwok, Y.R. Shen, and Y.T. Lee, Ann. Rev. Phys. Chem. **30**, 379 (1979)

11 C. D. Cantrell, S. M. Freund, J. L. Lyman, *Laser Handbook*, Vol. 3, Ed. M.L. Stitch (North-Holland, Amsterdam, 1979)

12 J.G. Black, P. Kolodner, M.J. Schultz, E. Yablonovitch, and N. Bloembergen, Phys. Rev. A **19**, 704 (1979)

13 J.G. Black, Ph.D. Thesis, Harvard University, May 1980

14 D.S. King and J.C. Stephenson, Chem. Phys. Lett. **66**, 33 (1979)

15 J.C. Stephenson and D.S. King, J. Chem. Phys. **78**, 1867 (1983)

16 R.C. Sharp, E. Yablonovitch and N. Bloembergen, J. Chem. Phys. **74**, 5357 (1981)

17 D.S. King and J.C. Stephenson, Chem. Phys. Lett. **51**, 48 (1977)

18 P.A. Schultz, Aa. S. Sudbø, D.J. Krajnovitch, H.S. Kwok, Y.R. Shen, and Y.T. Lee, Ann. Rev. Phys. Chem. **30**, 379 (1979)

19 V.N. Bagratashvili, Yu.G. Vainer, V.S. Dolzhikov, S.F. Kol'yakov, A.A. Makarov, L.P. Malyavkin, E.A. Ryabov, E.G. Silkis, and V.D. Titov, Appl. Phys. **22**, 101 (1980)

20 V.N. Bagratashvili, Yu.G. Vainer, V.S. Doljikov, S.F. Koliakov, A.A. Makarov, L.P. Malyavkin, E.A. Ryabov, E.G. Silkis, and V.D. Titov, Appl. Phys. **22**, 101 (1980)

21 V.N. Bagratashvili, Yu.G. Vainer, V.S. Dolzhikov, S.F. Kol'yakov, V.S. Letokhov, A.A. Makarov, L.P. Malyavkin, E.A. Ryabov, E.G. Sil'kis, and V.D. Titov, Sov. Phys. JETP **53**, 512 (1981)

22 V.N. Bagratashvili, V.S. Doljikov, V.S. Letokhov, A.A. Makarov, L.P. Maljavkin, E.A. Ryabov, E.G. Silkis, and Yu.G. Vainer, Opt. Comm. **38**, 31 (1981)

23 V.N. Bagratashvili, Yu.G. Vainer, V.S. Doljikov, V.S. Letokhov, A.A. Makarov, L.P. Malyavkin, E.A. Ryabov, and E.G. Sil'kis, Opt. Lett. **6**, 148 (1981)

24 Yu.S. Doljikov, V.S. Letokhov, A.A. Makarov, A.L. Malinovsky and E.A. Ryabov, Chem. Phys. Lett. **124**, 304 (1986)

25 V.S. Doljikov, Yu.S. Doljikov, V.S. Letokhov, A.A. Makarov, A.L. Malinovsky and E.A. Ryabov, Chem. Phys. **102**, 155 (1986)

26 Jyhpyng Wang, Kuei-Hsien Chen and Eric Mazur, Phys. Rev. A, **34**, 5 (1986) 3892

27 Kuei-Hsien Chen, Jyhpyng Wang and Eric Mazur, Phys. Rev. Lett, **59**, 24 (1987) 2728

28 Martin. Quack, *The Dynamics of coherent IR-multiphoton Excitation of Molecules*, talk at The Gordon Research Conference, Multiphoton Processes, New London, New Hampshire (1988)

29 J.R. Ackerhalt, H.W. Galbraith and P.W. Milonni, Phys. Rev. Lett. **51**, 1259 (1983)

30 J.R. Ackerhalt and P.W. Milonni, Phys. Rev. A **34**, 1211 (1986)

31 *Collected Work of Enrico Fermi* (University of Chicago Press, 1965), paper 266 and comments by S. Ulam

32 V.I. Arnold, Russ. Math. Surveys **18**, 9 (1963)

33 P.J. Robinson, K.A. Holbrook, *Unimolecular Reactions* (Wiley-Interscience, New York 1972)

34 H.S. Kwok, Ph.D. Thesis, Harvard University, August 1978

35 R.C. Sharp, Ph.D. Thesis, Harvard University, May 1980

36 H. Rabitz, Atomic and Molecular Processes with Short Intense Laser Pulses, Ed. André D. Bandrauk (Plenum Press, New York, 1988)

CHAPTER 2

THEORY OF SPONTANEOUS RAMAN SCATTERING

2.1 Introduction

This chapter presents a brief treatment of spontaneous Raman scattering. Both radiation field and molecular system are treated quantum mechanically. Vibrational level dependent Raman transition probabilities are derived from the interaction Hamiltonian of the radiation field and the molecular system. These transition probabilities are then used to derive the relation between the Raman intensities and mode energy. The expressions obtained in this chapter will be employed to interpret the experimental data discussed in the following chapters.

2.2 Theory

To describe the mechanism of Raman scattering we consider the interaction of the field with the induced polarization $\boldsymbol{P}$ of the molecule,

$$\boldsymbol{P} = \mu_o + \alpha \cdot \boldsymbol{E} \ , \tag{2.1}$$

where μ_o is the permanent dipole moment of the molecule, α a tensor representing the molecular polarizability, and $\alpha \cdot \boldsymbol{E}$ the induced dipole moment. The physical system is described by the Hamiltonian operator, which contains terms describing the molecular system and the electromagnetic radiation field, and a term representing the interaction between the molecular polarization and the field. This last term, the interaction Hamiltonian H_{int}, is responsible for the light scattering.

In the electric-dipole approximation one has

$$H_{\text{int}} = \boldsymbol{E} \cdot \alpha \cdot \boldsymbol{E} \ . \tag{2.2}$$

The molecular polarizability α can be expanded as a Taylor series of the generalized coordinate $\boldsymbol{q}$ of the molecular vibrational mode being considered

$$\alpha = \alpha_o + \left(\frac{\partial \alpha}{\partial q}\right)_0 q + \frac{1}{2}\left(\frac{\partial^2 \alpha}{\partial q^2}\right)_0 q^2 + \ldots \tag{2.3}$$

Substituting α into H_{int} we obtain,

$$H_{\text{int}} = \boldsymbol{E} \cdot \alpha \cdot \boldsymbol{E} + \boldsymbol{E} \cdot \left(\frac{\partial \alpha}{\partial q}\right)_0 \cdot \boldsymbol{E} q + \frac{1}{2} \boldsymbol{E} \cdot \left(\frac{\partial^2 \alpha}{\partial q^2}\right)_0 \cdot \boldsymbol{E} q^2 + \ldots . \tag{2.4}$$

The first term represents the Rayleigh scattering, the remaining terms first and higher order Raman scattering. Since higher order scattering is rejected in our experiment, we need only consider the term linear in q. In simple harmonic approximation we have[1]

$$q = (h/8\pi^2\mu\nu_R)^{1/2} [\ b^\dagger + b\ ], \tag{2.5}$$

where $b^\dagger$ and b are the creation and annihilation operator for the vibrational quanta respectively, and ν_R the frequency of the harmonic oscillator. The electromagnetic field is quantized similarly[2]

$$\boldsymbol{E}_\lambda = (2\pi h\nu_R/\varepsilon V)^{1/2} \sum \mathbf{e}_\lambda\, i [\ a_\lambda{}^\dagger - a_\lambda\ ]. \tag{2.6}$$

with $a^\dagger$ and a the creation and annihilation operators for the field, ε the relative permittivity, V the mode volume, and $\mathbf{e}_\lambda$ a unit vector representing the polarization of the light of wavelength λ. The linear term in the interaction Hamiltonian can therefore be written in the following form,

$$H_{int} \sim \left(\frac{\partial\alpha}{\partial q}\right) a_L b a^\dagger_{AS} + a_L b^\dagger a^\dagger_S\ (\mathbf{e}_L \quad \mathbf{e}_R)\ , \tag{2.7}$$

where the indices L, AS, S and R stand for laser, anti-Stokes, Stokes and Raman respectively. The first term in this expression annihilates a vibrational quantum and therefore corresponds to the anti-Stokes branch. The second term corresponds to the Stokes branch.

The interaction Hamiltonian can be used to obtain the transition probabilities between states. From the general perturbation theory,[1] the transition probability from an initial state $|i$ to a final state $|f$, is given by

$$W_{i \rightarrow f} = \left| \left\langle f \left| H_{int} \right| i \right\rangle \right|^2 . \tag{2.8}$$

For the eigenstates $|n\rangle$ of the harmonic oscillator one has[2]

$$b^{\dagger} |n\rangle = (n+1)^{1/2} |n+1\rangle , \tag{2.9}$$

and

$$b |n\rangle = n^{1/2} |n-1\rangle , \tag{2.10}$$

with n the vibrational quantum number corresponding to state $|n\rangle$.

From Eqs. (2.7) through (2.10) it follows that the transition probabilities for Stokes and anti-Stokes transitions depend on n+1 and n, respectively:

$$W_{n \rightarrow n+1} \sim n+1, \quad W_{n \rightarrow n-1} \sim n. \tag{2.11}$$

Hence the *total* intensity of the spontaneous Stokes and anti-Stokes Raman signals (summed over *all* vibrational levels of the particular vibrational mode considered), I_S and I_{AS}, are given by

$$I_S \sim \sum_{n=0} W_{n \rightarrow n+1} N(n) \sim \sum_{n=0} (n+1) N(n) = 1 + \sum_{n=1} n N(n)$$

$$I_{AS} \sim \sum_{n=0} W_{n \rightarrow n-1} N(n) \sim \sum_{n=1} nN(n) \tag{2.12}$$

with $N(n)$ the population of level n. Substituting the average energy in the mode, $E_R = h\nu_R \sum n\, N(n)$, we find for the summations in Eq. (2.12)

$$I_S = A\left(1 + \frac{E_R}{h\nu_R}\right), \qquad I_{AS} = A\left(\frac{E_R}{h\nu_R}\right). \tag{2.13}$$

where A is a proportionality constant related to the Raman cross section.

It is important to note that in the harmonic approximation the result obtained does not depend on the energy distribution $N(n)$, but only on the *average* energy E_R. Thus, the intensity of a Raman active mode is a measure for the *average energy content* of the mode. Without infrared pumping, at room temperature, T_o = 300 °K, the energy E_R^o of the Raman active mode can be obtained from the Boltzmann distribution,

$$E_R^o = \frac{h\nu_R}{e^{\frac{h\nu_R}{kT_o}} - 1}\,. \tag{2.14}$$

Since for vibrations $h\nu_R$ is generally much larger than kT at room temperature, E_R^o is much smaller than $h\nu_R$ in Eq. (2.13).

Now we define the I_{norm}, normalized anti-Stokes signal, by dividing the anti-Stokes signal, I_{AS}, by its corresponding Stokes signal at room temperature, I_S^o,

$$I_{norm} \equiv \frac{I_{AS}}{I_S^o} = \frac{\dfrac{E_R}{h\nu_R}}{1 + \dfrac{E_R^o}{h\nu_R}} \approx \frac{E_R}{h\nu_R} \quad . \tag{2.15}$$

So, the normalized anti-Stokes signal I_{norm} measures the average number of vibrational quanta in the Raman mode and is independent of the Raman cross section. Therefore I_{norm} can be used to compare the energy stored in different Raman modes. To remove the dependence on the Raman cross-section the experimental data in the following chapters is presented in terms of I_{norm}.

2.3 Conclusion

In this chapter, we derived relations between the intensity of the Raman signal and the vibrational energy in the Raman mode. These relations enable us to calculate the intramolecular vibrational energy distribution from the data of spontaneous Raman scattering experiments.

References

1 A.S. Davydov, *Quantum Mechanics*, 2nd Edition (Pergamon Press, New York, 1976)

CHAPTER 3

TIME RESOLVED SPONTANEOUS RAMAN SCATTERING
PART ONE: EXPERIMENTAL SETUP

3.1 Introduction

In this thesis the intramolecular vibrational energy distributions of infrared multiphoton excited molecules were studied by time resolved spontaneous Raman scattering. The layout of the experimental setup is shown schematically in Fig. 3.1. In this chapter we present a complete description of the laser systems, the Raman cell, the detection and data acquisition system, the calibration procedures and the data analysis software.

3.2 Laser systems

Two laser systems were used in the spontaneous Raman scattering experiments. A short-pulse CO_2 laser system (Fig. 3.2) serves as the pump laser, and a frequency-doubled ruby laser is used as the Raman probe laser. The CO_2 laser pulse originates in the 241-cm long cavity of a hybrid CO_2 laser, with a 62-MHz longitudinal mode spacing. The cavity consists of a transversely excited atmospheric-pressure (TEA) section and a low pressure

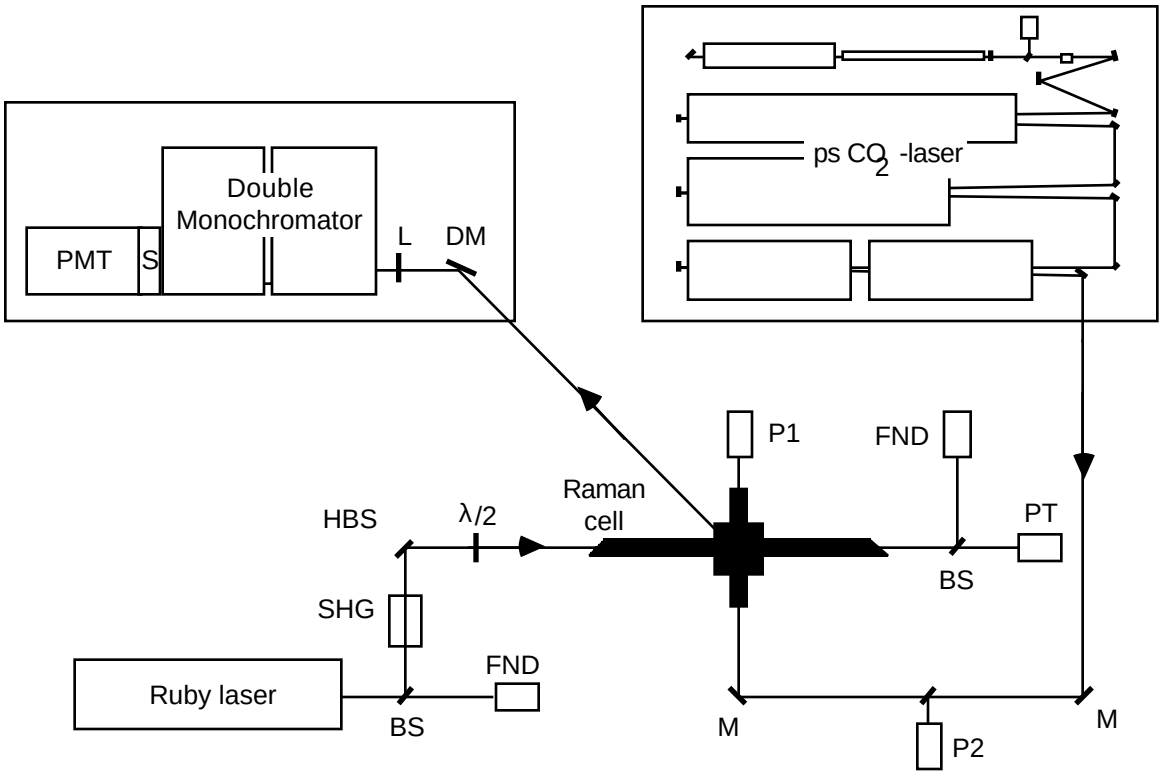

FIG. 3.1. Setup for measuring the spontaneous Raman scattering from infrared multiphoton excited molecules at low densities. Molecules excited by a CO_2-laser are probed by the second harmonic of a Ruby laser. BS = beam splitter, SHG = second harmonic generator, HBS = harmonic beamsplitter, $\lambda/2$ = half waveplate, FND = fast photodiode, PT = phototube, P1, P2 = pyroelectric detector, M = mirror, DM = dichroic mirror, L = quartz lens, S = shutter, PMT = photomultiplier tube. The detection (monochromator, photomultiplier, etc.) is located in a light-tight enclosure located directly above the Raman cell. Drawing not to scale.

(500 Pa) continuous wave (CW) discharge cell. Since the TEA section, a grating-tuned Taschisto Model 215 CO_2 laser head, has a 3.6-GHz bandwidth the laser can oscillate on many modes simultaneously. The low pressure section, which has a 55-MHz bandwidth, increases the laser gain of only one longitudinal mode, so that lasing will only occur on that single longitudinal mode.[1]

The 100-ns single-mode output pulses from this hybrid laser are truncated by a self-triggered plasma shutter.[2,3] The truncated pulses have a slow rise time—identical to the rise time of the 100-ns pulses—and an ultrashort fall time of about 10 ps. The pulses are further shortened by optical free induction decay (OFID) in a 4-m long low-pressure CO_2-cell.[4] The output pulse duration can be varied continuously from 30 to 250 ps by adjusting the pressure in the cell from 30 kPa to 4 kPa. The peak power of the short pulse is equal to that of the input pulse, while the total energy is decreased by the ratio of the duration of output and input pulses.

One Lumonics model 103 laser amplifier operating at atmospheric pressure and two 10-atm Lumonics model 280 amplifiers are used to increase the energy of the short laser pulse. The atmospheric pressure amplifier, which has the smallest bandwidth, limits the pulse duration to 500 ps. With the high pressure amplifiers, which have a much larger bandwidth, pulses as short as 50 ps can be amplified without significant stretching. The output beam is focused into the scattering cell by a cylindrical lens. Depending on the optical arrangement used, the beam waist is 2.2×0.18 mm or 6×0.35 mm. The average output energy is 100 mJ.

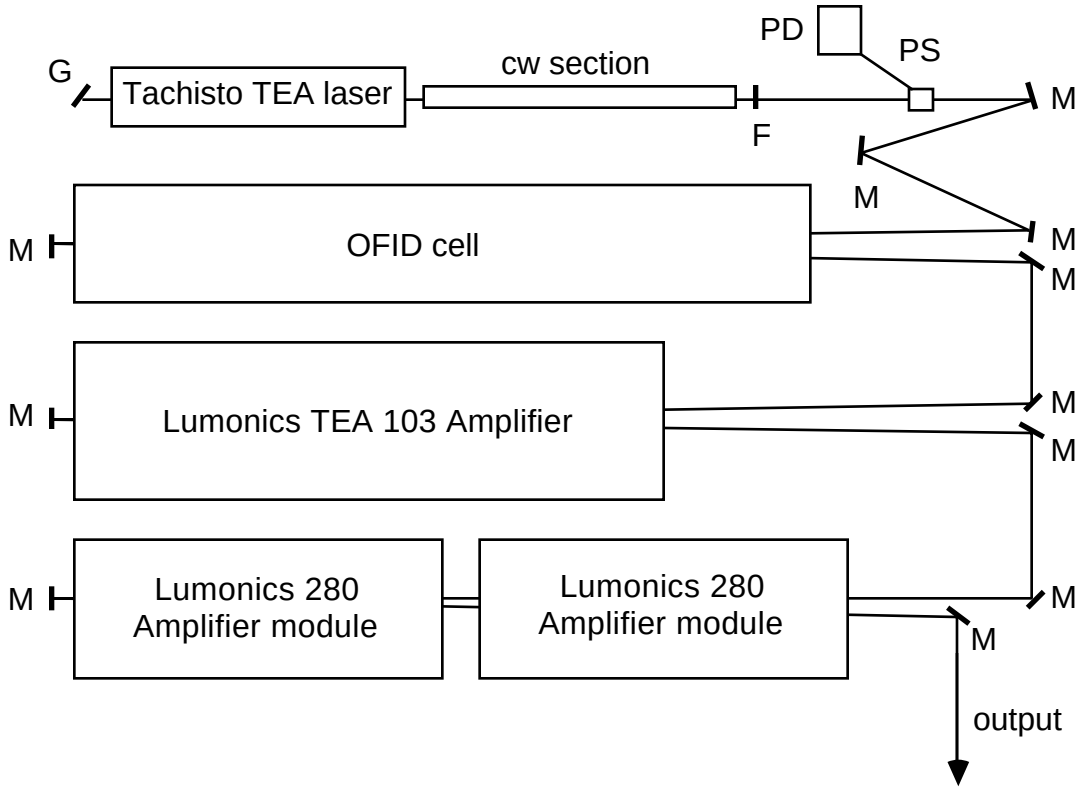

Fig. 3.2. The short-pulse CO_2 laser system used for the infrared multiphoton excitation of polyatomic molecules. G = grating, F = output coupler, S = beam splitter, PD = plasma detector, PS = plasma shutter, M = mirror.

The probe beam is generated by a frequency-doubled Raytheon model SS-420 *Q*-switched ruby laser. The second harmonic at 347.15 nm is vertically polarized, *i.e.* in the direction of detection. A half-wave plate rotates the polarization by 90° into the plane of the two laser beams to obtain a maximum cross-section for Raman scattering, see Eq. (2.7).

The beam is focused into the scattering region, where it crosses the infrared laser beam. The beam waist at the focal point is 500 μm, and the average probe pulse energy is 5 mJ.

3.3 Plasma detector

To avoid collisional effects in our experiment, it is very important that the duration of the CO_2 laser pulses is much shorter than the mean free time of the sample gas. Therefore, one has to make sure that the plasma shutter, the key device for generating short CO_2 laser pulses, fires properly every time the laser fires. A plasma detector (see Fig. 3.3) was constructed to monitor the operation of the plasma shutter.

Briefly, the operation of the detector is as follows. When a plasma is generated by the strong CO_2 laser radiation, the electric conductance between two electrodes placed across the plasma drops to zero. The output of a comparator, which monitors the electric conductance, is latched by a one shot circuit, and passed to the data acquisition system to flag the proper firing of the plasma shutter. Unflagged data can then be rejected by the computer system.

3.4 Raman cell

The Raman cell, in which the exciting and probing laser beams cross at right angles, is shown in Figs. 3.4 and 3.5. It consists of a cube-shaped aluminum body with two pairs of arms of circular cross-section. The arms for the exciting infrared beam are 0.15 m long, the ones for the probing ultraviolet beam 0.3 m. In order to minimize stray light from the windows the long arms have quartz windows at Brewster angle. In addition,

each of these arms contains six pairs of straight (see Fig. 3.5, D1) and conical (D2) baffles. The straight baffles collimate and restrict the probe beam, while the conical baffles trap any

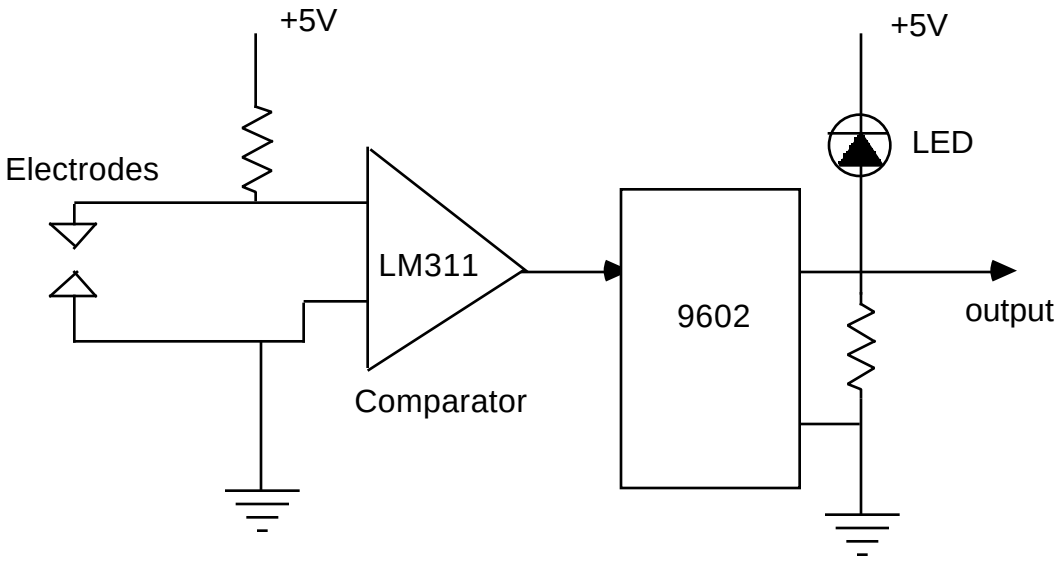

Fig. 3.3. Circuit diagram of the plasma detector.

light scattered along the path of the beam. The baffles are made separately from the arms and are installed by sliding them into the arms, so that they can be arranged in various configurations. Best results were obtained with apertures increasing from 2 mm nearest to the windows to 4 mm nearest to the center of the cell. In the center part of the cell, a vertical stray-light jacket (J) of circular cross-section prevents any light scattered by the last baffle from reaching the detection aperture directly. It has two 6-mm holes for the probe

beam and two 15-mm holes for the infrared beam. Light scattered at the intersection of the two beams is collected over a solid angle of $\pi/16$ sr and collimated by a quartz lens (L) that serves as a window. The focus of this lens coincides with the intersection of the two beams. All parts of the cell are vapor blasted and black anodized to absorb as much stray light as possible. A gas inlet on the bottom plate connects the cell to a gas-handling and vacuum system.

To simplify the alignment of the laser beams, the cell is mounted on four tightly fitting posts (P) shown in Fig. 3.6. It can easily be removed and put back accurately by lifting a black nylon shaft (S) through which the collimated scattered light reaches the detection. To align the pump and probe laser beams, the pulsed probe beam is first aligned through the cell. Then the cell is removed and the infrared beam is adjusted until the two beams produce overlapping burnspots on a piece of thermosensitive paper.

3.5 Detection

The scattered light is detected in a light-tight enclosure on a raised platform above the scattering cell, see Figs. 3.1 and 3.6. The scattered light that exits the cell consists of Stokes and anti-Stokes Raman signals, Rayleigh scattering and stray light. A dichroic mirror and a quartz lens image the scattering region onto the entrance slit of a tandem Jarrel-Ash 0.25-m Ebert-type monochromator with 2400-grooves/mm gratings. The linear dispersion of the system is 1.65 nm/mm. Most measurements were carried out at a resolution of 3 nm, enough to prevent elastically scattered light from reaching the detector. The imaging ratio of the detection lenses is 2:1, so that the 6×2 mm entrance slit of the monochromator corresponds to a 3×1 mm area of the scattering region. Additional spatial

filtering between the two monochromators further reduces stray light. The total throughput of the two monochromators is about 4%. The output of the monochromator is detected with an Amperex XP2020Q photomultiplier tube (1-ns time resolution, 1.5-kHz dark count rate, 25% quantum efficiency). A mechanical shutter (S) protects the tube when the detection box is opened.

The overall signal-to-noise ratio of cell and detection is excellent. Even though single photons are detected for each laser pulse, the measurements can be performed in daylight or with room lights on. The amount of ambient light that reaches the photomultiplier after the spatial and spectral filtering is well below the 1.5-kHz dark count rate of the photomultiplier tube, and therefore entirely negligible.

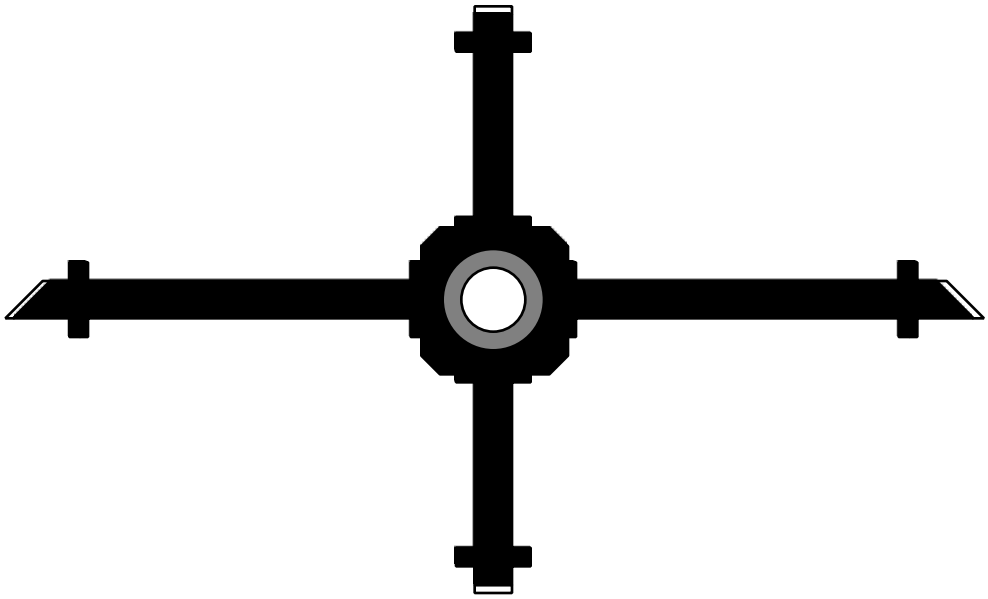

FIG. 3.4. Top view of the low pressure Raman cell. The CO_2-laser beam (pump) enters through the short arms, while the probing UV beam enters through the long arms. Scattered light exits through a collimating lens at the top.

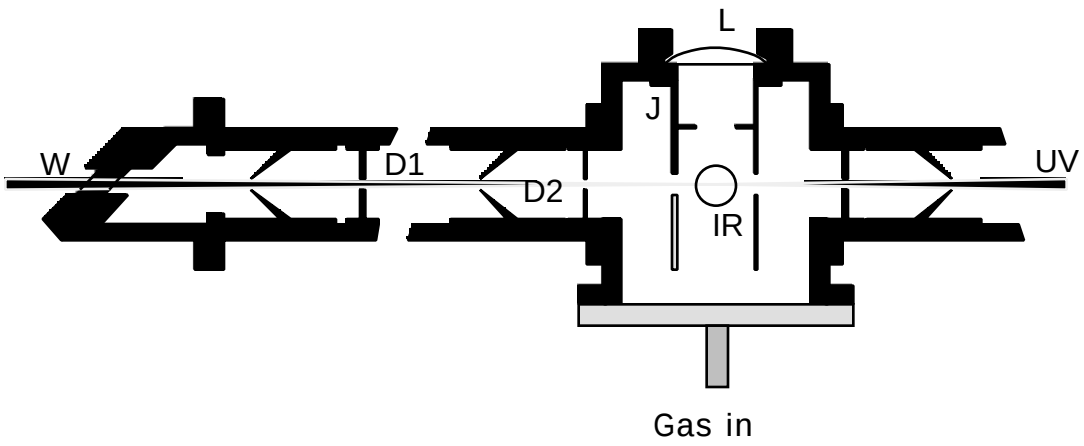

Fig. 3.5. Cross-sectional view of the Raman cell. W = quartz window, D1, D2 = straight and conical baffles, J = stray light jacket, IR = position of IR pump beam, UV = probing UV beam, L = collimating lens. The window holder has been rotated by 90° to show the Brewster angle mounting.

In addition to the Raman signals, the following signals are measured during an experimental run:

1. The energy of the infrared pump pulse, detected by a Molectron P1-15 pyroelectric detector.
2. The energy of the probe ultraviolet pulse, detected by a Hamamatsu phototube.
3. The time-delay between the pump pulse and the probe pulse. The time of arrival of the infrared pulse is monitored by a Molectron P1-10 fast pyroelectric detector and the arrival of the ultraviolet pulse is monitored by a EG&G FND

100 photodiode. The delay time between the two pulses is measured by a EG&G Ortec 457 time-to-pulse-height converter.

4. The output energy of the ruby laser, detected by a EG&G FND 100 photodiode. By comparing the output of the ruby laser with the energy of the ultraviolet pulse, the efficiency of the RDA frequency doubling crystal can be monitored.

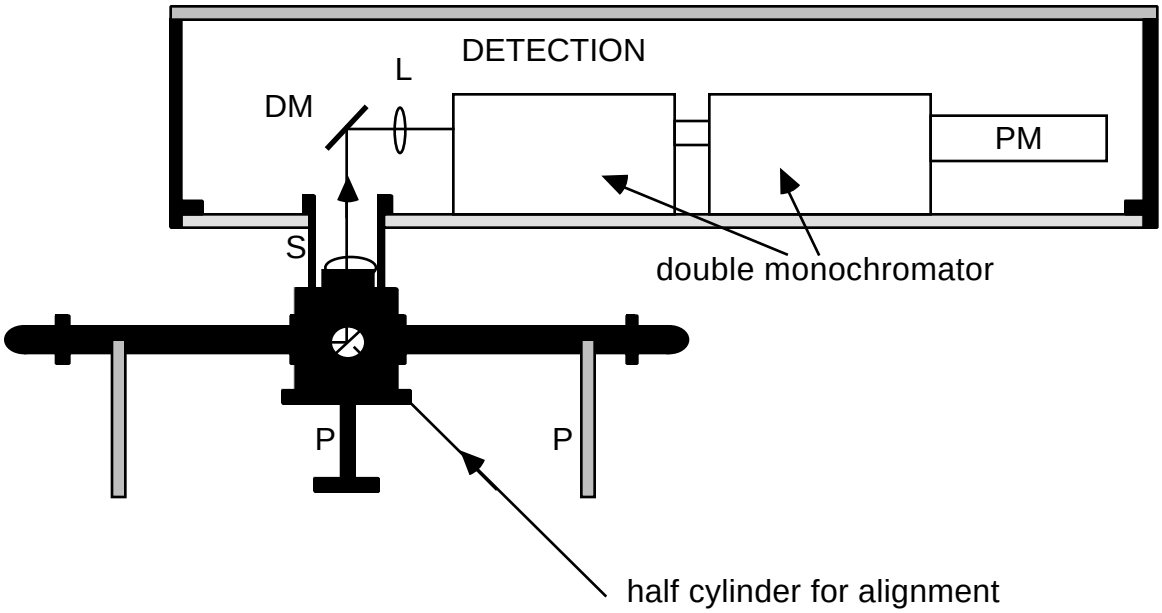

Fig. 3.6. Detection of Raman signals. The cell is mounted on four posts, P, from which it can easily be removed by lifting the light shaft, S, through which the scattered light reaches the detection hardware. DM = dichroic mirror, L = quartz lens, PM = photomultiplier

5. The output of the plasma detector. The circuit and function of the plasma detector were discussed above.
6. The output of the fluorescence detector. The circuit and function of the fluorescence detector are discussed in chapter 6.

All signals are displayed on a computer terminal during the measurements, so that online diagnosis and adjustments can be made.

3.6 Alignment

Spontaneous Raman scattering is a weak process: in our setup, at sample gas pressures of 130 Pa (1 Torr), the signal level drops into the photon counting regime. Aligning such a small signal is difficult. The Raman photons of interest are emitted from the center of the Raman cell where the two laser beams cross each other. To align the detection, a white teflon half cylinder is placed in the center of the Raman cell with its axis parallel to the CO_2 laser beam and its flat side tilted 45° with respect to the ruby laser beam. Then, a He-Ne laser is aligned along the path of the ruby laser. The He-Ne light scattered by the teflon can then be used to align the optical path of the detection system, i.e. the collecting lens, the monochromators and the photomultiplier.

3.7 Data Acquisition

The data acquisition system consists of an optically-isolated laser control trigger module, 10 pulse integrators, 10 sample-and-hold circuits, a 4-channel EG&G Ortec model 934 constant-fraction discriminator, an EG&G Ortec model 457 time-to-pulse-height converter, a Gould Biomation 8100 transient waveform digitizer with a Standard Engineering model GIO-816 CAMAC input/output register and interface, a Kinetic Systems model 3531 multiplexer, a Kinetic Systems model 3553-Z1C 12-bit analog-to-digital converter, a Kinetic Systems model 3988-G2A GPIB CAMAC crate controller and a DEC Pro 350 computer (see Fig. 3.7).

The home-built laser trigger module controls the timing sequence of the firing of the CO_2 laser, and the flash and *Q*-switch of the ruby laser. The trigger circuits are optically isolated to prevent radio-frequency interference from the laser-firing on the data acquisition.

Synchronization of the two lasers is achieved by adjusting the time delay between the CO_2 laser and the ruby laser *Q*-switch triggers.

After triggering the lasers, the multiplexer sequentially scans the outputs of the sample-and-hold circuits to the 12-bit analog-to-digital converter, which is then read by the computer. To correct for the output offset, the output of the integrators are sampled twice in each data-acquisition cycle, once 180 ms before and once immediately after the lasers fire. The computer then takes the difference of the two readouts. Because of this, the system is insensitive to possible base line drifts during long measurements.

To minimize the effect of dark counts on the small Raman signals, the high-gain photomultiplier output must be measured only during the probe pulse. Therefore it is integrated by a pulse integrator with a decay time much shorter than the inverse of the dark count rate, and then recorded by the transient waveform digitizer. Since the digitizer has a 10-ns resolution, the recording window can be chosen narrow enough to gate out the dark counts. In other words, the recording window is chosen so narrow that the probability of recording a dark count is negligible. Narrowing the window does not affect the measurement of the Raman signals as long as the width of the window is larger than the rise time of the integrator. In our setup, it was set to 1 μs. The recorded waveform is read out by the computer in the second half of the data acquisition cycle through the GIO-816 CAMAC input/output register and interface. The short decay time of the integrator will not affect the accuracy of the measurement, provided that it also is much longer than the probe pulse. The decay time-constant of the pulse-integrator was chosen to be 10 μs. For the other channels, where dark count is not a problem, the decay time-constant was set to 10 ms, much longer than the 6-μs tracking time required by the sample-and-hold circuits.

The time delay between the pump and the probe pulse is recorded by an EG&G Ortec 457 time-to-pulse-height converter. The output pulses from a pyroelectric detector (for the infrared pulse) and FND 100 photodiode (for the ultraviolet pulse) are first processed by an EG&G Ortec 934 constant fraction discriminator so that the timing of the pulses does not vary with the pulse height. Without this process, stronger pulses will trigger the time-to-pulse-height converter earlier than weaker pulses, because the triggering threshold is reached earlier.

The digitized data from all channels are transmitted to the computer via an IEEE-488 interface bus. Data are stored on a hard disk for later analysis. All data of each data-acquisition cycle are displayed on the computer screen. This allows adjustments to be made during the measurements.

3.8 Calibration

For performing quantitative measurements it is necessary to carefully calibrate all measured quantities. Calibrations were therefore carried out before each individual measurement to account for possible drifts or changes in the alignment. Calibration of the ultraviolet phototube, which measures the Raman probe beam energy, is carried out with a Molectron J3-05DW calibrated pyroelectric detector. During a calibration run, the output of both phototube and pyroelectric detector are recorded by the computer, while the laser output is varied manually. After the calibration run, a computer procedure is used to calibrate the computer reading of the phototube. Calibration of infrared pumping energy is

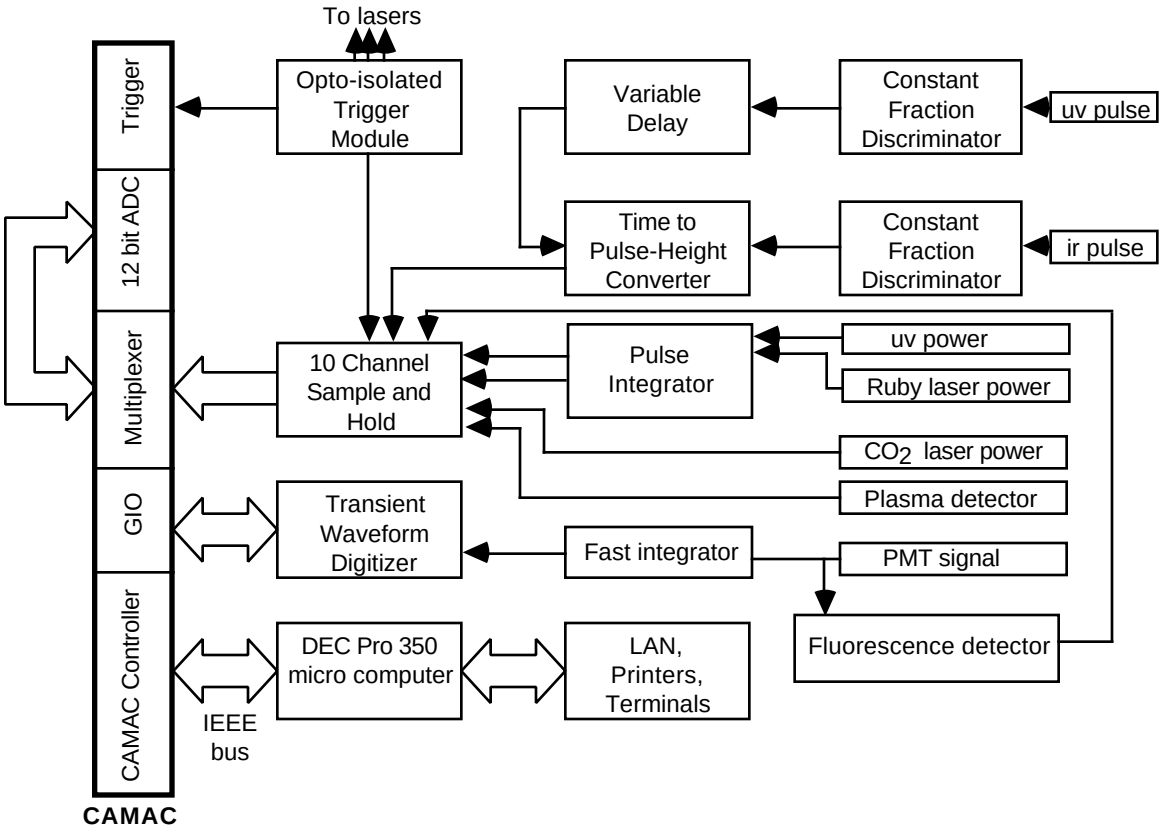

Fig. 3.7. Schematic diagram of the computer controlled multichannel data-acquisition system.

done in a similar way with a Scientech 365 Joule meter. A typical calibration result is shown in Fig. 3.8.

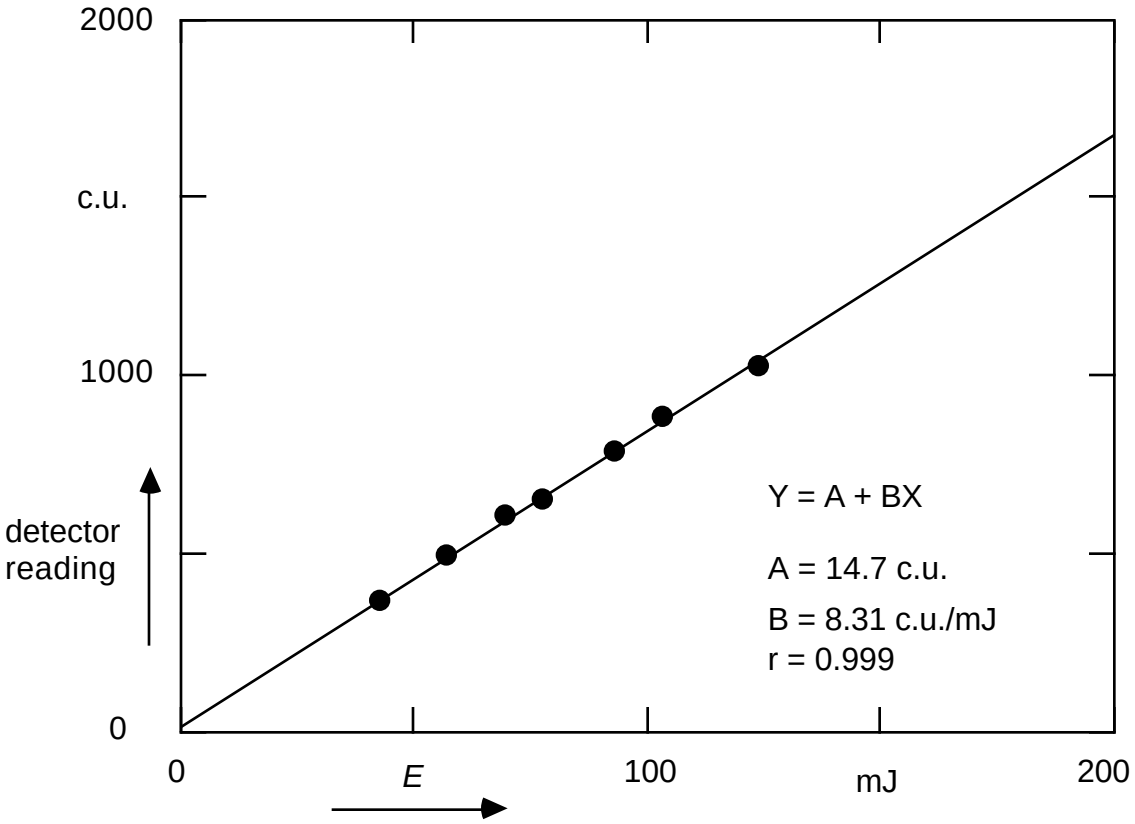

Fig. 3.8. Calibration of the infrared detector. The vertical axis is the computer reading of the pyroelectric detector output in uncalibrated "computer units" (c.u.), and the horizontal axis the readout of the Scientech 365 Joule meter. In the graph, "r = 0.999" indicates that the correlation between the two quantities is 0.999.

Beam profile calibration is done with a 10-μm pinhole and a pyroelectric detector mounted on a micrometer-driven two-dimensional translation stage. During calibration, the pinhole scans through the beam profile. Typically, 10 points are measured along the beam

profile, and for each point about 10 laser shots are averaged. For each shot, in addition, the readout is normalized with the pulse energy to eliminate the effect of laser intensity fluctuations. The beam profiles obtained in this way are fitted with Gaussian curves. Their width, together with the calibrated pulse energy, can then be used to calculate the fluence (average energy per unit area) of the laser beams. A typical beam profile calibration is shown in Fig. 3.9.

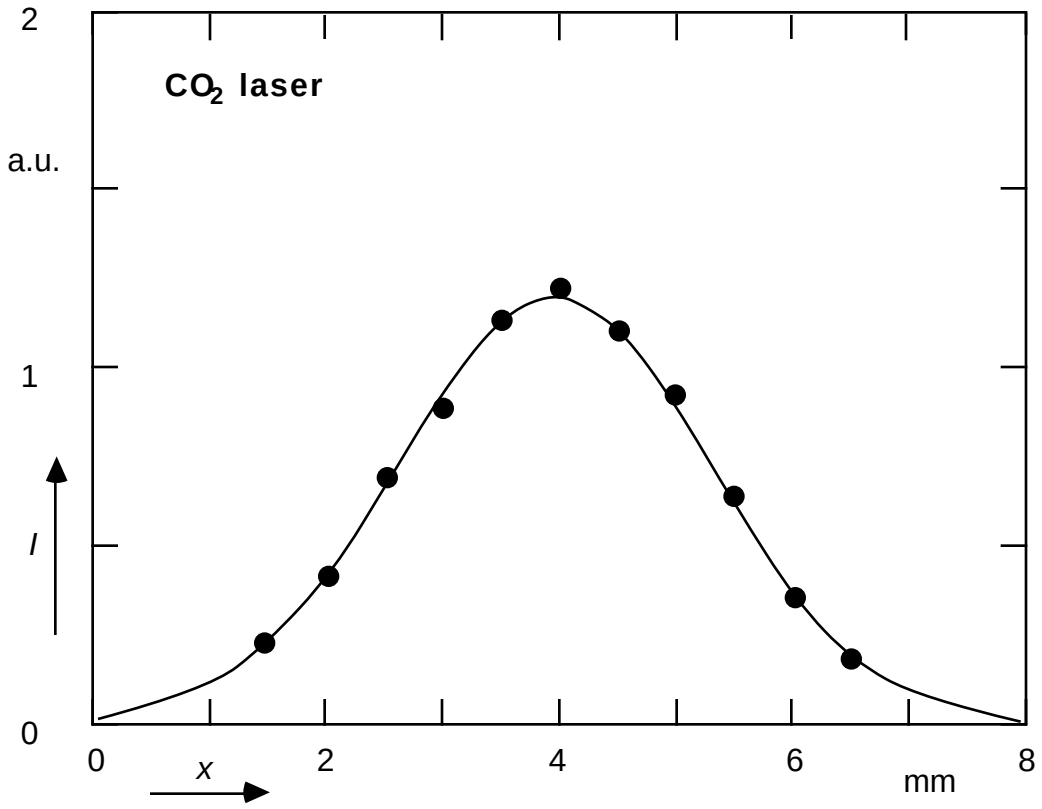

Fig. 3.9. Horizontal beam profile of the CO_2 laser. Each data point in the graph is the average of 10 shots.

Because of the intramolecular energy transfer, the recorded Raman intensities depend not only on the intensity of the Raman probe beam, but also on the infrared pump energy. The measured signal is thus a convolution of the two beam profiles, and therefore the beam profile calibration is also needed for the deconvolution of the Raman signals.

Since the quantity of interested is the ratio of anti-Stokes signal to room-temperature Stokes signal (see Eq. (2.15) in chapter 2), there is no need to calibrate the Raman signals. This makes our measurements insensitive to possible long term drifts in the gain of the photomultiplier tube or drifts in the signal alignment. For absolute measurements, one would need to calibrate the detection system in addition to the calibrations mentioned above.

3.9 Data analysis

Due to the low signal level, a large number of data must be averaged to obtain a satisfactory signal-to-noise ratio. Fluctuations in laser power and laser timing, however, make it necessary to first collect and sort out the data. During the experiment, eight data channels are recorded by the computer. Five of these, the ultraviolet Raman probe intensity, the infrared pumping intensity, the time delay between pump and probe, the intensity of the Raman signal, and the monochromator wavelength reading are necessary for data analysis, while the other three, the ruby laser energy, the plasma detector signal and the fluorescence detector signal (see chapter 6) are used for diagnosis and data rejection. The data analysis procedure consists of four stages: rejection, normalization, sorting and averaging.

During data rejection the following shots are rejected. Shots where either the time delay between the two laser pulses or the CO_2 laser intensity lies outside the range of interest due to fluctuation, shots where the plasma shutter did not fire correctly, or shots where fluorescence was detected (see chapter 6). These rejected shots result from

inevitable laser fluctuation or other stochastic processes which are irrelevant to our measurement.

Next, since the Raman scattering intensity is proportional to the energy of the probe pulse, the Raman signals are divided by the probe pulse energy. After this normalization, the data are sorted and averaged according to the energy of the infrared pulse, to obtain the pump fluence dependence. As a result of the central limit theorem,[5] after averaging, the signal-to-noise ratio is inversely proportional to the square root of the number of shots in each fluence slot. Therefore, the wider the slots for sorting and averaging, the better the signal to noise ratio. This, of course, is at the expense of the number of points on of the fluence axis. Typically 10,000 raw data points are needed to plot 10 data points with a 10% error bar.

For each measurement, the infrared pumping fluence dependence is always analyzed first within a fixed time delay range. The Raman signal can then be normalized with the analyzed fluence dependence, to eliminate the effect of CO_2 laser fluctuations. Finally the Raman data can be analyzed as a function of other parameters such as time-delay, wavelength, sample gas pressure etc.

The data analysis procedure explained above cannot be done without advanced computer programming. For each measurement of 10,000 shots, 80,000 floating point numbers are recorded. The data analysis program not only has to deal with a large amount of data and long calculations, but also with a large number of data analysis options. A program that integrates the four stages mentioned above including graphic display of the data was developed to minimize the turn-around time of the data analysis. The interprocess communication feature of the UNIX operating system was employed for maximum efficiency, and to allow great flexibility in entering data-analysis options, such as

normalization schemes and data rejection criteria. The program allows arbitrary user-defined mathematical and statistical operations on the data. A partial source code listing of the data-analysis programs and interprocess communication routines can be found in Appendix B.

3.10 Choice of molecular systems

To find suitable molecular systems for the present experiment, certain conditions have to be satisfied. First of all, the molecule must have a strong infrared active mode in resonance with the CO_2 laser. Because of the low efficiency of the free induction decay cell, the resonant frequency must correspond to those CO_2-laser lines that have strong enough oscillator strength. Secondly, the molecule must be able to absorb a large number of infrared photons before dissociating. If the molecule dissociates, laser-induced fluorescence signals from the dissociation fragments may mask the much weaker Raman signals. Thirdly, the molecule must have at least one (and preferably more) Raman active mode which is strong enough to be detected at low pressure. Fourth, the molecule must not generate laser-induced fluorescence in ground state. These four conditions limit the number of candidate molecules. Four molecules, which satisfy these conditions, SF_6, CF_2Cl_2, CH_3CHF_2 and CF_2HCl, were selected for the experiment.

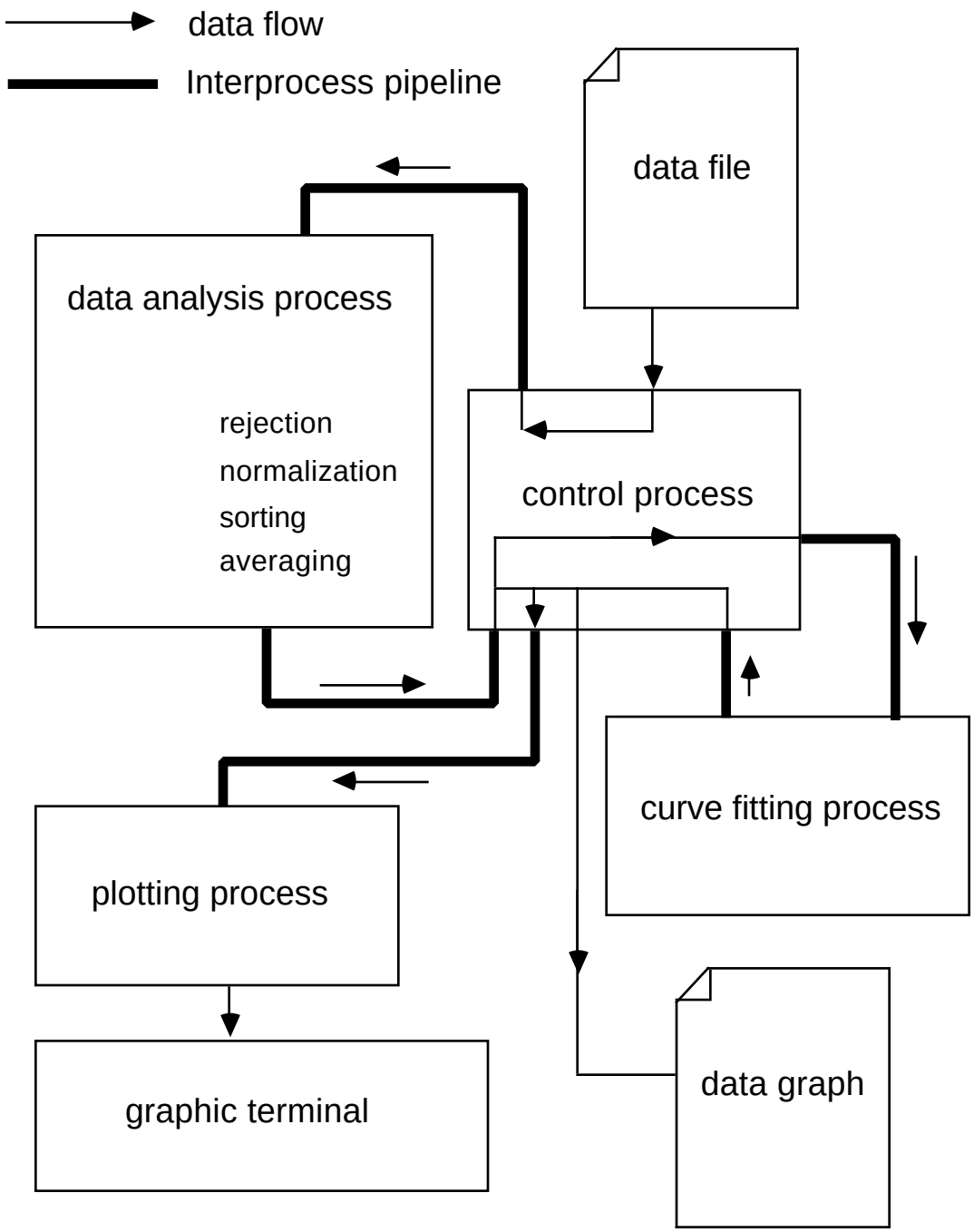
data flow
Interprocess pipeline
data file
data analysis process
rejection
normalization
sorting
averaging
control process
curve fitting process
plotting process
graphic terminal
data graph

Fig. 3.10. Flow chart of data analysis program.

References

1 A. Gondhalekar, N.R. Heckenberg, and E. Holzhauer, IEEE J. Quantum. Electron. **QE-11**, 103 (1975)

2 H.S. Kwok, and E. Yablonovitch, Appl. Phys. Lett. **27**, 583 (1975)

3 H.S. Kwok, and E. Yablonovitch, Opt. Comm. **21**, 252 (1977)

4 E. Yablonovitch and J. Goldhar, Appl. Phys. Lett. **25**, 580 (1974)

5 See *e.g.*: W. Feller, *An introduction to Probability Theory and Its Applications* (Wiley, New York, 1971)

CHAPTER 4

TIME RESOLVED SPONTANEOUS RAMAN SCATTERING
PART TWO: SF_6

4.1 Introduction

Sulfur hexafluoride has both a strong infrared absorption mode in the CO_2 laser frequency range and a strong Raman active mode. Spectroscopic data of the vibrational modes of SF_6 are listed in Table 4.1. Unlike other molecules of this size, SF_6 can absorb 40-100 infrared photons before dissociation,[1] making it possible to study highly excited molecules without dissociation.

In our experiments the ν_3 mode of SF_6 was pumped by short CO_2 laser pulses ranging from the P(12) to the P(28) line of the 10.6 μm branch of the CO_2 laser (937 cm^{-1} – 951 cm^{-1}). Raman signals were obtained at a 775 cm^{-1} frequency shift, corresponding to the vibrational frequency of the ν_1 Raman active mode. Two different CO_2 laser pulse durations, 0.5 ns and 15 ns, with fluences up to 7×10^4 J/m^2 were employed to study intensity effects.

Section 4.2 though 4.6 present the experimental results obtained. A full discussion of the results can be found in section 4.7.

Mode	k (cm^{-1})	ν (THz)	symmetry	degeneracy	activity
ν_1	775	23.25	A_{1g}	1	Raman (s)
ν_2	644	19.32	E_g	2	Raman (w)
ν_3	965	28.95	F_{1u}	3	infrared
ν_4	617	18.51	F_{1u}	3	infrared
ν_5	524	15.72	F_{2g}	3	Raman (w)
ν_6	363	10.89	F_{2u}	3	inactive

Table 4.1 Vibrational modes of SF_6, taken from Ref. 2 (s = strong, w = weak).

4.2 Raman spectrum

Figure 4.1 shows the Raman spectrum of SF_6 around the ν_1 symmetric breathing mode with and without infrared pumping on the ν_3 mode. The central peak is due to elastically scattered light. The figure clearly shows that there is no contribution from this elastically scattered light at the position of the Raman lines. The spectral resolution, which is determined by the slit of the monochromator, is 3 nm.

Without infrared pumping, only a Stokes shifted peak is observed. This is because at room temperature less than 3% of the molecules are in excited states of the Raman active mode. With infrared pumping, it is seen that both Stokes and anti-Stokes signals increase. Since the ν_3 and ν_1 modes have opposite symmetry, they do not couple at low excitation. The graph, however, clearly shows that under infrared multiphoton excitation on the ν_3

mode the energy distribution of the Raman active ν_1 mode is changed. The remainder of the experimental results are obtained at fixed frequencies, 356.7 nm and 338 nm for the Stokes and anti-Stokes lines, respectively.

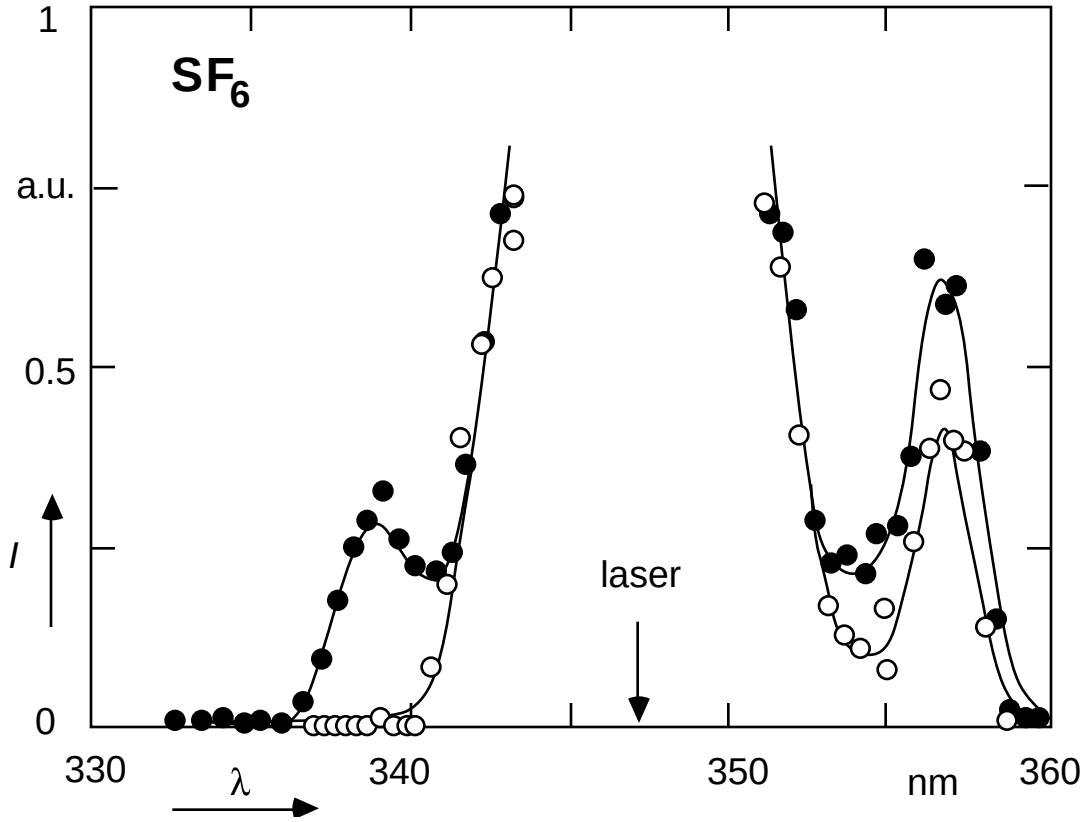

Fig. 4.1. Raman spectrum of SF_6, with (closed symbols) and without (open symbols) infrared multiphoton excitation. Infrared excitation: 10.6 μm P(20) line, 0.5 ns pulse duration, and average fluence 0.6×10^4 J/m^2. The small arrow shows the position of the laser radiation at 347.15 nm.

4.3 Fluence dependence

The infrared fluence dependence of the Stokes and anti-Stokes signal is shown in Figs. 4.2 and 4.3 for different pressures and pulse durations. The results shown were obtained in different runs, each one calibrated individually. The spread in data therefore provides an indication of the absolute accuracy and reproducibility of the experimental data. Figure 4.3 shows that both Stokes and anti-Stokes signals increase by the same amount, in agreement with Eq. (2.13).

4.4 Time dependence

Figure 4.4 shows the increase of both Stokes and anti-Stokes signals as a function of the time delay between the infrared pump and the probe pulse for two infrared pulse durations, 0.5 ns and 15 ns, respectively, at a pressure of 67 Pa and an average infrared fluence of 0.8×10^4 J/m^2. As explained in chapter 2, Raman signals are normalized with the thermal Stokes signal. Negative time delay, $t < 0$, means that the molecules are probed before the infrared multiphoton excitation, *i.e.* the molecules are in thermal equilibrium at room temperature. Within the 20 ns time resolution of the experiment, determined by the duration of the ultraviolet pulse, a *collisionless* (see section 4.5) increase of both Stokes and anti-Stokes signals is observed. The increase is consistent with the result obtained in Eq. (2.13), *i.e.* for each pulse duration both Stokes and anti-Stokes signal increase by the same amount. After the initial increase the signals remain constant, even on a time scale on which collisional vibrational energy relaxation starts to play a role (the vibrational relaxation time constant, $\tau_{V\text{-}V}$, is given by $p\tau_{V\text{-}V} \approx 70$ μsPa).[3] Clearly, collisions do not affect the

total intensity of the anti-Stokes signal, showing that intramolecular equilibrium is reached on a time scale shorter than the time resolution. Since the intensity of the signal is

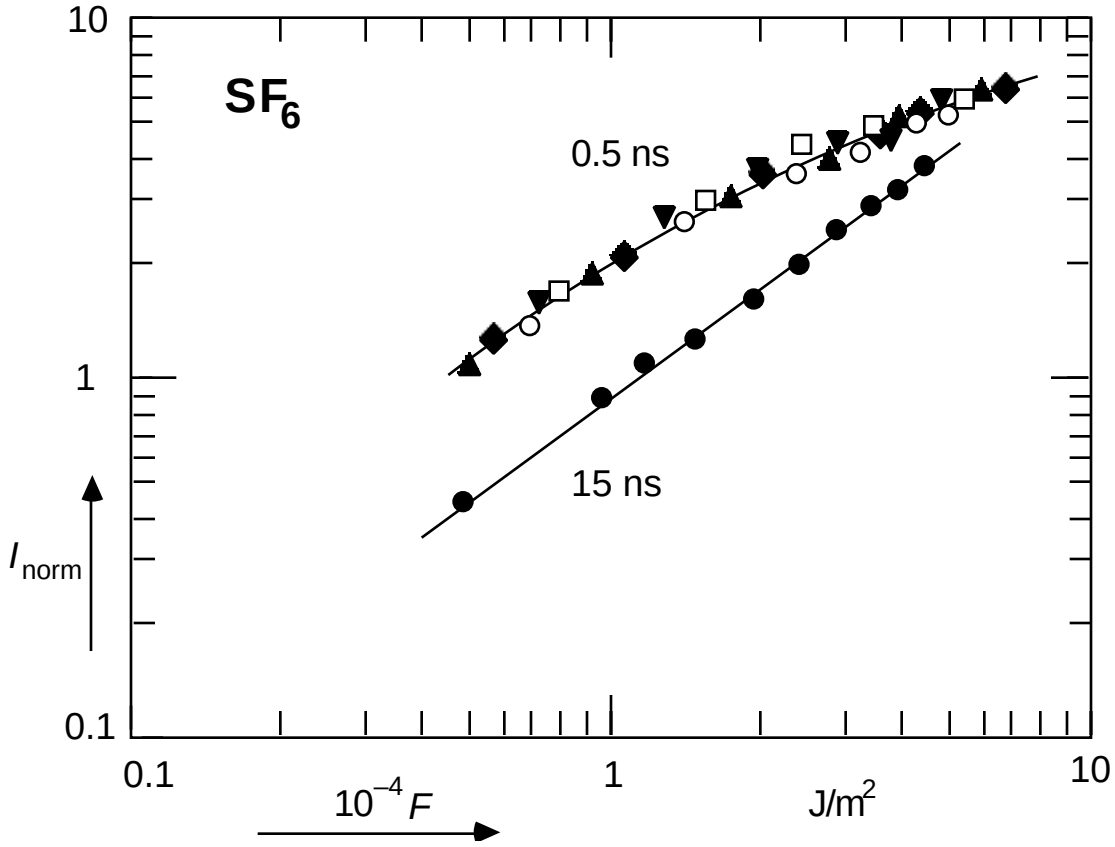

Fig. 4.2. Relative anti-Stokes signal as a function of the infrared pumping fluence for various pressures and two infrared pulse durations at the 10.6 μm P(20) line: 0.5 ns (open symbols) and 15 ns (closed symbols). This graph shows the reproducibility of the data from measurement to measurement. □: 33 Pa; ○: 67 Pa; ▲: 133 Pa; ▼: 200 Pa; ◆: 267 Pa; ●: 133 Pa.

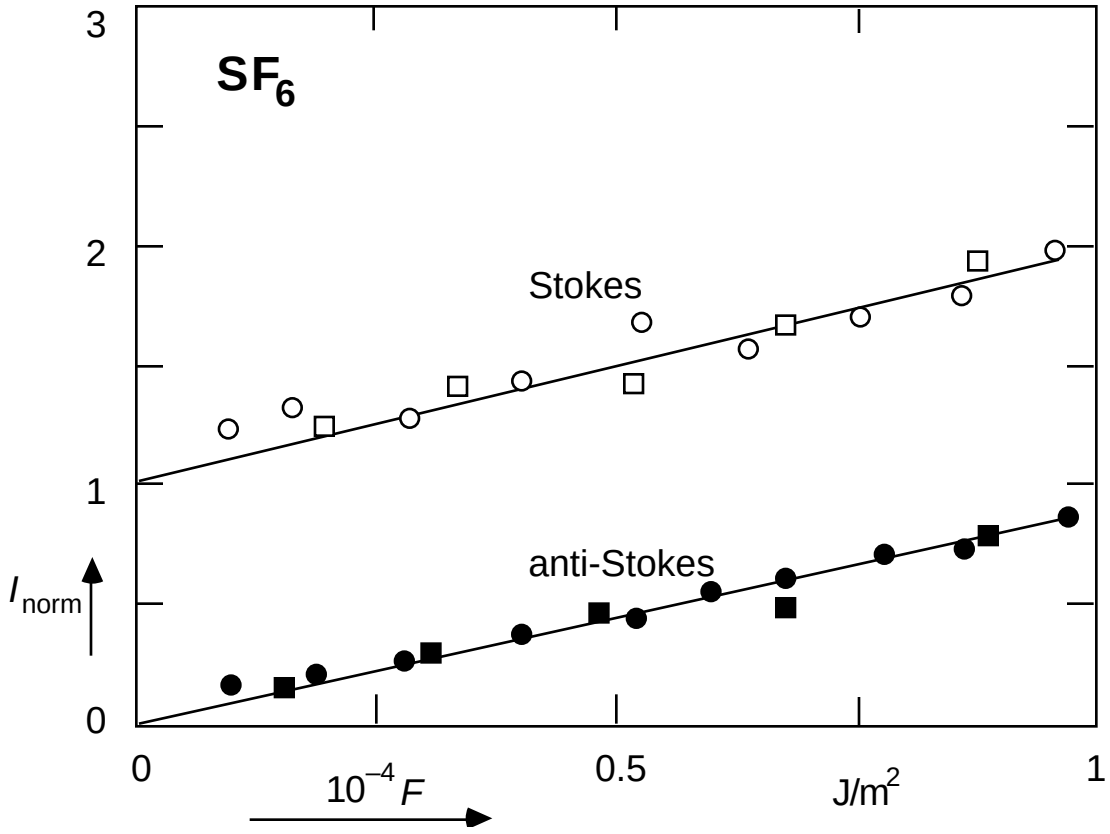

Fig. 4.3. Relative Stokes (open symbols) and anti-Stokes (closed symbols) signal as a function of the infrared pumping fluence at the 10.6 μm P(20) line for 15 ns pulses at two different pressures: p = 27 Pa (squares), and p = 133 Pa (circles).

determined by the average energy in the Raman active mode *only*, intermolecular vibrational-vibrational energy transfer will not affect the Raman signals once intramolecular equilibrium is reached.

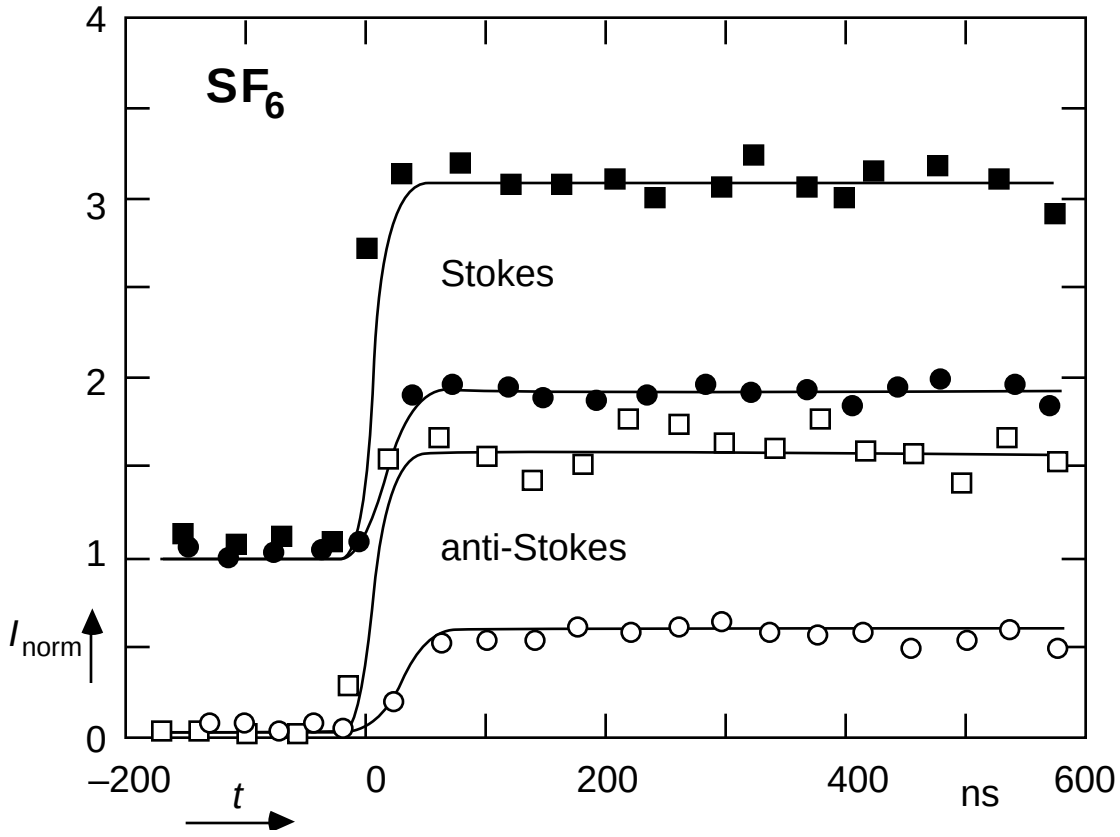

Fig. 4.4. Intensity of Stokes (closed symbols) and anti-Stokes (open symbols) signal as a function of the time delay between pump and probe pulses at a pressure of 67 Pa. The data are normalized to the thermal Stokes signal. Negative time delay means that the signals are measured before the infrared multiphoton excitation. The rise time in the curves reflects the 20 ns FWHM duration of the probe pulse. Results are shown for two different durations, 0.5 ns (squares) and 15 ns (circles). Infrared excitation at the 10.6 μm P(20) line, with an average fluence of 0.8×10^4 J/m^2.

The long-time evolution of the anti-Stokes signal, measured at two different gas pressures, 70 and 270 Pa is shown in Fig. 4.5. The observed decay in the signals is about ten times faster than the relaxation time reported for collisional transfer of vibrational energy to translational degrees of freedom ($p\tau_{V-T} \approx 16\,\mathrm{ms\,Pa}$).[4] Moreover, the low pressure signal decays faster than the high pressure signal, showing the decay is not caused by collisional energy relaxation, but by diffusion of the excited molecules out of the interaction region—a process inversely proportional to pressure. Indeed, the data points obtained at the higher pressure can be made to overlap the low pressure points by scaling the horizontal axis with pressure (see curves in Fig. 4.5).

4.5 Pressure dependence

Figure 4.6 shows the pressure dependence of the Raman signal, obtained by varying the pressure in a single experimental run. Both the anti-Stokes signal from infrared multiphoton excited molecules as well as the thermal Stokes signal from unexcited molecules are shown. The points lie on straight lines, which account for the trivial dependence of the signals on particle density. This figure excludes the possibility that the observed changes in Raman signal are caused by a collisional process, in which case one would see a p^2-dependence.

4.6 CO_2 laser frequency dependence

Figure 4.7 shows the anti-Stokes signal for excitations at different CO_2-lines. Each point shown represents a separate experimental run in which the anti-Stokes signal was measured at a particular laser line. From each of these measurements, carried out with two

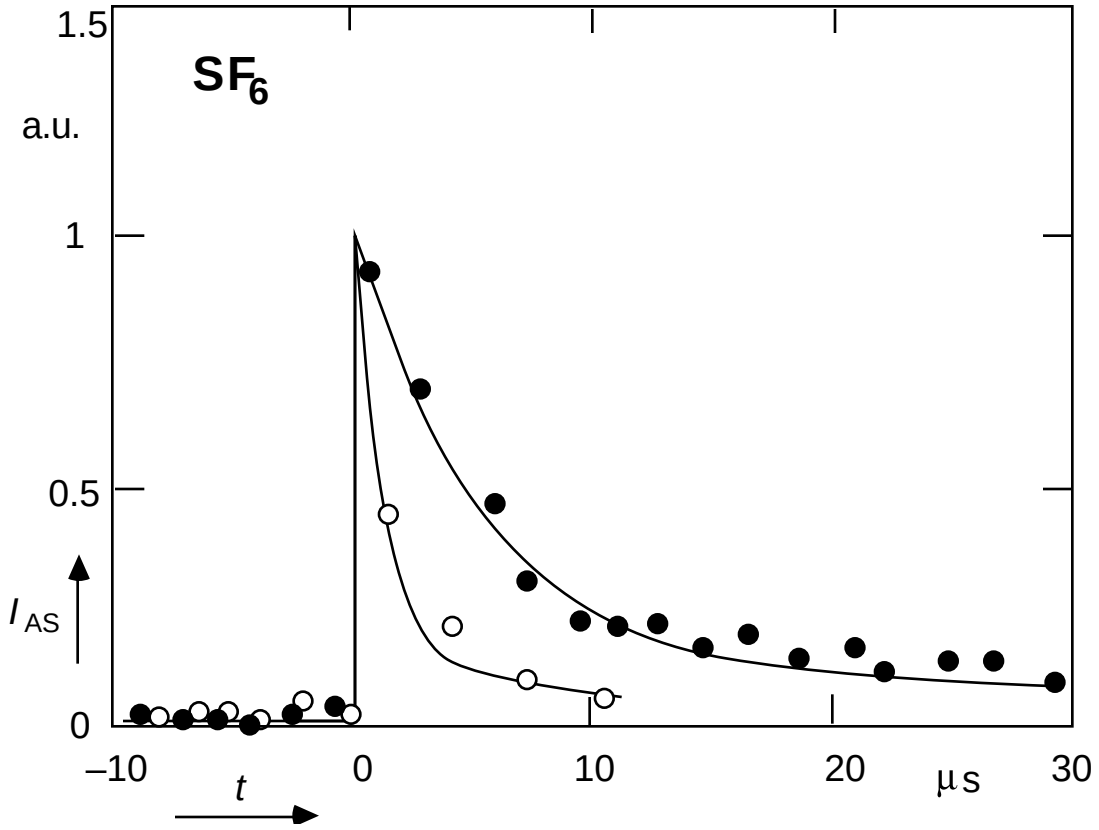

Fig. 4.5. Long time behavior of the anti-Stokes signal for two pressures: p = 70 Pa (open symbols) and p = 270 Pa (closed symbols). The signal is normalized to one at t = 20 ns. Infrared excitation: 10.6μm P(20) line, 0.5 ns pulse duration, and average fluence 10^4 J/m^2. The decay of the curves, which is due to diffusion of the excited molecules out of the interaction region, scales with pressure.

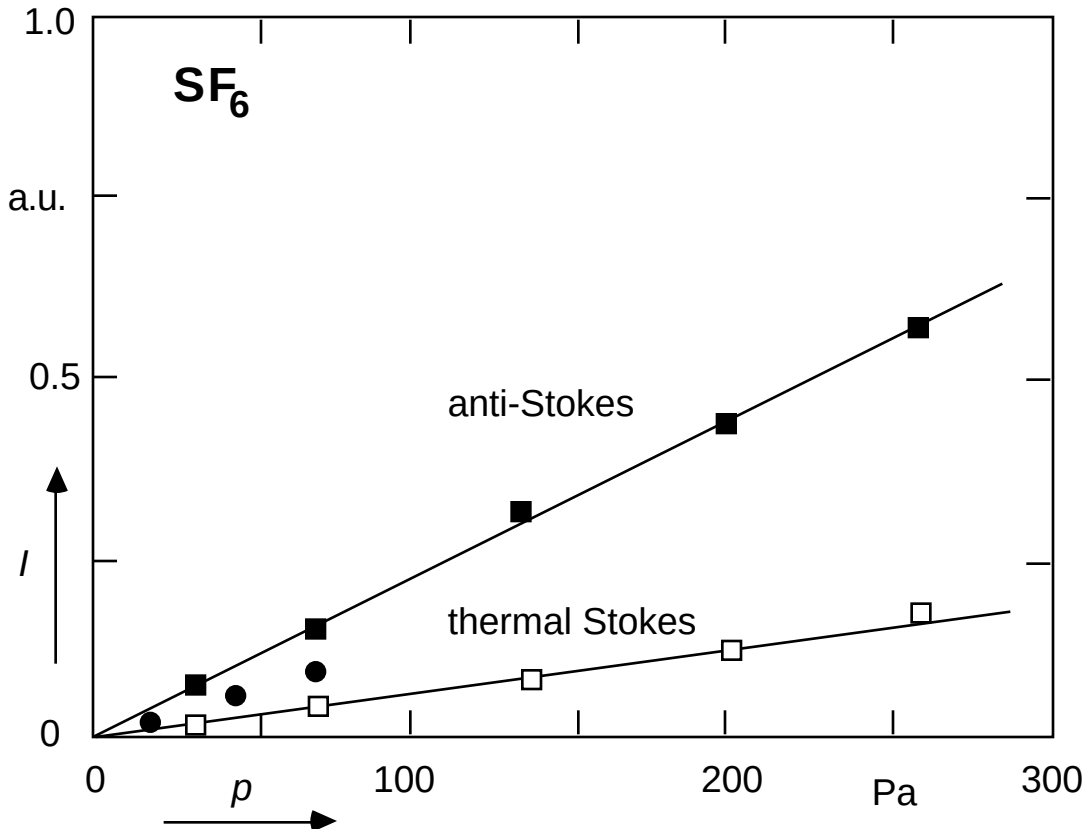

Fig. 4.6. Pressure dependence of anti-Stokes (closed symbols) and thermal Stokes (open symbols) signal. Infrared excitation for anti-Stokes data: 10.6 μm P(20) line, 0.5 ns (squares) and 15 ns (circles) pulse duration, and average fluence 2×10^4 J/m^2.

different pulse durations, the infrared fluence dependence was obtained, yielding graphs similar to Fig. 4.3. One point from each of these fluence dependencies (at a fluence of 10^4 J/m^2) is shown here. As a reference the linear absorption profile of the ν_3 pump mode is also plotted.[5]

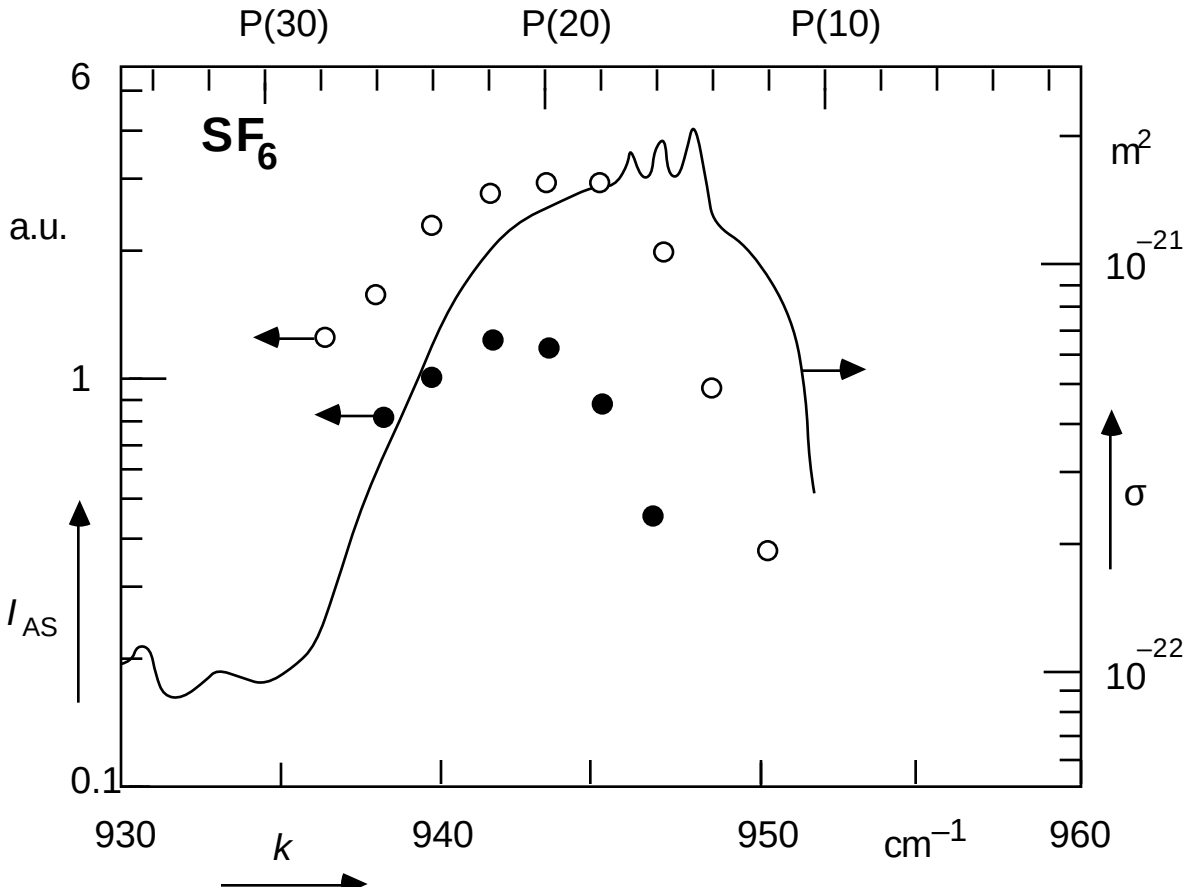

Fig. 4.7. Anti-Stokes signal for excitations at different CO_2-lines. The curve shows the one photon absorption cross section (see scale on the right). A clear red-shift can be observed. Data for two different pulse durations at an average fluence of 10^4 J/m^2 are shown: 0.5 ns (open symbols) and 15 ns (closed symbols). The position of the data points with respect to the right hand vertical scale is arbitrary.

4.7 Discussion

Within the 20 ns time-resolution of the experiment, a collisionless increase of the anti-Stokes signal is observed after excitation. Since the Raman signals remain constant (within the 10% experimental accuracy) for 1 μs after infrared multiphoton excitation, it suggests that intramolecular vibrational energy equilibrium is established within the time-resolution of the experiment. If the energy distribution among the different vibrational modes were not in equilibrium, collisions would alter the energy in the Raman active mode, and consequently change the Raman signal intensity.

Further evidence of an intramolecular equilibrium is obtained by comparing the present results with the results obtained from photoacoustic measurements.[1] Since the Raman signals are proportional to the energy stored in the Raman active mode, the energy can be obtained from the relative increase in anti-Stokes signal,

$$E_R = h\nu_R \, I_{norm} / [1 - \exp(-h\nu_R / kT_o)], \tag{4.1}$$

where I_{norm} is the ratio between the anti-Stokes signal and the Stokes signal at room temperature as defined in Eq. (2.15), k the Boltzmann factor, and T_o room temperature. This equation is obtained by substituding Eq. (2.14) into Eq. (2.15). If one assumes intramolecular equilibrium among the different vibrational modes, the energy distribution of the different modes should correspond to a common temperature. The total increase in vibrational energy of the molecule can thus be calculated from this temperature, and compared to the total absorbed energy, obtained from the photoacoustic measurements. The result of this comparison is shown in Fig. 4.8 and Table 4.2. The average total

energy absorbed per molecule in units of pumping infrared photons is plotted as a function of infrared fluence. The data points are obtained from the current experiments, while the curves show the results of the photoacoustic measurements from Ref. 1. The agreement between the two measurements is remarkable, providing strong evidence for an intramolecular equilibrium.

It should be pointed out that the photoacoustic measurements monitor all molecules absorbing one or more infrared photons, while the Raman measurements only involve the fraction of molecules absorbing enough photons to reach the region where the infrared and Raman active mode couple to each other, a region frequently referred to as the quasicontinuum.[6] Consequently the curve of the Raman experiment should fall off more rapidly for low fluences than the one for the photoacoustic experiment, since the fraction of excited molecules is smaller. This is indeed observed for fluences below 10^4 J/m^2.

Another remarkable feature is that a collisionless increase in anti-Stokes signal within 20 ns can still be observed at infrared fluences as low as 3×10^2 J/m^2,[7] where the average infrared absorption of SF_6 is reported to be below 1 photon per molecule.[1] At these fluences the *inter*molecular vibrational energy distribution—in contrast to the *intra*molecular distribution—is not in equilibrium. Apparently even at low infrared fluence a small but measurable fraction of molecules is excited high enough to show a change in Raman spectrum, while most molecules remain unexcited. Such a bimodal distribution, consisting of some highly excited molecules and the others unexcited, is consistent with a recent observation of two or three photon transitions in a pulse jet of SF_6 at infrared fluences below 2×10^3 J/m^2.[8] At higher fluences direct experimental evidence for a bimodal distribution was obtained from high resolution Raman experiments.[9]

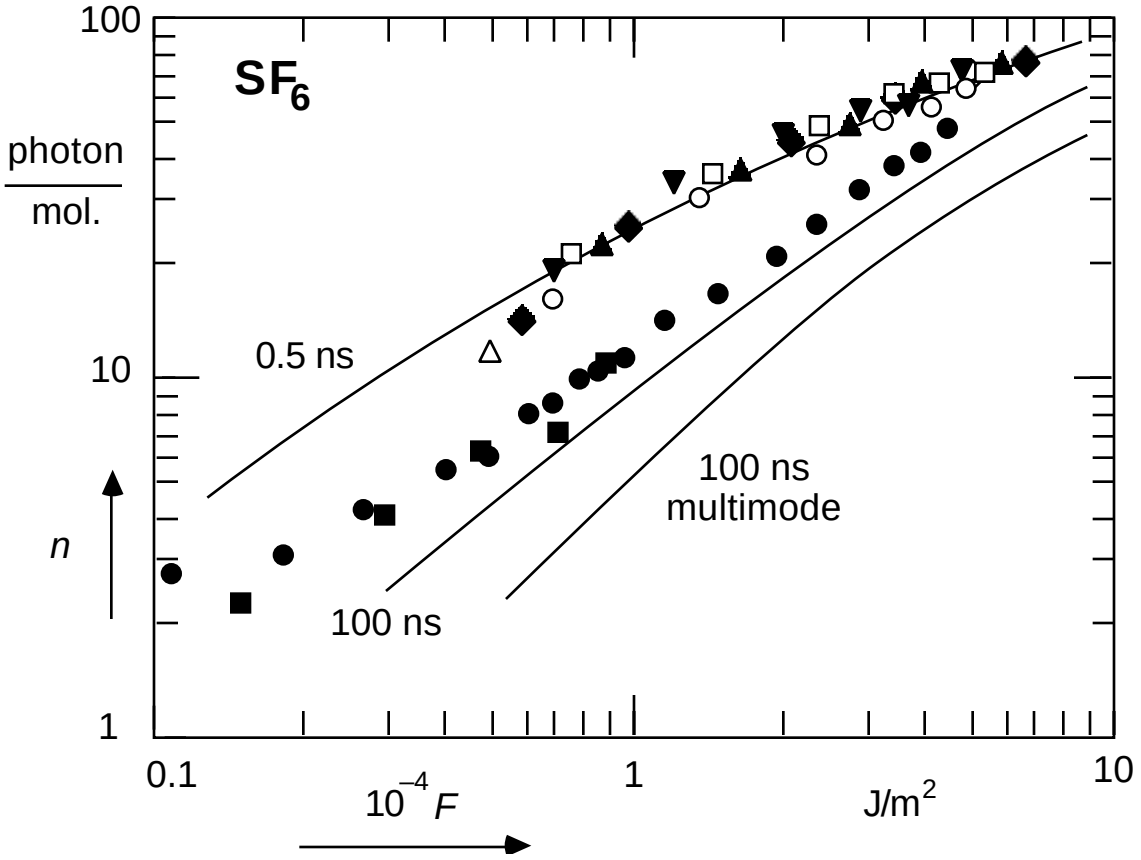

Fig. 4.8. Average number of infrared photons absorbed per molecule as a function of infrared fluence. The data points shown were obtained from the ones shown in Figs. 4.2 and 4.3, assuming thermal equilibrium between all vibrational modes immediately after infrared multiphoton excitation. See those figures for an explanation of the symbols. The solid lines are the average number of infrared photons obtained from the photoacoustic measurements reported in Ref. 1. The results show a remarkable agreement.

F (10^4 J/m^2)	I_{norm}	E_{775} (cm^{-1})	E_{total} (cm^{-1})	E_{PA} (cm^{-1})
0.5	1.1	850	13000	15000
1.0	2.0	1600	23000	23000
2.0	3.3	2700	39000	39000
4.0	5.0	3900	57000	57000
7.0	6.8	5300	78000	78000
0.5	0.44	340	5000	–
1.0	0.9	700	10300	–
2.0	1.8	1400	20600	–
4.0	3.6	2800	41300	–

TABLE 4.2. Relative intensity and vibrational energy of the 775 cm^{-1} vibrational mode, E_{775}, of SF_6 after infrared multiphoton excitation with 0.5 ns (top) and 15 ns (bottom) pulses. The total vibrational energy of the molecules, E_{total}, calculated assuming intramolecular equilibrium, is compared with the result obtained from photoacoustic measurement, E_{PA}.

The fluence dependence in Fig. 4.2 shows that the ratio of the anti-Stokes signals obtained for the 0.5 and 15 ns pulses decreases as the fluence increases. This observation, which is in agreement with the photoacoustic results,[1] shows that in the low fluence range intensity plays a more important role in the infrared multiphoton excitation of SF_6 than in the high fluence range. At low excitation high intensity is needed to overcome the anharmonic shift of the energy levels.[10] In this regime the fraction of molecules excited high enough to show a change in Raman spectrum depends more on intensity than it does the in high fluence range. Once the molecules are excited to a regime where the many intramolecular couplings help excitation, only fluence plays a role. Therefore the increase in anti-Stokes signal, which is a direct consequence of intramolecular couplings, depends also somewhat on intensity in the low fluence regime.

In Fig. 4.7 the dependence of the anti-Stokes signals on the infrared pumping wavelength is shown for both 15 ns and 0.5 ns multiphoton excitation. For comparison, the linear absorption profile of the ν_3 pump mode is also plotted in the graph. Since the total profile is the convolution of the profile for each individual absorption step, it should be narrower than the linear absorption profile. However, this expected narrowing effect seems to be compensated by power broadening and anharmonicity shifts.

Because of the anharmonicity shift of the levels at high excitation, the signals shift toward the red by about 5 cm^{-1} from the center of the linear absorption profile. The present data matches the absorption profiles for SF_6 at a temperature of 450 °K,[11] much lower than the 2800 °K final temperature corresponding to the average absorption of 25 infrared photons per molecule at 10^4 J/m^2.

The results shown in Fig. 4.7 agree with the infrared multiphoton absorption profile[12] and the frequency dependence of the infrared multiphoton dissociation

probability[13,14] for SF_6 reported in the literature. This implies that the anti-Stokes Raman signal is proportional to the total vibrational energy stored in the molecule for all the CO_2-lines within the absorption profile, and not only for the center frequency. Therefore a rapid intramolecular vibrational energy equilibrium appears to be established for collisionless infrared multiphoton excitation at all frequencies that lie within the absorption profile of SF_6.

References

1 J.G. Black, P. Kolodner, M.J. Schultz, E. Yablonovitch, and N. Bloembergen, Phys. Rev. **A19**, 704 (1979)

2 G. Herzberg, *Molecular spectra and molecular structure*, Vol. 2 (Van Nostrand Reinhold, New York, 1979)

3 R.D. Bates Jr., J.T. Knudtson, G.W. Flynn and A.M. Ronn, Chem. Phys. Lett. **8**, 103 (1971)

4 J.I. Steinfeld, I. Burak, D.G. Sutton and A.V. Nowak, J. Chem. Phys. **52**, 5421 (1970)

5 W. Fuss and J. Hartmann, J. Chem. Phys. **70**, 5468 (1979)

6 N. Bloembergen and E. Yablonovitch, Physics Today **5**, 23 (1978)

7 E. Mazur, I. Burak, and N. Bloembergen, Chem. Phys. Lett. **105**, 258 (1984)

8 V.M. Apatin, V.M. Krivtsun, Yu.A. Kuritsyn, G.N. Makarov, and I. Pak, Opt. Comm. **47**, 251 (1983)

9 V.N. Bagratashvili, Yu.G. Vainer, V.S. Doljikov, V.S. Letokhov, A.A. Makarov, L.P. Malyavkin, E.A. Ryabov, and E.G. Sil'kis, Opt. Lett. **6**, 148 (1981)

10 T.B. Simpson, J.G. Black, I. Burak, E. Yablonovitch and N. Bloembergen, *J.* Chem. Phys. **83**, 628 (1985)

11 A.V. Nowak, and J.L. Lyman, J. Quant. Spectrosc. Radiat. Transfer **15**, 945 (1975)

12 D.O. Ham and M. Rothschild, Opt. Lett. **1**, 28 (1977)

13 F. Brunner, T.P. Cotter, K.L. Kompa, and D. Proch, J. Chem. Phys. **67**, 1547 (1977)

14 F. Brunner and D. Proch, J. Chem. Phys. **68**, 4936 (1978);

CHAPTER 5

TIME RESOLVED SPONTANEOUS RAMAN SCATTERING PART THREE: CF_2Cl_2, CH_3CHF_2 AND CF_2HCl

5.1 Introduction

This chapter presents the results of the spontaneous Raman scattering experiments on infrared multiphoton excited CF_2Cl_2, CH_3CHF_2 and CF_2HCl. These three molecules all have three or more Raman active modes that are accessible to our experimental setup. As indicated in Eq. (2.15), this allows direct comparison of the vibrational energy of different modes after infrared multiphoton excitation. Among these three molecules, CF_2Cl_2 was studied most extensively. We will therefore first present the experimental results for CF_2Cl_2 in sections 5.2 through 5.6, then a brief summary of the results on CH_3CHF_2 and CF_2HCl in section 5.7, followed by conclusions.

Freon-12, CF_2Cl_2, is an interesting molecules because three of its nine vibrational modes are accessible to our experimental setup. In addition, two of these three modes can be pumped by a CO_2 laser. This allows one to pump the molecule at two different infrared absorption modes, and also to monitor directly the excitation in the pump mode. In our experiments on CF_2Cl_2, either the ν_8 mode (923 cm^{-1}) or the ν_1 mode (1098 cm^{-1}) was

pumped by short CO_2 laser pulses. At the same time Raman signals of these two modes as well as the signal from the ν_2 mode, were monitored. Spectral data for CF_2Cl_2 are listed in Table 5.1.

All experiments on CF_2Cl_2 were carried out with 15-ns CO_2-laser pulses. Because the CO_2 laser frequencies employed to pump this molecule are away from the peak of the CO_2 laser gain profile, not enough energy was available to perform the experiments with shorter pulses.

Unlike SF_6, where no significant dissociation occurs, for CF_2Cl_2 a fraction of the molecules dissociate at a fluence of 3×10^4 J/m^2. When the CF_2Cl_2 molecules dissociate, the Raman probe beam induces fluorescence from the dissociation fragments. Since the laser induced fluorescence is much stronger the Raman signal, it is important to ensure that this fluorescence signal is not interpreted as a Raman signal. One possibility is to limit the infrared pumping fluence to small enough values so that no dissociation occurs. However, since the probability of dissociation increases with increasing fluence and since the dissociation does not have a sharp threshold, one would have to limit the fluence to no more than 1.5×10^4 J/m^2. At such a low fluence the changes in Raman signal due to infrared excitation are barely observable. To solve this problem, a fluorescence detector that is able to distinguish between Raman signals and laser induced fluorescence was constructed. A detailed description of this device, which was essential for measuring the Raman signals of infrared multiphoton excited CF_2Cl_2, is presented in chapter 6.

5.2 Raman spectrum of CF_2Cl_2

Figure 5.1 shows the Raman spectrum of CF_2Cl_2, obtained with and without

Mode	k (cm^{-1})	symmetry	degeneracy	activity
ν_1	1098	A_1	1	Raman (m) & Infrared (s)
ν_2	667		1	Raman (s) & Infrared (s)
ν_3	457.5		1	Raman (s)
ν_4	261.5		1	Raman (s)
ν_5	322	A_2	1	Raman (w)
ν_6	1167	B_1	1	Raman (w) & Infrared (s)
ν_7	446		1	Infrared (w)
ν_8	923	B_2	1	Raman (w) & Infrared (s)
ν_9	433		1	Raman (m) & Infrared (w)

Table 5.1 Vibrational modes of CF_2Cl_2, taken from Ref. 1
(s = strong, m = medium, w = weak).

infrared pumping on the ν_8 mode. As in the Raman spectrum of SF_6, the large central peak in the spectrum corresponds to elastic scattering. Because of the low population of excited levels at room temperature, only Stokes signals can be detected in the absence of infrared pumping. These room temperature data are shown in the right hand side of the graph; the corresponding anti-Stokes side of the spectrum has been omitted. After excitation large anti-Stokes signals appear. The Stokes and anti-Stokes peaks marked by arrows, at 356.5 nm and 336 nm respectively, correspond to the pumped ν_8 mode. The large difference in the height of the Stokes peaks on the right hand side of the graph reflects the large variation in Raman scattering cross section of the Raman modes. The peak closest

to the central Rayleigh scattering peak, which belongs to the ν_2 mode, has the largest Raman cross section. The smallest peak, marked by an arrow, belongs to the ν_8 mode which is pumped by the CO_2 laser. One can obtain an indication of the average excitation in each mode by comparing the intensity of the anti-Stokes peaks with the intensities of the corresponding Stokes peaks in this graph, as suggested in Eq.(2.15). From such a simple comparison it already becomes clear that the pump mode is much more highly excited than the other modes.

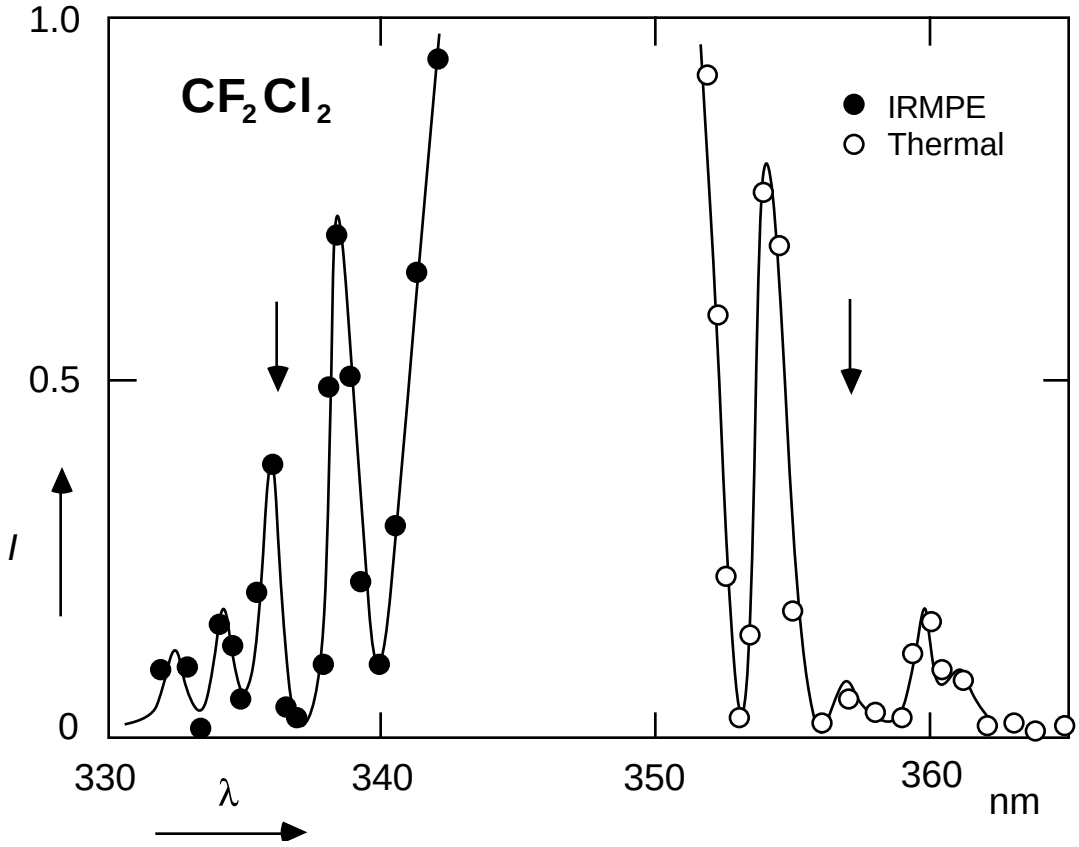

Fig. 5.1. Raman spectrum of CF_2Cl_2, with (closed circles) and without (open circles) infrared multiphoton excitation. Infrared excitation with 15 ns pulses at the 10.6 μm P(32) line. The arrows mark the position of the infrared pump mode.

5.3 Fluence dependence

Figure 5.2 and 5.3 show the fluence dependence of the normalized anti-Stokes signals for CF_2Cl_2 for excitation of the ν_8 and ν_1 mode, respectively. Each set of data was obtained in a single measurement by changing the monochromator wavelength every two thousand laser shots (corresponding to about two hours of measurement) and averaging the data. In contrast to the linear fluence dependence of SF_6, all three modes have an exponential fluence dependence, both for the ν_8 and ν_1 excitation. The graphs also show clearly that the exponential rate of increase is about the same for the ν_8 and ν_1 modes and is drastically different for the ν_2 mode.

5.4 Time dependence

Figure 5.4 shows the time dependence of the three accessible Raman active modes of CF_2Cl_2 for infrared excitation of the ν_8 mode with 15 ns pulses. Each of the anti-Stokes signals is normalized with its corresponding Stokes signal at room temperature. Just as for SF_6, anti-Stokes signals appear for all three modes after excitation at $t = 0$, but the signals decay much more rapidly, and although the time dependences are similar for the various modes, the maximum relative intensities differ.

5.5 The effect of buffer gas

The normalized anti-Stokes signals of CF_2Cl_2 were also studied in the presence of N_2 buffer gas. Figure 5.5 shows the intensity ratio of the anti-Stokes signals with and

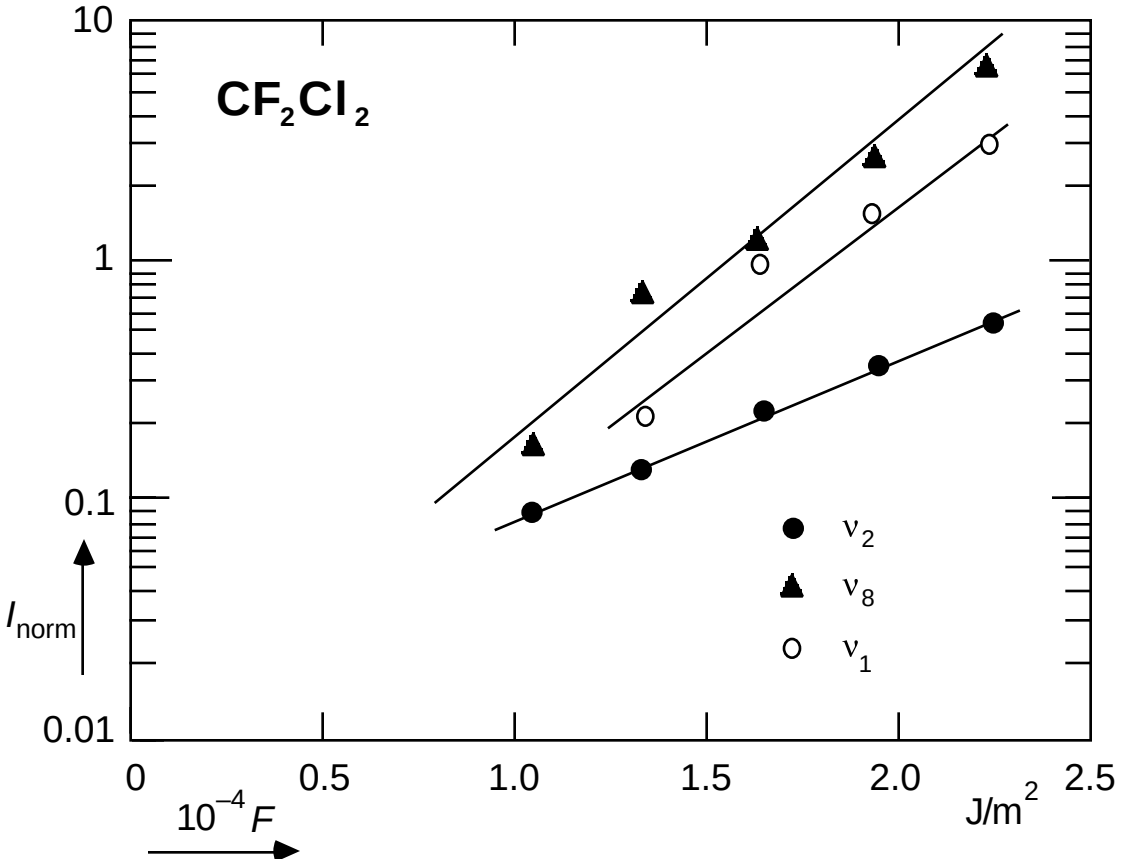

Fig. 5.2. Semilogarithmic plot of the fluence dependence of the anti-Stokes signals of CF_2Cl_2 at 400 Pa. The dependence is exponential for all three modes. Infrared excitation of ν_8 mode with 15 ns pulses at the 10.6 μm P(32) line.

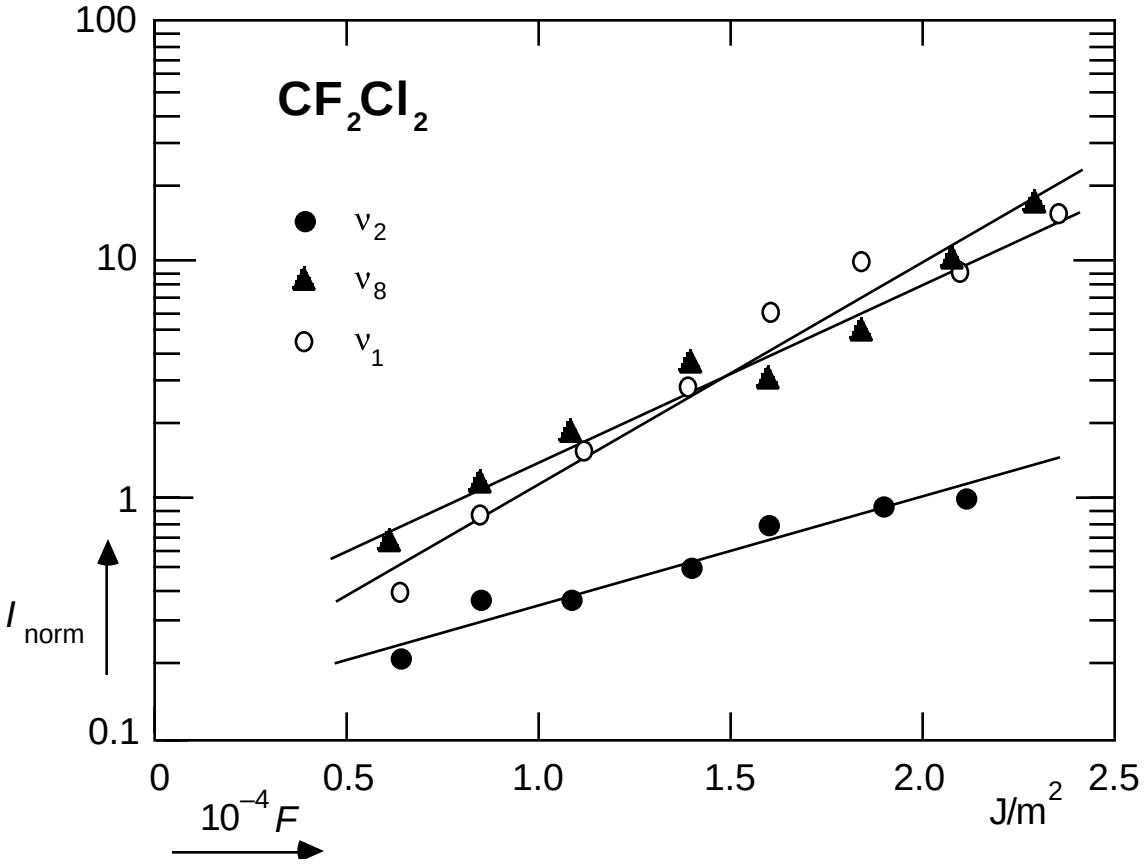

Fig. 5.3. Semilogarithmic plot of the fluence dependence of the anti-Stokes signals of CF_2Cl_2 at 400 Pa. The dependence is exponential for all three modes. Infrared excitation of ν_1 mode with 15 ns pulses at the 9.4 μm R(24) line.

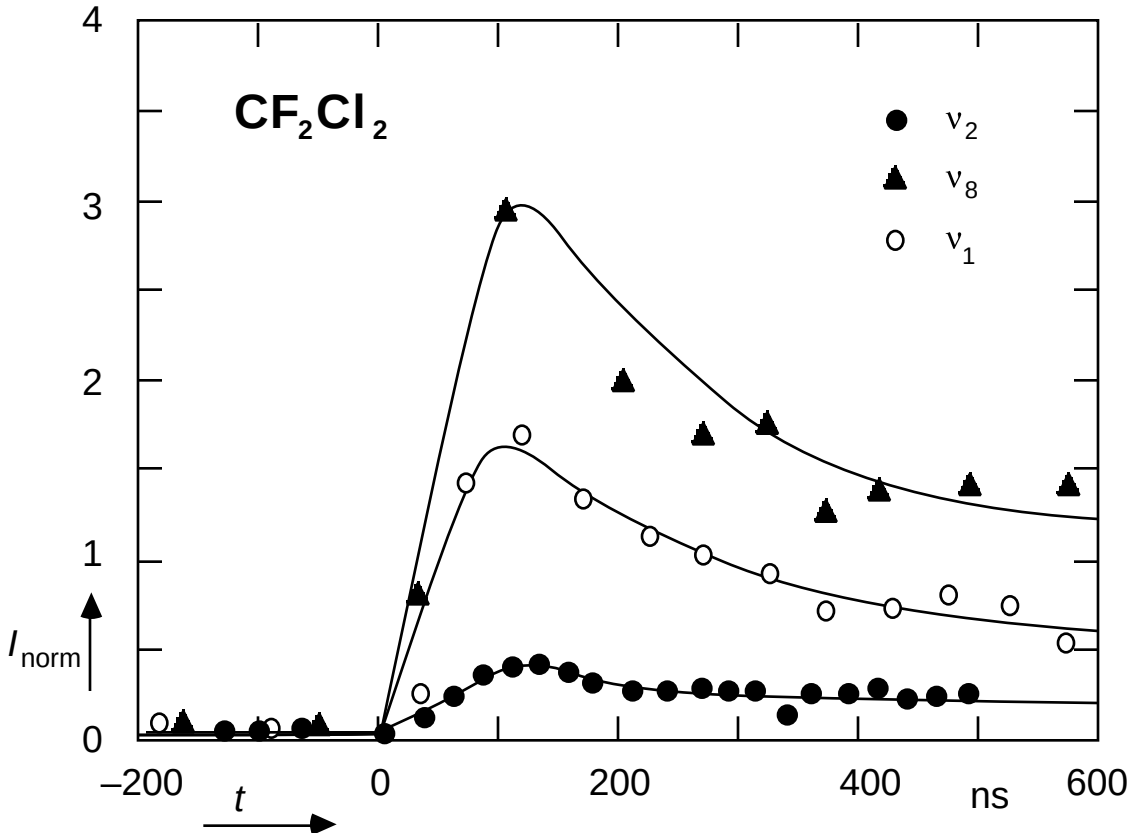

Fig. 5.4. Intensity of the anti-Stokes signals as a function of the time delay between pump and probe pulse for CF_2Cl_2 at 400 Pa. Infrared excitation of the ν_8 mode with 15-ns pulses on the 10.6 μm P(32) line with average fluence 1.8×10^4 J/m^2.

without buffer gas. Each of the anti-Stokes signals rapidly decreases with increasing buffer gas pressure, while at the same time the differences between them become smaller. No data are available for the anti-Stokes signal of the ν_8 mode at 26 kPa buffer gas

pressure. Since the Raman cross-section of the ν_8 mode is much smaller than that of the other two modes, this peak falls below the noise level at high buffer gas pressure.

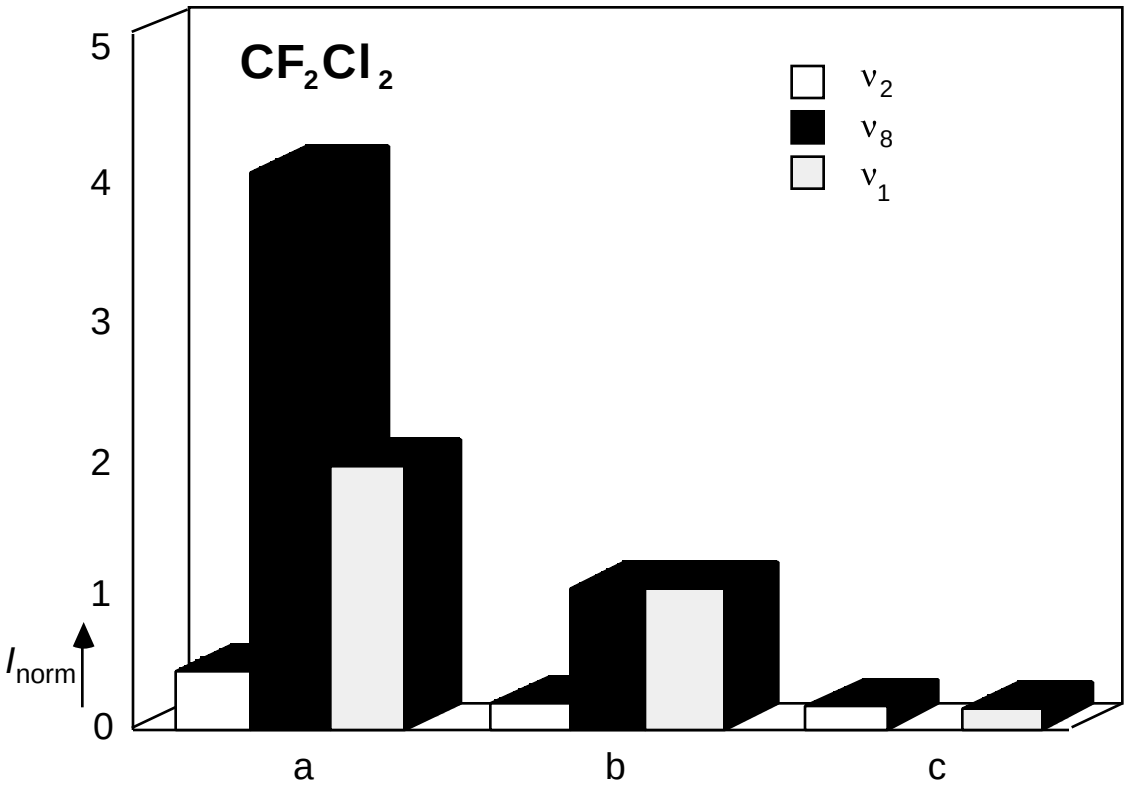

Fig. 5.5. Comparison of anti-Stokes intensities for CF_2Cl_2 at an average fluence of 2.1×10^4 J/m^2 and a pressure of 400 Pa, without buffer gas (*a*), and with 13 kPa (*b*), and 26 kPa (*c*) of N_2 buffer gas. Excitation of the ν_8 vibrational mode.

5.6 Laser induced fluorescence spectrum of the dissociation fragments

Figure 5.6 shows the spectrum of the laser induced fluorescence from the infrared multiphoton dissociated CF_2Cl_2 at three different fluences, ranging from 2 to 4×10^4 J/m^2, again with the excitation of the ν_8 mode. These results were obtained by analyzing only those laser shots where fluorescence was detected by the fluorescence detector (see chapter 6). The fluorescence signal was recorded in 10 nm increments from 290 nm to 340 nm. Although the intensity increases with increasing fluence, the spectral shape of the broadband emission does not change. In addition it should be noted that the fluorescence extends to the blue side of the incident laser field at 347.15 nm. The cut-off wavelength of the fluorescence is about 290 nm, which means that some of the dissociation fragments carry as much as 5000 cm^{-1}, or about 5 infrared photons, of internal energy.

5.7 Discussion

In general, for infrared multiphoton excited molecules, the intramolecular vibrational energy distribution depends on the excitation region, which in turn is determined by the infrared fluence. At low fluence the energy is essentially confined to the pumped mode, just as in ordinary one photon spectroscopy (region I). In this case the energy of other modes does not change after excitation, and the Raman signals simply reflect the thermal population of these modes. At higher pumping fluences the molecule may absorb many infrared photons and reach the high excitation region where the vibrational modes are strongly coupled (region II). In this region, modes which are not in resonance with the CO_2 laser also acquire energy during the excitation through the coupling with the pump mode. At even higher pumping fluence, dissociation of the molecules

occurs (region III).[2–5] Except for the fluorescence spectrum of infrared multiphoton dissociated CF_2Cl_2, all the experiments discussed in this chapter were done in region II.

As one can see from Figs. 5.2 and 5.3, CF_2Cl_2 shows a nearly exponential fluence dependence. Above 10^4 J/m^2, the excitation is a steep function of the pumping fluence and the Raman signals double roughly every 0.3×10^4 J/m^2 increment. Since CF_2Cl_2 is

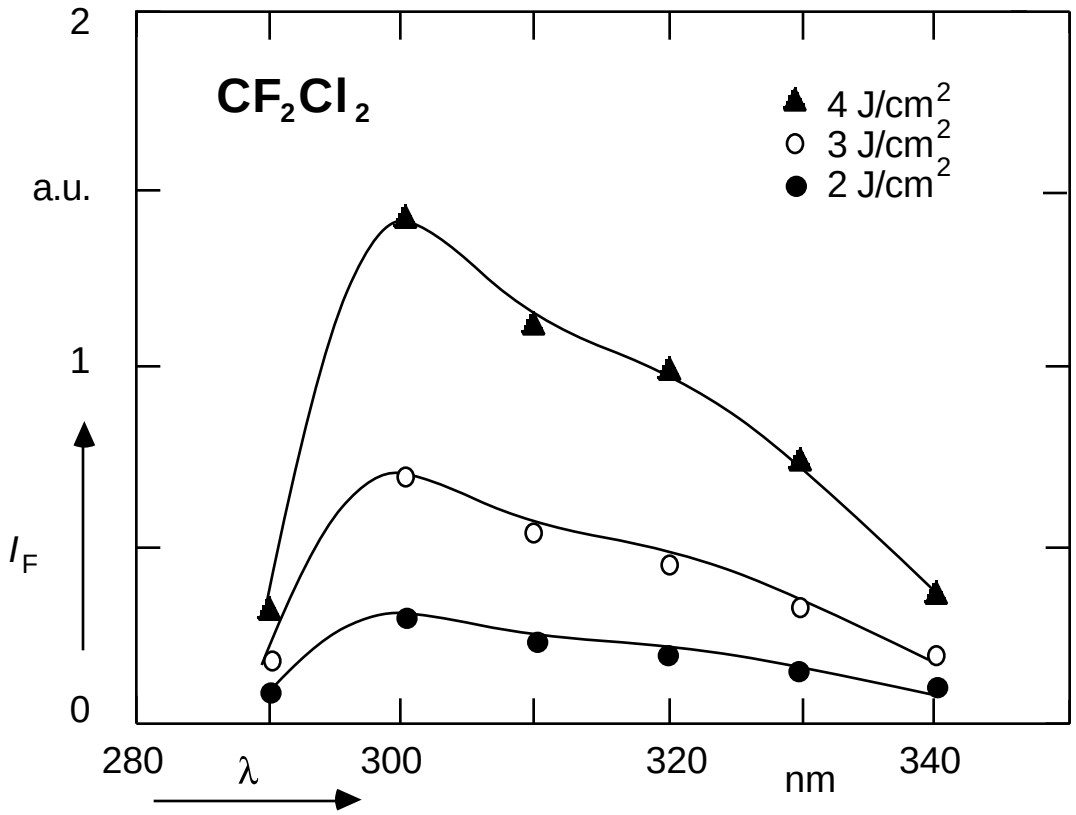

Fig. 5.6. Laser induced fluorescence spectrum from the dissociation fragments of CF_2Cl_2 after infrared excitation of the ν_8 mode. Note that only the intensity of the fluorescence increases with increasing fluence; the spectral shape does not change.

smaller than SF_6, fewer vibrational modes are available and one expects a strong bottleneck effect in CF_2Cl_2. The observed slow rise of the signals at low fluence, which is in sharp contrast with the linear fluence dependence of SF_6, indeed suggests that this is the case.

Measurements of the Raman signal for shorter pulses would provide a better understanding of the role of intensity effects.

Since the normalized anti-Stokes signal I_{norm} is a direct measure of the average number of vibrational quanta in the Raman active mode, one can evaluate the vibrational energy distribution of CF_2Cl_2 after infrared multiphoton excitation from the normalized intensities. According to Eq. (2.15) in thermal equilibrium the intensities of the normalized signals are given by

$$I_{\text{norm}} = \frac{1}{e^{h\nu/kT} - 1} \quad , \tag{5.1}$$

and the mode with lowest frequency will have the largest anti-Stokes signal. The results in Figs. 5.2 and 5.3, which are tabulated in Table 5.2, however, show that the signal intensities after infrared multiphoton excitation cannot be described by Eq. (5.1) at any fluence. In particular, the pump mode always contains the highest vibrational energy, and the 667 cm^{-1} mode the lowest. A comparison of the intramolecular energy distribution after excitation of the ν_8 and ν_1 mode with thermal distributions is shown in Figs. 5.7 and 5.8, respectively. The left side of the graphs shows the energy distribution after infrared multiphoton excitation, with and without buffer gas, while the right side of the graphs shows a thermal distribution. The temperature for the thermal cases was chosen such that the total energy in the three modes equals the measured total energy in the three modes in the multiphoton excitation case. From Fig. 5.7 it can be clearly seen that the energy distribution approaches the thermal one as buffer gas is added. At the same time, the overall signal intensity is reduced due to loss of energy to the buffer gas.

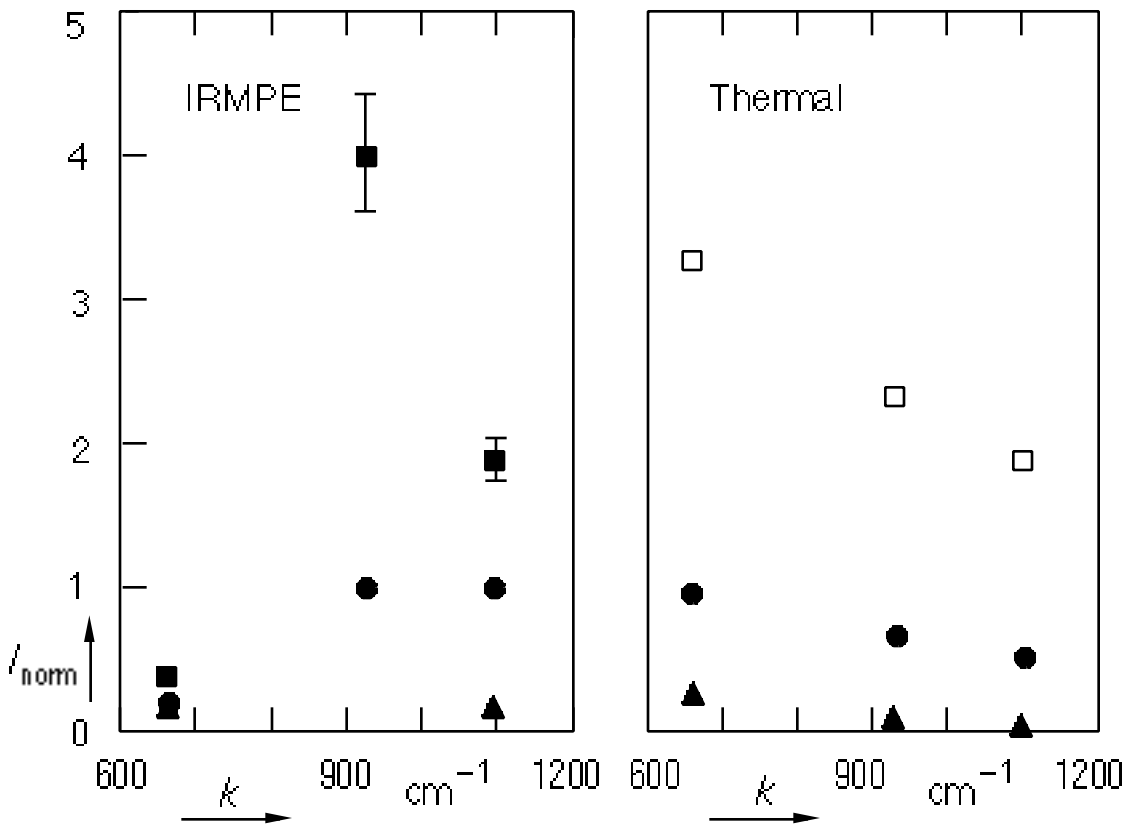

Fig. 5.7. Comparison of the observed normalized anti-Stokes signals after excitation of the ν_8 mode with calculated equilibrium values. The lower data points show the effect of collisional relaxation. N_2 buffer gas pressure: 0 kPa (squares), 13 kPa (circles), and 26 kPa (triangles).

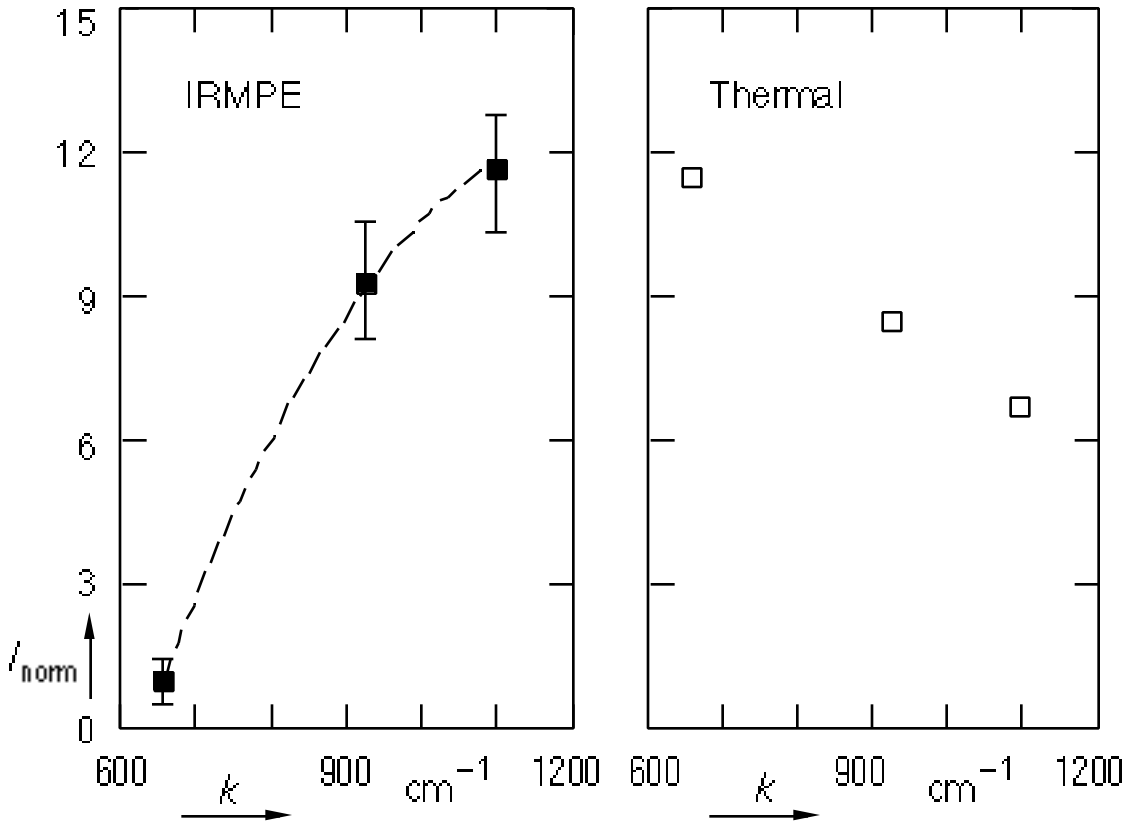

Fig. 5.8. Comparison of the observed normalized anti-Stokes signals after excitation of the ν_1 mode with calculated equilibrium values.

As can be seen in Figs. 5.2 and 5.3, the exponential rate of increase of the Raman signals with respect to the increase of the pumping fluence are about the same for the ν_8 and ν_1 modes and significantly lower for the ν_2 mode. From the data in Table 5.2, one can see that although the intensities of the anti-Stokes signals increase steeply with increasing pumping fluence, the intensity *ratio* does not change much. This rules out the

possibility that the observed nonequilibrium distribution is a result of averaging a 'hot' equilibrium ensemble and a 'cold' bottlenecked ensemble. If that were the case, the intensity ratio would change toward its equilibrium value as the fraction of molecules in the hot ensemble becomes larger with increasing fluence. If one calculates the energy content of the three modes for CF_2Cl_2 from Fig. 5.8 and adds up the obtained energies, it appears that a complete randomization of energy only occurs above at least 21,000 cm^{-1} of excitation for excitation of the ν_1 mode.

One expects collisions to relax the nonequilibrium energy distribution induced by the infrared multiphoton excitation. Even though the decay times of the anti-Stokes signals shown in Fig. 5.4 are different, it is not possible to draw any quantitative conclusions from these data because the signals drop below the noise level before equilibrium is reached. When buffer gas is added, the collision rate increases and the energy distribution should reach equilibrium more quickly. The intensity ratios shown in Fig. 5.7 indeed tend toward equilibrium with increasing buffer gas pressure. At a buffer gas pressure of 13 kPa the relative intensities of the ν_8 and the ν_1 mode become nearly identical. At 26 kPa, equilibrium is established between the ν_2 and the ν_1 modes. At this pressure, however, the overall signal has decreased so much because of vibration-translation relaxation that the anti-Stokes signal from the ν_8 pump mode becomes too small to be detected.

The time dependence of the Raman signals for CF_2Cl_2 shown in Fig. 5.4 is quite different from that of SF_6. The signals do not remain constant as for SF_6, especially for the two highly excited modes (ν_8 and ν_1). This decay is most likely due to collisional transfer of energy to other, initially 'cold', vibrational modes. Because of the limited sensitivity and spectral range, however, this cannot be verified in the present experimental setup.

F (10^4 J/m^2)	p_{N_2} (kPa)	I_{norm} ratio	E_{ν_2} (cm^{-1})	E_{ν_8} (cm^{-1})	E_{ν_1} (cm^{-1})
0	–	3.4 : 1 : 0.45	28	11	6
1.2	–	0.21 : 1 : 0.23	70	480	130
1.5	–	0.15 : 1 : 0.41	120	1140	560
1.8	–	0.12 : 1 : 0.48	180	2160	1240
2.1	–	0.10 : 1 : 0.48	280	3800	2190
2.4	–	0.10 : 1 : 0.48	440	6300	3620
2.1	13	0.20 : 1 : 1.00	130	920	1100
2.1	26	0.17 : – : 0.15	110	< 450	160

TABLE 5.2. Average vibrational energy and relative intensity ratio for three Raman active modes, ν_2 (667 cm^{-1}), ν_8 (923 cm^{-1}) and ν_1 (1098 cm^{-1}), of CF_2Cl_2 after infrared multiphoton excitation. The top line gives the (calculated) room temperature equilibrium values. At a N_2 buffer gas pressure of 26 kPa the anti-Stokes signal of the ν_8 mode drops below the noise level.

Fluorescence. As can be seen in Fig. 5.6, the laser induced fluorescence from the dissociation fragments of infrared multiphoton dissociated CF_2Cl_2 extends far into the blue side of the Raman probe. This indicates that the dissociation fragments carry up to

5000 cm^{-1} of excitation energy, corresponding to five infrared photons. It should also be noted that the shape of the spectrum does not change with increasing fluence. This implies that an increase in fluence does not change the energy distribution of the dissociation fragments, but only increases the *number* of dissociated molecules. Therefore the unimolecular dissociation rate of infrared multiphoton excited CF_2Cl_2 must be much smaller than the excitation rate.

Fermi resonances. Questions have been raised about the influence of possible Fermi resonances on the interpretation of the Raman spectra of highly vibrationally excited molecules.[6] The interaction of a fundamental vibration with an overtone or with a combination mode may cause Fermi resonances when certain symmetry requirements are satisfied.[7] Basically, if the frequency of an overtone or a combination mode happens to lie close to the frequency of a fundamental mode, and if the interaction between the two is strong enough, the nature of the two processes mix and the energy levels are displaced. As a result the vibrational spectrum can be misinterpreted. One well-known example is the mixing of the 1300 cm^{-1} vibrational mode and the overtone of the 667 cm^{-1} vibrational mode of CO_2, which causes *two* peaks, instead of one single peak, to appear in the Raman spectrum of CO_2 around 1300 cm^{-1}. Since this problem is related to the interpretation of the anti-Stokes signals of highly excited molecules in our experiment, the possible effect of Fermi resonances on our experimental data must be examined.

Let us consider an anti-Stokes transition in the kth vibrational mode of a certain molecule. For simplicity we assume that the initial state ψ_k corresponds to the first excited state of the kth vibrational mode, and that the final state of the Raman transition is the ground state ψ_o. We further assume that the frequency ν_k of this Raman active vibrational mode lies close to the sum of the frequencies of two other fundamental modes, $\nu_k \approx \nu_i + \nu_j$,

where i, j represent the ith and jth vibrational modes respectively (see Fig. 5.9). In addition we assume that the interaction matrix element between the doubly

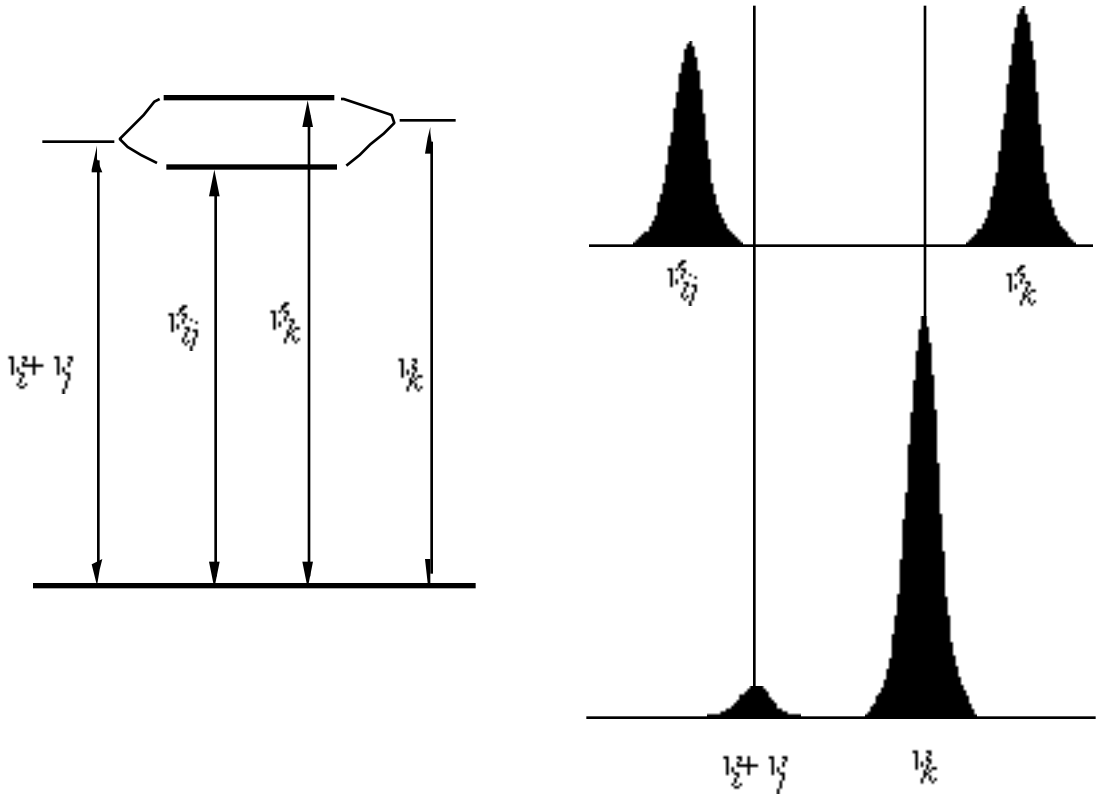

Fig. 5.9. The effect of a Fermi resonance on the molecular energy levels and spectrum. The interaction between the $\nu_i+\nu_j$ combination and the ν_k fundamental transitions shifts the energy levels and redistributes the spectral intensity. The bottom spectrum is the expected one without Fermi resonance, the top one shows the actual spectrum.

excited combination state ψ_{ij} and ψ_k,

$$W_{ij,k} = \int \psi_{ij}^{*}\ W \psi_k \, \mathrm{d}^3x \,, \tag{5.2}$$

with W the interaction operator, is nonzero. The actual energy levels $E' = h\nu'$, with $\nu' = \nu'_{ij}, \nu'_k$, of these interacting states will then be determined by the secular equation

$$\begin{vmatrix} (\nu_i+\nu_j)-\nu' & W_{ij,k} \\ W_{ij,k} & \nu_k-\nu' \end{vmatrix} = 0. \tag{5.3}$$

The wavefunctions of the interacting states will be superpositions of the original wavefunctions,

$$\psi'_{ij} = a\psi_k + b\psi_{ij} \tag{5.4}$$

and

$$\psi'_k = c\psi_k + d\psi_{ij} \,, \tag{5.5}$$

where the transformation matrix with coefficients a, b, c and d is unitary. These two equations show the effect of Fermi resonances on the intensities of the two transitions: the peak corresponding to the inherently weak combination mode ψ_{ij} grows considerably because it 'borrows' intensity from the wavefunction of the fundamental mode ψ_k, while at the same time the intensity of the fundamental is reduced. Clearly, in high resolution spec-

troscopy the displacement of the line positions and the redistribution of line intensities between interacting combination and fundamental modes can be misleading.

In the present experiment, however, the situation is quite different. To accommodate the change in level spacing due to the anharmonicity of the vibrational mode, the measurements are done at low spectral resolution. Thus all Raman photons scattered from different excitation levels will be collected and integrated. If the displacements due to Fermi resonances are smaller than the resolution of the monochromator (1.5 nm) this means that one measures the *spectrally integrated* signal,

$$\left| \psi'_{ij} \middle| R_{ij} + R_k \middle| \psi_o \right|^2 + \left| \psi'_k \middle| R_{ij} + R_k \middle| \psi_o \right|^2$$

$$= \left| a^* \psi_k \middle| R_k \middle| \psi_o + b^* \psi_{ij} \middle| R_{ij} \middle| \psi_o \right|^2 + \left| c^* \psi_k \middle| R_k \middle| \psi_o + d^* \psi_{ij} \middle| R_{ij} \middle| \psi_o \right|^2$$

$$= \left| \psi_k \middle| R_k \middle| \psi_o \right|^2 + \left| \psi_{ij} \middle| R_{ij} \middle| \psi_o \right|^2 \approx \left| \psi_k \middle| R_k \middle| \psi_o \right|^2, \qquad (5.6)$$

with R_{ij} and R_k the combination mode and Raman scattering operators, respectively, and where we have used the unitary properties of the transformation matrix. Equation (11) demonstrates that the spectrally integrated signal is *identical* to the one without Fermi resonance. Therefore the measured signal is the sum of the 'real' Raman signal $\left| \psi_k \middle| R_k \middle| \psi_o \right|^2$ plus a much smaller quantity $\left| \psi_{ij} \middle| R_{ij} \middle| \psi_o \right|^2$, whether or not Fermi resonances occur.

In addition to this general observation, a closer look at the available spectroscopic data for SF_6 and CF_2Cl_2 further reveals that there are no Fermi resonances with the Raman modes studied in this thesis. The only candidate for a Fermi resonance with the ν_1 mode (775 cm^{-1}) of SF_6 is the overtone of the ν_6 mode (363 cm^{-1}). However the ν_6 mode is spectroscopically inactive because of its F_{2u} symmetry. For CF_2Cl_2, the only reported Fermi resonance is due to the combination mode $\nu_3+\nu_9$ (882 cm^{-1}), which is infrared, not Raman active.

Summarizing the above remarks, we may conclude that Fermi resonances cannot affect our experimental data. Therefore, in our experiment the observed anti-Stokes signals can be used as a measure of the average number of vibrational quanta in each of the modes, with or without Fermi resonances.

5.8 Measurements on CH_3CHF_2 and CF_2HCl

Both CH_3CHF_2 and CF_2HCl show only small or no changes in Raman intensities after infrared multiphoton excitation.

CH_3CHF_2. The largest molecules studied, CH_3CHF_2, has four accessible Raman active modes. The wavenumbers of the Raman active modes are 870 cm^{-1}, 1140 cm^{-1}, 1460 cm^{-1} and 2980 cm^{-1}. Among the four Raman active modes, only the 870 cm^{-1} mode shows a small increase in Raman intensity after infrared multiphoton excitation.

The Raman spectrum of CH_3CHF_2 at various infrared pumping fluences is shown in Fig. 5.10. The anti-Stokes signal has a distinctive peak at low infrared fluence. However, as the infrared fluence increases, it is replaced by a broadband laser induced fluorescence from the dissociation fragments, just as for CF_2Cl_2. The graph, which is

semilogarithmic, clearly shows that the intensity of the fluorescence is much stronger than the Raman signal.

A comparison of Fig. 5.11 with Fig. 5.4 shows that the time dependence of the Raman signals for CH_3CHF_2 are very similar to the one for CF_2Cl_2. From the normalized intensities it follows that at an infrared fluence 1.5×10^4 J/m^2, the energy of the Raman active mode corresponds to 0.15 vibrational quanta. Fig. 5.10, on the other hand, shows that at this fluence the molecules roughly start to dissociate. The small amount of energy in the Raman active mode at this fluence therefore strongly suggests that the vibrational energy distribution of infrared multiphoton excited CH_3CHF_2 is nonequilibrium.

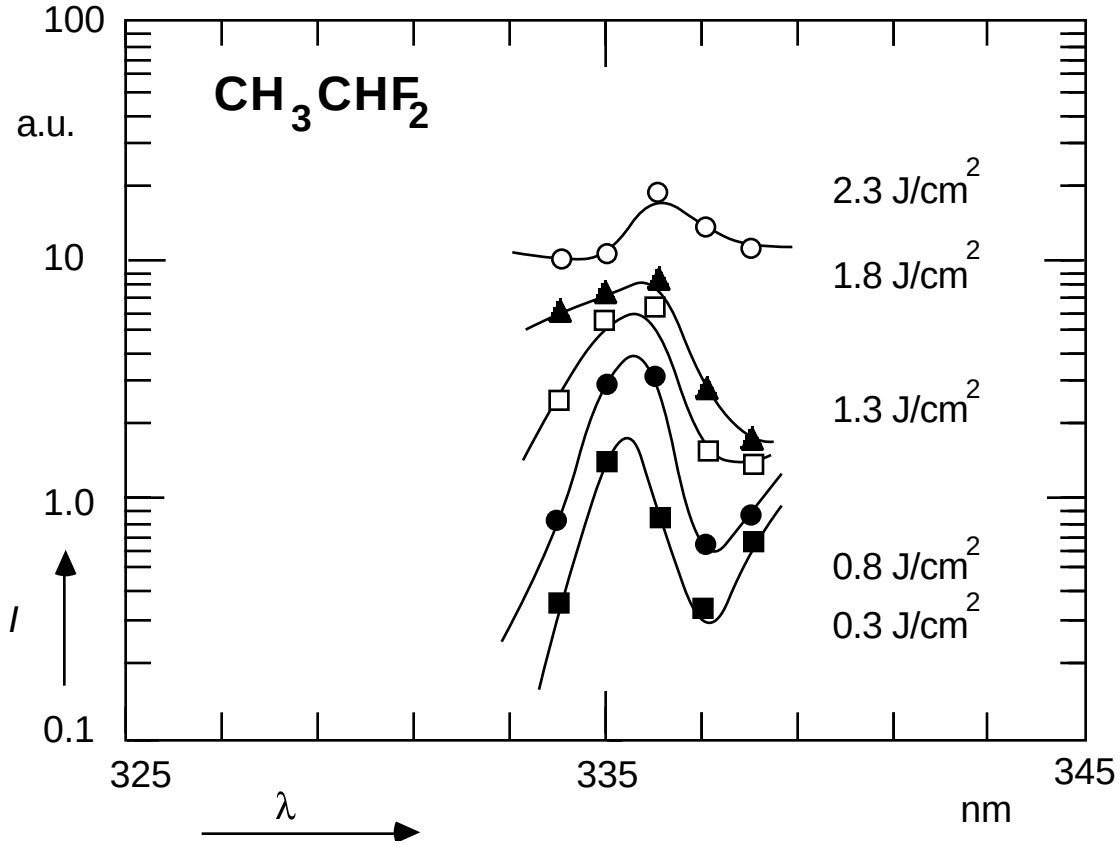

Fig. 5.10. Anti-Stokes signal of the 870 cm^{-1} mode of infrared multiphoton excited CH_3CHF_2 at various fluences. Infrared excitation: 10.6 μm P(20) line, 0.5 ns pulse duration. At high fluence, laser-induced-fluorescence from the dissociation fragments replaces the Raman signal.

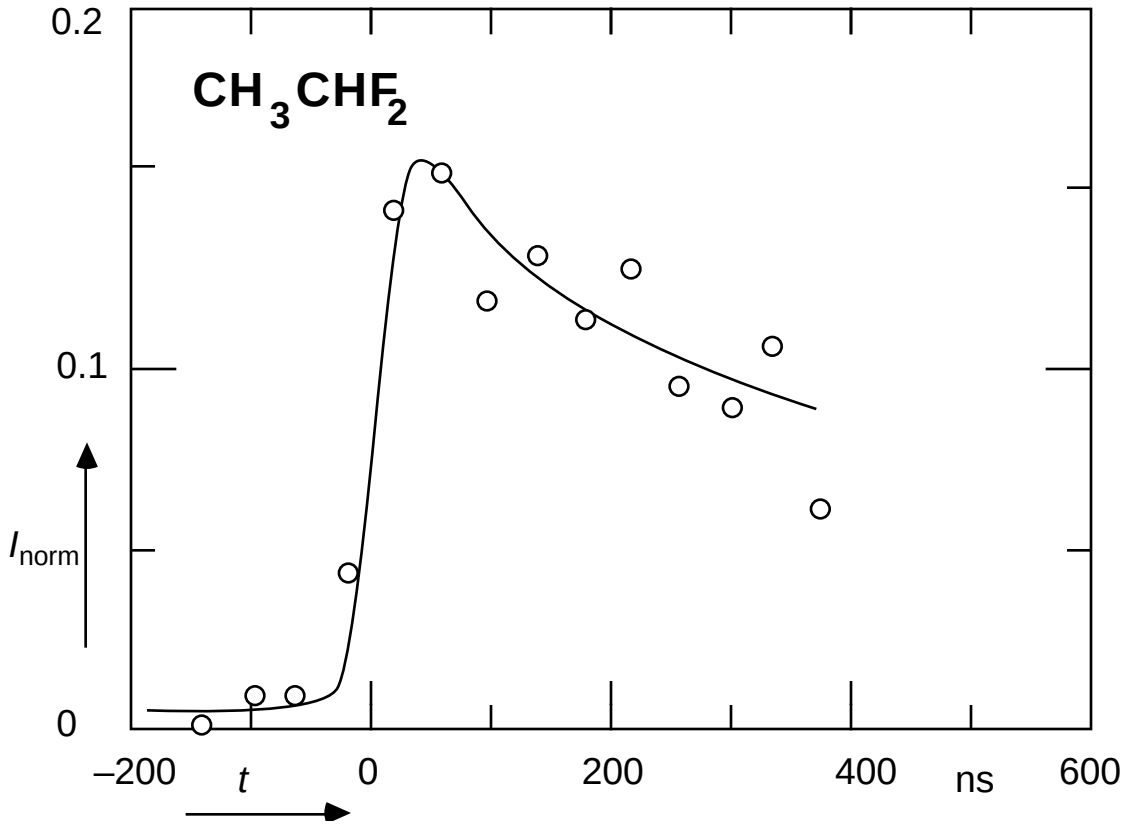

Fig. 5.11. Intensity of the anti-Stokes signals as a function of the time delay between pump and probe pulse for CH_3CHF_2 at 660 Pa. Infrared excitation: 10.6 μm P(20) line, 0.5 ns pulse with average fluence 1.5×10^4 J/m^2.

CF_2HCl. The density of states of CF_2HCl is estimated to be much lower than other molecules of the same size.[8] This estimate is supported by the experimental observation that CF_2HCl has a much stronger intensity dependence in infrared multiphoton excitation.[9]

In our experiment, none of the five accessible Raman active modes of CF_2HCl show any change after infrared multiphoton excitation, even at a fluence of 2×10^4 J/m^2, when the average number of photons absorbed per molecule is reported to be about ten.[10] This experimental result is consistent with the density-of-state estimate, as well as the intensity dependence in infrared multiphoton excitation, and again strongly suggests that the energy distribution is nonequilibrium.

5.9 Conclusion

We have presented the time-resolved Raman spectra of infrared multiphoton excited CF_2Cl_2, CH_3CHF_2 and CF_2HCl. Intramolecular vibrational energy distributions after infrared multiphoton excitation were obtained by comparing the normalized anti-Stokes intensity, a direct measure of the energy in the mode, for different Raman active modes. The experimental results show that for all three molecules, the distribution is nonequilibrium. For CF_2Cl_2, in addition, the fluence dependence shows that the nonequilibrium distribution cannot be the result of averaging a 'hot' equilibrium ensemble and a 'cold' bottlenecked ensemble. This leads to the conclusion that even at high excitation the intramolecular vibrational distribution is still nonequilibrium, with an excess of energy in the pumped mode. It should be emphasized, however, that these conclusions hold for molecules in region II, and not for dissociating molecules since the signal from those molecules is rejected. Therefore the above conclusions do not contradict the observation[2] that the infrared multiphoton *dissociation* of molecules is consistent with RRKM theory.[11]

References

1 T. Shimanouchi, J. Phys. Chem. Ref. Data **6**, 993 (1977)

2 David S. King and John C. Stephenson, Chem. Phys. Lett. **51**, 48 (1977)

3 J.W. Hudgens, J. Chem. Phys. **68**, 777 (1978)

4 R.J.S. Morrison and E.R. Grant, J. Chem. Phys. **71**, 3573 (1979)

5 Aa.S. Sudbø, P.A. Schulz, E.R. Grant, Y.R. Shen, and Y.T. Lee, J. Chem. Phys. **70**, 912 (1979)

6 D.W. Lupo, and M. Quack, Chem. Rev. **87**, 181 (1987)

7 F. Albert Cotton, *Chemical Applications of Group Theory* (Wiley-Interscience, New York, 1971)

8 J.L. Lyman, G.P. Quigley and O.P. Judd, *Single-Infrared-Frequency Studies of Multiple-Photon Excitation and Dissociation of Polyatomic molecules,* ed. C. Cantrell (Springer-Verlag, Heidelberg, 1980)

9 David S. King and John C. Stephenson, Chem. Phys. Lett. **66**, 33 (1979)

10 T.B. Simpson, J.G. Black, I. Burak, E. Yablonovitch and N. Bloembergen, J. Chem. Phys. **83**, 628 (1985)

11 P.J. Robinson, K.A. Holbrook, *Unimolecular Reactions* (Wiley-Interscience, New York 1972)

CHAPTER 6

REJECTION OF STOCHASTIC BACKGROUND NOISES IN RAMAN EXPERIMENTS

6.1 Introduction

Among the methods for low level light detection with photomultiplier tubes, digital photon counting and analog charge integration are the two commonly used ones. Although photon counting can provide an excellent signal-to-noise ratio in CW experiments, charge integration must be used when the distribution of the arrival time of the photons is too narrow for digital photon counting. This is usually the case when short, intense laser pulses are used to achieve high time resolution. In the experiments described in chapters 4 and 5, charge integration with an Amperex XP2020Q high gain photomultiplier was used to detect the Raman photons scattered from infrared multiphoton excited molecules. Since the signal level is extremely low (0–3 Raman photons per laser shot), the rejection of stochastic background noise is very important in our experiment.

There are two main sources of noise in our experiment: one is the afterpulse[1] from the photomultiplier tube, the other is the fluorescence induced by the Raman probe laser.

Afterpulses originate from the collisions between the photoelectrons and residual atoms in the photomultiplier. The collisions generate positive ions which are accelerated toward the photocathode and induce the emission of secondary electrons. Afterpulses increase with time because of the diffusion of He atoms into the photomultiplier, especially in a He rich environment.

The laser induced fluorescence comes from the highly excited dissociation fragments of the sample gas, when a fraction of the molecules are dissociated by the CO_2 laser. Since the probability of dissociation increases with increasing CO_2 laser fluence and does not have a sharp threshold, one cannot completely eliminate the dissociation by simply reducing the power of the CO_2 laser.

Both of these two sources of noise contribute irregularly because of their stochastic nature. Although usually they appear in only 5-20% of the laser shots (depending on the aging of the photomultiplier and the intensity fluctuation of the CO_2 laser), the signal-to-noise ratio of the experiment can be seriously degraded because of the high intensity of these noises.

The laser induced fluorescence has a life time longer than the width of our Raman probing pulses. Afterpulses of the photomultiplier also appear after the real output pulses generated by Raman scattered photons. Therefore whether or not the noise appears in a specific laser shot can be determined by monitoring the coincidence of the photomultiplier signal with the Raman probing pulse. Shots with photomultiplier output pulses not in coincidence with the Raman probing pulse should be rejected. A noise rejection system was therefore built to monitor the coincidence between the photomultiplier output and the Raman probe pulse shot by shot. The system is designed in such a way that it does not affect the operation of the charge integrator.

6.2 Electronic scheme

Figure 6.1 is the block diagram of the noise rejection system. The signal from the photomultiplier tube (PMT) is sent to a charge integrator consisting of a low pass filter and an low noise amplifier. For most of the frequency components of the photomultiplier pulses, the charge integrator appears as a 50 Ω cable terminator, therefore it is not required to be placed very close to the photomultiplier. The photomultiplier signal is also monitored by a wide band RF amplifier which, together with a constant fraction discriminator (ORTEC 934), records the arrival time of the photons. The time interval when the Raman probe pulse is present is recorded by a photodiode and another constant fraction discriminator. The output pulses of both constant fraction discriminators are compared in the coincidence circuit. If any of the photomultiplier output pulses appears when the Raman probe pulse is not present, the coincidence circuit sends a flag to the computer and the data is rejected.

Special care must be taken that the RF amplifier will not interfere with the charge integrator. If the input impedance of the RF amplifier is too high it will not have the required fast time response. On the other hand, if it is too low it will make the relaxation time of the integrator too short to record the integrated signal accurately. The RF amplifier used here is an ORTEC 574 timing amplifier, with its 50 Ω input terminator removed. The modified amplifier has a 2.5 kΩ input impedance, resulting in a 25 μs (2.5 kΩ × 0.01 μF) charge integrator relaxation time constant. This is long enough for the transient waveform digitizer to record the signal. In addition, because the 2.5 kΩ input impedance of the RF amplifier is much higher than that of the charge integrator (50 Ω), the amount of charge taken away from the charge integrator by the amplifier is negligible. When the amplifier is

placed close to the integrator, its time response will not be affected by the cable configuration since the charge integrator terminates the cable correctly at 50 Ω.

Figure 6.2 shows the details of the coincidence circuit. It consists of two one-shot circuits. The first one triggers at the end of the Raman probe pulse. The output pulse must be made (via R1, C1) just long enough to cover the interval where the afterpulses and fluorescence might appear. If any signal appears in this range, the second one-shot circuit will be triggered and the flag signal will be low. The length of the flag must be made (via R2, C2) long enough for the computer to read. Since the output pulse from the ORTEC 934 constant fraction discriminator is a negative voltage pulse, a pull-up resistor and a capacitor coupler is used in front of the one-shot circuits to shift the level. The output pulse-width of the constant fraction discriminator channel monitoring the photomultiplier tube should be made as short as possible to respond to the individual photons. The output pulse-width of the other constant fraction discriminator channel monitoring the photodiode, however, need not be identical to that of the Raman probe pulse, since in addition to reflecting the Raman probe pulse, the pulse-width should be adjusted to compensated the time delay due to the intrinsic path difference between the photomultiplier signal and photodiode signal.

6.3 Conclusion

The noise rejection system discussed above has been successfully applied in the Raman experiments described in chapters 4 and 5. In particular, it has enabled us to extend our studies to highly excited molecules where laser induced fluorescence from dissociation fragments occurs. Also it allows us to extend the life time of expensive photomultiplier

tubes by rejecting the afterpulse noise resulting from the aging of the tubes. The application of this noise rejection system is not limited to Raman experiments only. It can be applied to any low level light detection pump and probe experiment provided that the desired signal is in coincidence with the probe.

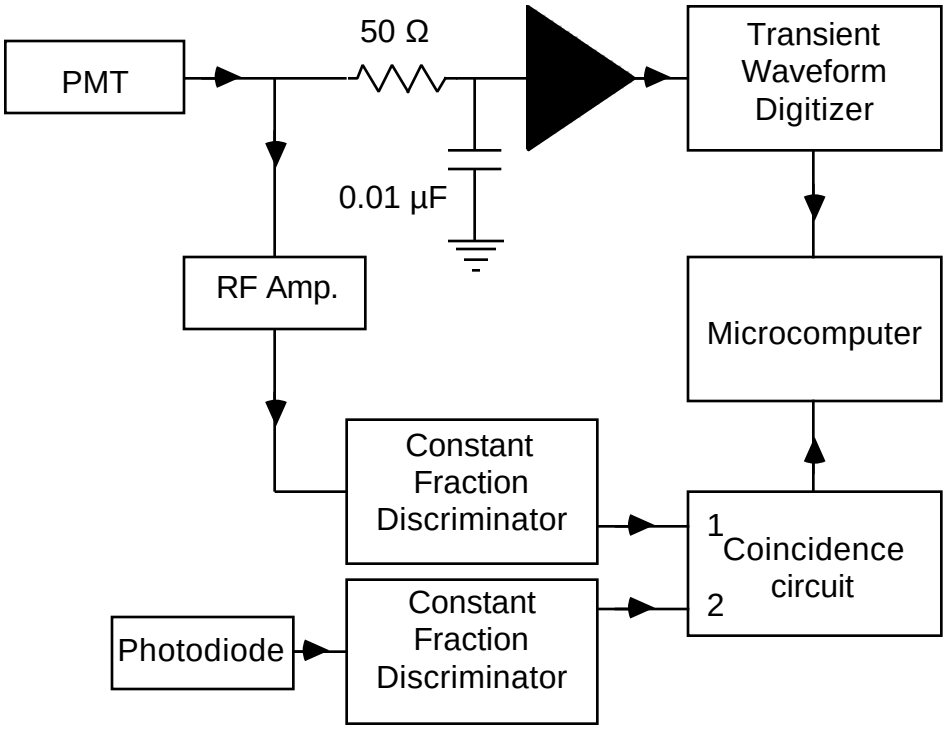

Fig. 6.1. Block diagram of the noise rejection system. PMT = Amperex XP2020Q photomultiplier, RF amplifier = modified ORTEC 574 timing amplifier. The constant fraction discriminators are two of the four channels in an ORTEC 934 module. Transient waveform digitizer, a Biomation 8100, can be replaced by an AD582 sample-and-hold chip for a less expensive setup. Details of the coincidence circuit are shown in Fig. 6.2.

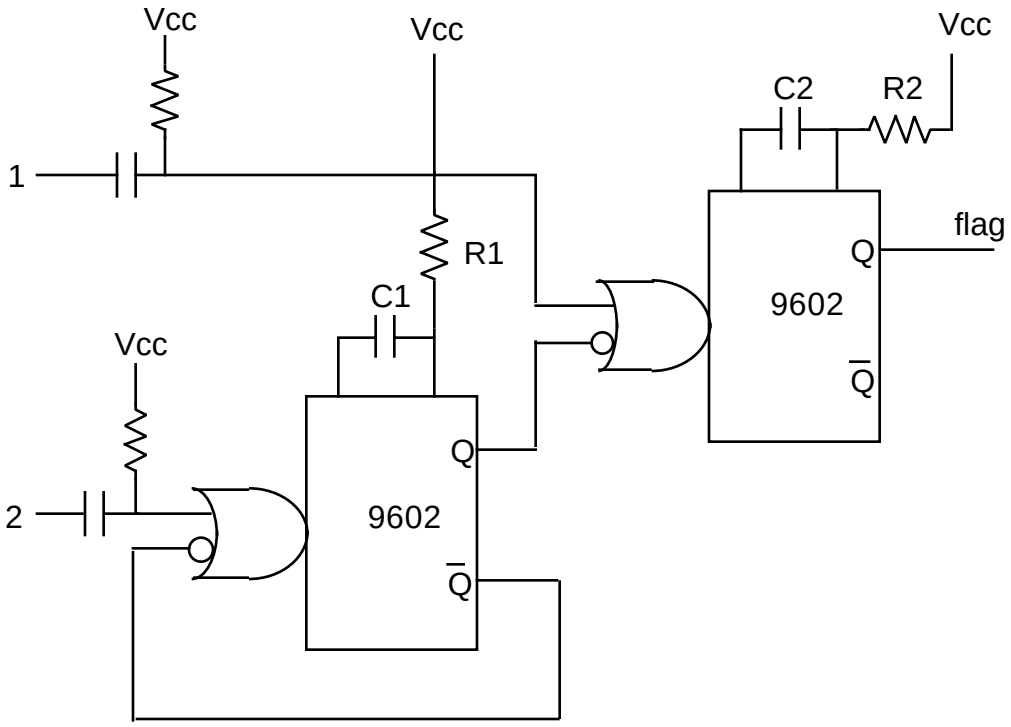

Fig. 6.2. Circuit diagram of the coincidence circuit. A pull-up resistor and a capacitor coupler are used in front of each one-shot (9602) circuit to shift the negative voltage input pulses into negative logic pulses. The first one-shot circuit triggers at the end of the input pulse from terminal 2 (the rising edge of a negative logic pulse). The output pulse of this one-shot lasts for 400 ns. If there are any pulses coming from terminal 1 during these 400 ns, the second one-shot circuit will trigger and send flag signal to the computer.

References

1 S. Torre, T. Antonioli and P. Benetti, Rev. Sci. Instrum. 54, 1777 (1983).

CHAPTER 7

COHERENT ANTI-STOKES RAMAN EXPERIMENTS

7.1 Introduction

In chapters 4 and 5, spontaneous Raman scattering was employed to measure the total energy in each of the Raman active modes. From this energy, in turn, the intramolecular energy distribution was obtained. Since the spontaneous Raman signals from the different energy levels within a vibrational ladder have different frequencies due to the anharmonicity, in principle, one can also measure the energy distribution within the vibrational ladder by resolving the spontaneous Raman signals from each level individually. In practice, however, the low signal level of the spontaneous Raman scattering in our setup does not allow such a high spectral resolution. Therefore, to study the energy distribution within a vibrational mode, high resolution coherent anti-Stokes Raman spectroscopy[1–4] was employed.

In coherent anti-Stokes Raman scattering, two beams with frequency ω_L and ω_S are mixed via the third order nonlinear susceptibility $\chi^{(3)}$ in the sample, to generate a new frequency $\omega_c = 2\omega_L - \omega_S$. If the difference of the two driving frequencies $\omega_L - \omega_S$ matches an allowed transition in the sample, the magnitude of the coherent anti-Stokes

Raman signal at frequency ω_c is greatly enhanced. Coherent anti-Stokes Raman scattering has several advantages over spontaneous Raman scattering:

1) Given the typical nonlinear susceptibility of a molecular system, and the high laser powers available today, the signal level of coherent anti-Stokes Raman scattering can be several orders of magnitude larger than that of spontaneous Raman scattering.
2) The output beam of the coherent anti-Stokes Raman scattering is highly collimated, allowing high rejection of possible fluorescence, which always is nondirectional.
3) The spectral resolution of coherent anti-Stokes Raman scattering is determined by the linewidth of the lasers, which can be made very narrow with single-mode dye lasers.

High resolution coherent anti-Stokes Raman spectroscopy can resolve the individual Raman transitions in the vibrational ladders, so that information on the population of individual vibrational levels within a vibrational mode can be obtained. Its high signal levels also allows one to use a picosecond streak camera to resolve the output photons in time. With a streak camera it thus become possible to resolve the population changes *during* the infrared excitation.

This chapter presents a description of the coherent anti-Stokes Raman scattering setup used in our laboratory for studying infrared multiphoton excitation, and a discussion of some preliminary results.

7.2 Theory

The goal of this section is not to derive a complete and rigorous theory of coherent anti-Stokes Raman scattering, but rather to highlight the basic underlying physics of the

technique which forms the basis of our experiment. Although we will avoid using tensor notations, all the equations in this section can be generalized into a tensor formalism without changing the underlying physics.

As with spontaneous Raman scattering, for coherent anti-Stokes Raman scattering we should again consider the induced polarization. The difference between the two processes is that spontaneous Raman scattering is determined by the linear term of the electric susceptibility $\chi^{(1)}$, while coherent Raman scattering is determined by the third order susceptibility $\chi^{(3)}$. To take nonlinear susceptibilities into account, the polarization can conveniently be expanded as a power series of the electric field,[5]

$$P = \chi^{(1)}E + \chi^{(2)}E^2 + \chi^{(3)}E^3 \ldots . \tag{7.1}$$

In this expression, P is the polarization, E is the electric field and the $\chi^{(i)}$ the ith-order susceptibility. The susceptibilities in Eq. (7.1) depend on various molecular parameters such as the vibrational frequencies, as well as the state of the molecule. In a typical light scattering experiment, one of the $\chi^{(i)}$'s is measured and from this quantity information on the parameters and/or the state of the molecule can be obtained.

There are many terms in $\chi^{(3)}$ corresponding to different third-order nonlinear phenomena. The term responsible for coherent anti-Stokes Raman scattering, $\chi_c^{(3)}$, gives rise to an induced polarization $P^{(3)}$ in the presence of two laser fields E_L and E_S at frequencies ω_L and ω_S,

$$P^{(3)}(z, t) = \frac{3}{8}\chi_c^{(3)}E_L^2E_S e^{i[(2k_L - k_S)z - (2\omega_L - \omega_S)t]} + \text{complex conjugate}, \tag{7.2}$$

where k_L and k_S are the wavevectors of the laser field. This induced polarization $P^{(3)}$ is the driving term in the Maxwell equation

$$\nabla^2\vec{E} - \frac{n^2}{c^2}\frac{\partial^2\vec{E}}{\partial t^2} = \frac{4\pi}{c^2}\frac{\partial^2\vec{P}}{\partial t^2}, \tag{7.3}$$

with n the index of refraction and c the speed of light. For simplicity, let us assume that the fields E_L and E_S, and the induced polarization have the same direction to avoid using tensor notations, and also that the amplitude of the electric field is a slowly varying function of both space and time. We may then write

$$E = \frac{1}{2}\left[E_c(z,t)e^{i(k_c z - \omega t)} + E_c(z,t)e^{-i(k_c z - \omega t)}\right], \tag{7.4}$$

where the slowly varying function $E_c(z, t)$ represents the amplitude of the coherent anti-Stokes signal. Substituting Eqs. (7.2) and (7.4) into (7.3), and neglecting the second derivatives of E_c because of the slowly varying approximation, we obtain

$$\frac{\partial E_c}{\partial z} + \frac{n_c}{c}\frac{\partial E_c}{\partial t} = \frac{2\pi i\omega_c}{n_c c}\left(\frac{3}{4}\right)\chi_c^{(3)}E_L^2 E_S e^{i(2k_L - k_S - k_c)z}, \tag{7.5}$$

where n_c is the index of refraction at $\omega_c = 2\omega_L - \omega_S$. Assuming the system is in a steady state ($\partial E_c/\partial t = 0$) and integrating (7.5) over the length L of the sample, we obtain

$$E_c = \frac{3\pi\omega_c\chi_c^{(3)}E_L^2 E_S}{2n_c c(2k_L - k_S - k_c)}\left(e^{i(2k_L - k_S - k_c)L} - 1\right). \tag{7.6}$$

Since the intensity I of an radiation electric field E is given by

$$I = \frac{cn}{8\pi} EE \quad , \tag{7.7}$$

we finally obtain for the coherent anti-Stokes intensity

$$I_c(z = L) = \frac{144\pi^4 \omega_c^2 \left|\chi_c^{(3)}\right|^2 I_L^2 I_S L^2}{c^4 n_c n_L^2 n_S} \times \frac{\sin^2[(2k_L - k_S - k_c)L/2]}{[(2k_L - k_S - k_c)L/2]^2} \quad , \tag{7.8}$$

with I_L and I_S the intensities of the incident laser beams.

In the above expression we can see that the coherent anti-Stokes intensity is proportional to the square of the interaction length L and the product of the intensities of the input beams. In the gas phase, the coherent anti-Stokes intensity is also proportional to the square of the sample gas density, because $\hat{e}\chi_c^{(3)}\acute{u}$ is proportional to density. The phase matching condition is expressed in the function

$$\frac{\sin^2[(2k_L - k_S - k_c)L/2]}{[(2k_L - k_S - k_c)L/2]^2} \quad ,$$

which has a maximum for $2k_L - k_S - k_c = 0$.

7.3 Experimental setup

The goal of the coherent anti-Stokes Raman experiment is to resolve the population distribution of the individual vibrational states *within* the vibrational modes of infrared-

multiphoton-excited molecules. To achieve this goal, either a single-mode Littman dye laser,[6] or the second harmonic of a Nd:YAG laser was employed to provide radiation at ω_L, and a broadband dye laser for the radiation at ω_S. The bandwidth of the broadband dye laser is broad enough to cover anharmonic shifts, typically 200 cm^{-1}. This particular arrangement, usually referred to as multiplex coherent anti-Stokes Raman scattering,[2] allows one to measure the coherent anti-Stokes signal simultaneously from many vibrational states within a vibrational mode (see Fig. 7.1). The various components of the coherent anti-Stokes signal are separated by a monochromator, and detected by a detector array, allowing one to obtain coherent anti-Stokes Raman spectra in a single shot. In this scheme the spectral resolution is determined by the monochromator, and is usually less than for conventional coherent anti-Stokes Raman spectroscopy. The single shot capability, however, offers a much higher reliability in comparing the coherent anti-Stokes signals from the different vibrational levels.

A diagram of the coherent anti-Stokes Raman spectroscopy setup is shown in Figure 7.2. Details of the picosecond CO_2 laser used for the excitation of the molecules can be found in chapter 3. The single-mode Littman dye laser and the broad band dye laser have a bandwidth of 0.01 cm^{-1} and 200 cm^{-1}, respectively. Both lasers consist of an oscillator and two amplifier stages which are synchronously pumped by a frequency doubled Nd:YAG laser. The pulse widths of the two dye lasers after amplification are 5 ns, and the output energies are 10 mJ and 25 mJ, for the Littman dye laser and the broadband dye laser, respectively.

The coherent anti-Stokes scattering cell is 6 cm long, with anti-reflection coated windows at the ends, and NaCl window at the sides for the infrared laser beam. In the center of the cell, the infrared laser beam intersects the dye laser beams at 90°.

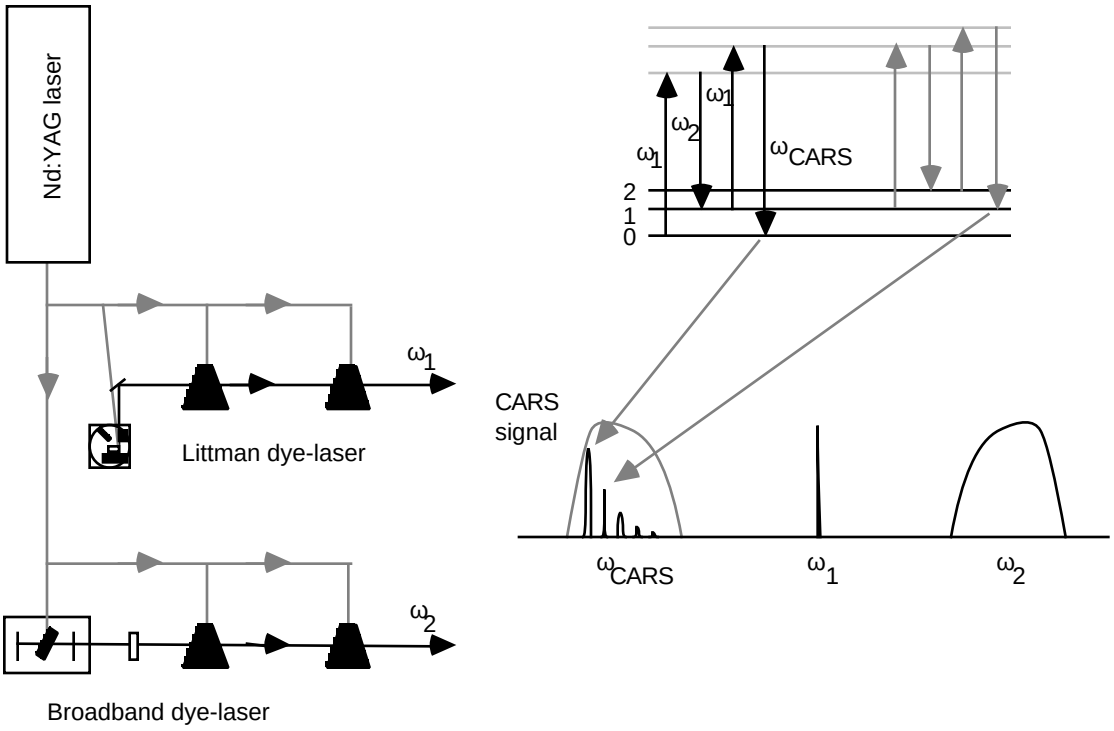

Fig. 7.1. Multiplex coherent anti-Stokes Raman spectroscopy for probing molecular vibrational levels.

Since the difference in the index of refraction of the sample gas at the two dye laser frequencies is negligible, the phase matching condition can be satisfied in both the "boxcars" and colinear configurations.[2] In the colinear configuration, the two dye laser beams are mixed through a half-reflection beam splitter and travel in the same direction.

The coherent anti-Stokes signal then travels in the same direction as the input laser beams. Since in our application the frequency of the coherent anti-Stokes output beam is very close to those of the two pumping dye lasers, it is difficult to filter out the pump beam in the colinear configuration. In the "boxcars" configuration, the two dye lasers intersect each other at an angle of 1–3 degrees. In this case, the phase matching condition is used to calculate the direction of the output beam. Because the direction of the output beam is different from the input beams, it is much easier th reject the input beams. An additional advantage of the "boxcars" configuration is that a high spatial resolution is obtained, since the coherent anti-Stokes signal is only generated at the intersection of the input beams. For these reasons the "boxcars" configuration was chosen in the experiments described below.

The detection and data acquisition systems are similar to those described in chapter 3. Either a photomultiplier or a streak camera, mounted on the back of the monochromator, is used for the detection. When a photomultiplier is used, the monochromator is scanned to obtain a spectrum. With the streak camera, the spectrum can be obtained in one single shot. As before, the energy of the CO_2 laser and dye lasers are recorded shot-by-shot for sorting and normalization of the coherent anti-Stokes signal according to Eq. (7.8). A synchronization circuit (see Fig. 7.3) was added to the laser systems to synchronize the 10-Hz Nd:YAG laser with the 0.3-Hz CO_2 laser. The circuit first issues the triggers to the flash lamp and the CO_2 laser spark gap, then it waits for the feedback signal of a high voltage sensor on the discharge plates of the CO_2 laser before issuing the *Q*-switch signal to the Nd:YAG laser. Since the firing of the Nd:YAG laser, controlled by the *Q*-switch signal, is locked to the high voltage discharge of the CO_2 laser, the intrinsic jitter between the two lasers is reduced from 200 ns to 20 ns.

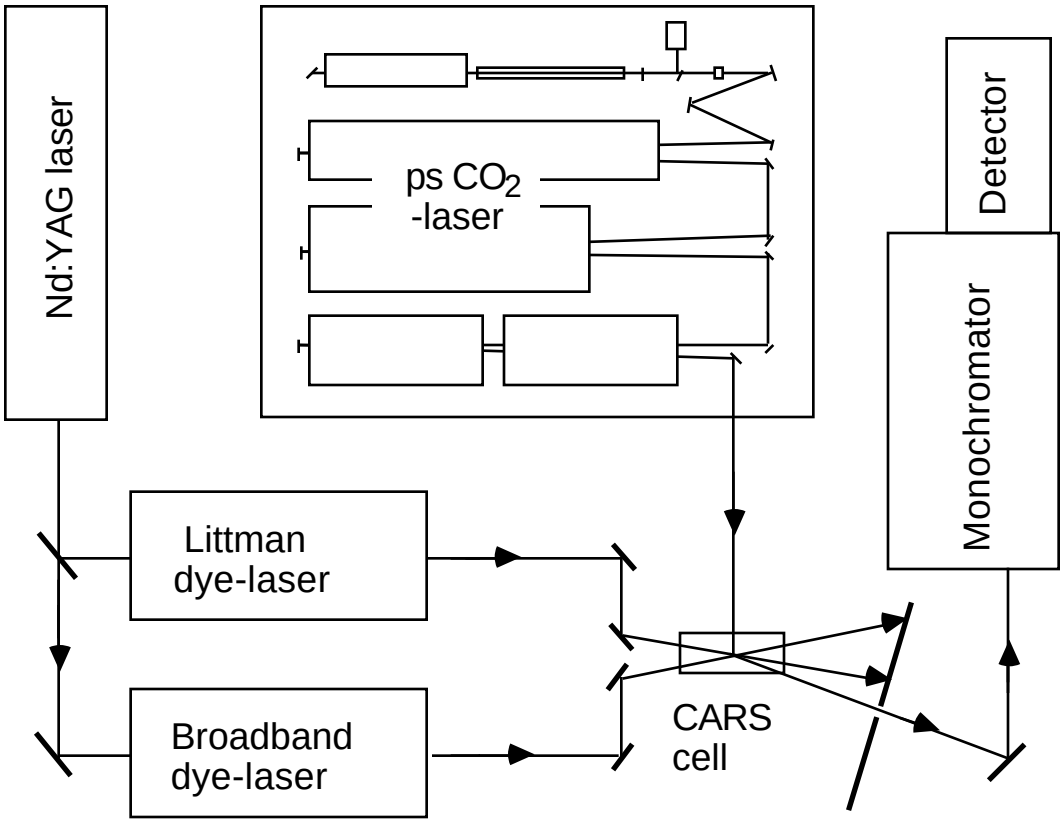

Fig. 7.2. Setup for the coherent anti-Stokes Raman spectroscopy of infrared multiphoton excited molecules. Sample molecules are excited by a picosecond CO_2 laser, and probed by coherent anti-Stokes Raman scattering. The coherent anti-Stokes Raman probe consists of a Littman single-mode dye laser and a broadband dye laser, both pumped by a Nd:YAG laser. Details of the picosecond CO_2 laser is described in chapter 3.

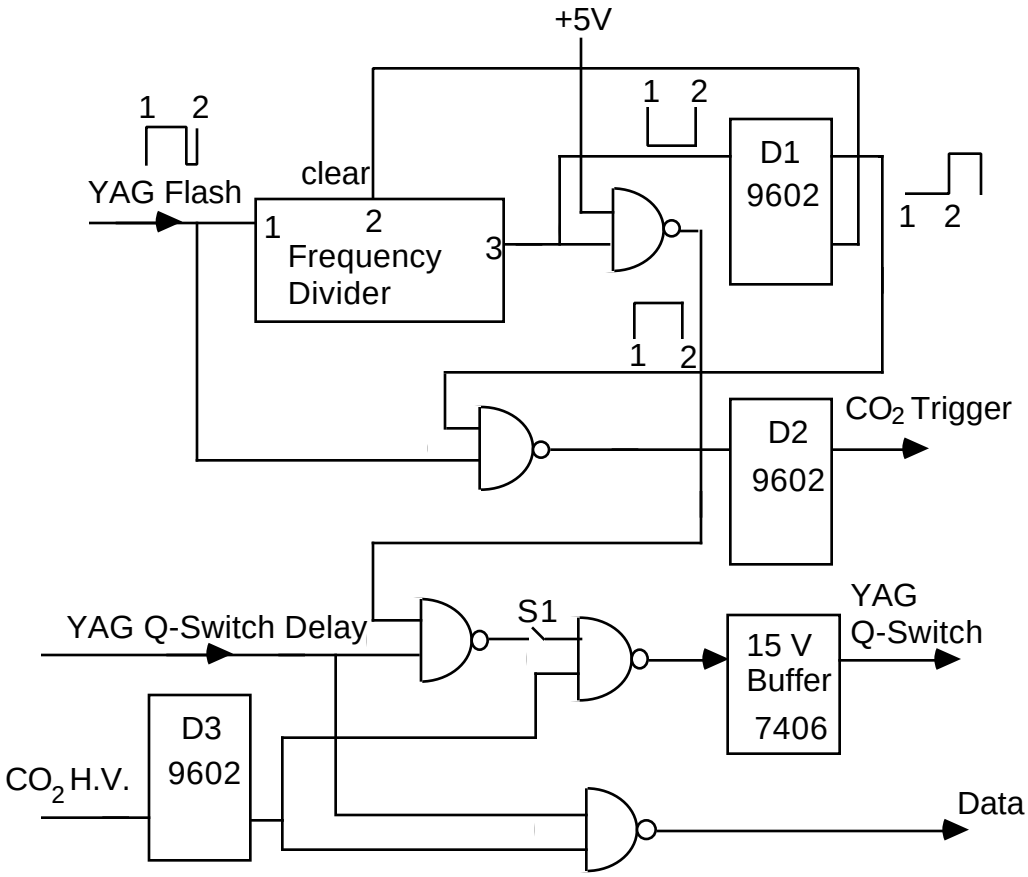

Fig. 7.3. Synchronization circuit for the Nd:YAG laser and CO_2 lasers. The frequency-divider reduces the triggering frequency of the Nd:YAG laser from 10 to 0.31 Hz. D1–D3: delay circuits.

7.4 Preliminary results

To test the coherent anti-Stokes Raman spectroscopy setup, we carried out two measurements. First, we measured the ground-state line profile of the ν_2 mode of CF_2Cl_2.

The result of this measurement is shown in Fig. 7.4. The peak of the profile is centered at 667 cm^{-1}, in agreement with the spectroscopic data reported in Refs. 7 and 8. Since the sample gas is measured at room temperature, rotational lines are not resolved. Each data point in the graph is the average of only 30 laser shots. In other words, with the 10-Hz repetition rate of the Nd:YAG laser, a measurement like this one can be performed in less than three minutes. Clearly, because of the high signal level, the data collection rate is much faster than that of the spontaneous Raman setup.

Next, we measured the population changes in the ν_1 mode of SF_6 after infrared multiphoton excitation. As in the spontaneous Raman experiment, the CO_2 laser was tuned to the 10.6 μm P(20) line, which is in resonance with the ν_3 mode of SF_6 at 965 cm^{-1}. The measurement was performed at a sample gas pressure of 1.3 kPa with 15 ns infrared pulses.

Fig. 7.5 shows the coherent anti-Stokes signal from the $0 \rightarrow 1$ transition as well as the signal from highly excited states in the quasicontinuum, shifted by 20 cm^{-1} from the band head. The graph clearly shows that as the infrared fluence increases, the coherent anti-Stokes signal from the $0 \rightarrow 1$ transition decreases quickly because of the depletion of the ground state population, while the coherent anti-Stokes signal from the quasicontinuum increases. This clearly indicates that the vibrational energy of the ν_1 mode increases as a result of the infrared pumping of the ν_3 mode, in agreement with the results of the spontaneous Raman experiments presented before.

According to Eq. (7.8), the coherent anti-Stokes signal is proportional $|\chi^{(3)}|^2$. For the $0 \rightarrow 1$ transition one has $|\chi^{(3)}|^2 \propto (\rho_1 - \rho_0)^2$ (see Ref. 2), where ρ_1 and ρ_0 are the population density of the first excited and ground state, respectively. In the spontaneous Raman experiments in chapter 4 and 5, we determined the total energy stored in the ν_1 mode as a function of infrared fluence. If one assumes an equilibrium energy distribution

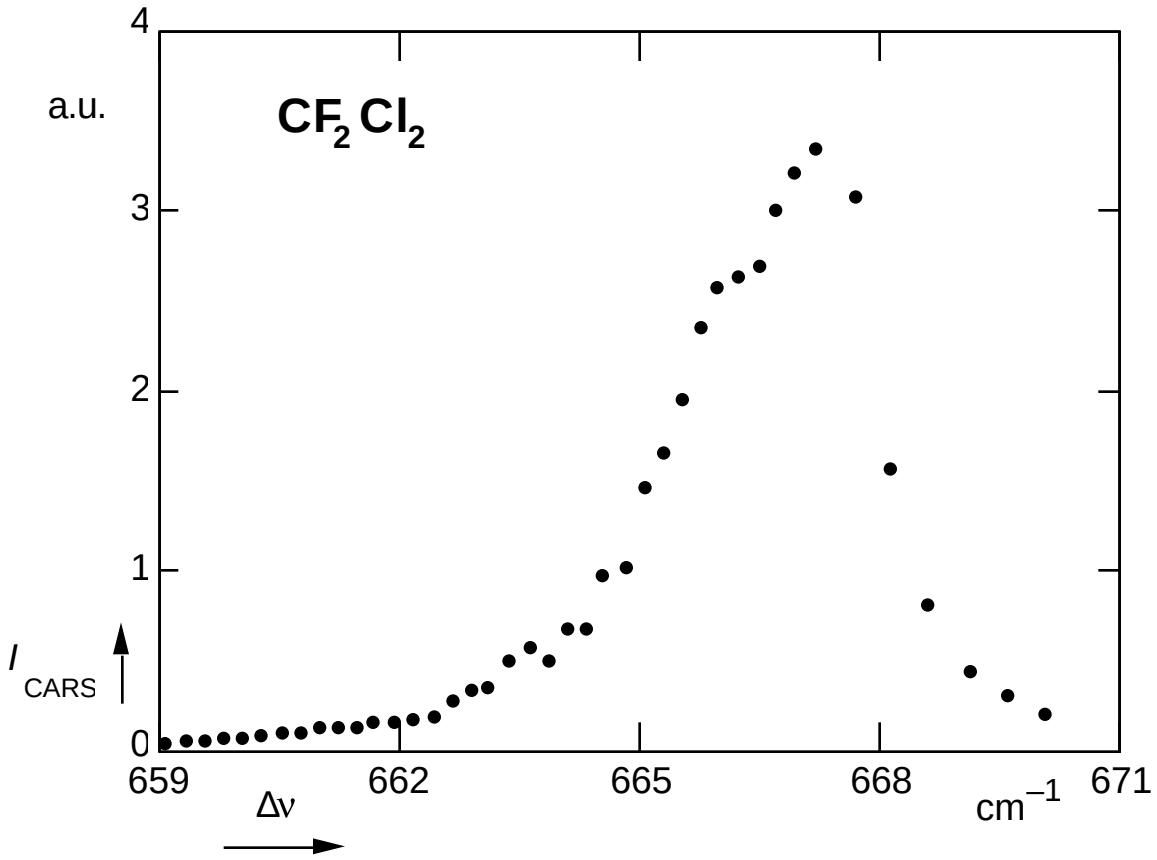

Fig. 7.4. Line profile of the ν_2 vibrational ground state of CF_2Cl_2, measured at 3.9 kPa (30 Torr) without infrared multiphoton excitation. The peak is centered at 667 cm^{-1}, in agreement with the spectroscopic data reported in Refs. 7 and 8.

within the ν_1 ladder, one can calculate the population difference $\rho_1 - \rho_0$ from the total energy. Fig. 7.6 compares the measured ground state coherent anti-Stokes signal to the

calculated value of $(\rho_1 - \rho_0)^2$. The excellent agreement suggests that the distribution within the ν_1 mode is close to equilibrium. Although this conclusion seems to be inconsistent with the result of Ref. 9, which suggests that the vibrational energy distribution within the mode is bimodal, it should be pointed out that our measurement was done at much higher fluences where the "bottlenecked" low excitation ensemble may be negligible. Also, since our measurement was done at 1.3 kPa (10 Torr) with 15 ns infrared pump pulses, it may not be completely free from collisional effects.

Although the population in the quasicontinuum must increase as the population in the low excitation states is depleted, the results in Fig. 7.5 do not show a large increase in the signal from the quasicontinuum region. This can be attributed to the fact that the coherent anti-Stokes signal from level n is proportional to $(\rho_{n+1} - \rho_n)^2$. In the quasicontinuum, for large n, the population difference between adjacent levels can be expected to be small.

7.5 Discussion

As we have seen in the previous section, coherent anti-Stokes Raman spectroscopy is a powerful tool for studying molecular dynamics. Even the preliminary experiments have produced useful results. Several improvements of the current setup of coherent anti-Stokes Raman spectroscopy are being implemented:

1) The current CO_2 laser system will be replaced with a 10-Hz picosecond mode-locked CO_2 laser. Combined with the streak camera, the system will have picosecond time resolution. In addition, the higher repetition rate will result in a better signal-to-noise ratio.

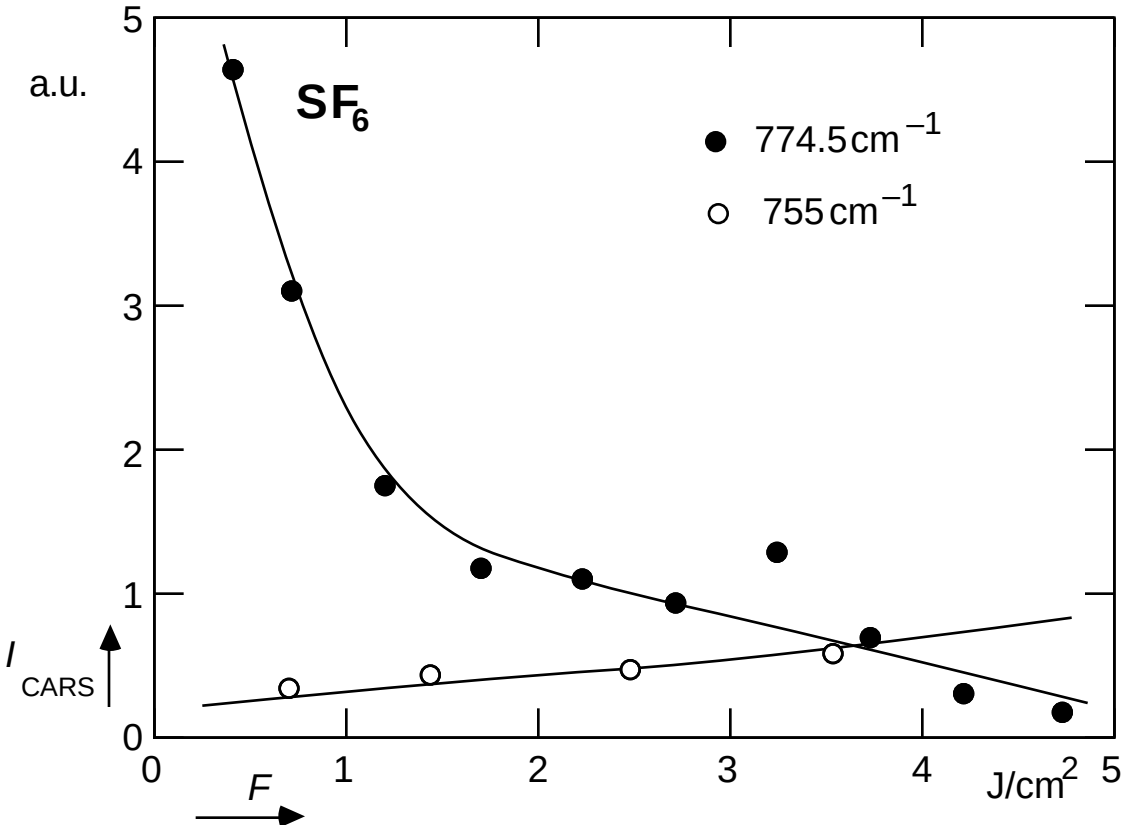

Fig. 7.5. Coherent anti-Stokes signals of the vibrational energy levels of the ν_1 mode of SF_6 measured at 1.3 kPa (10 Torr) with infrared multiphoton excitation. Closed symbols represent the signal from the transition between the ground state and the first excited state. Open symbols represent the signal from the higher excited states.

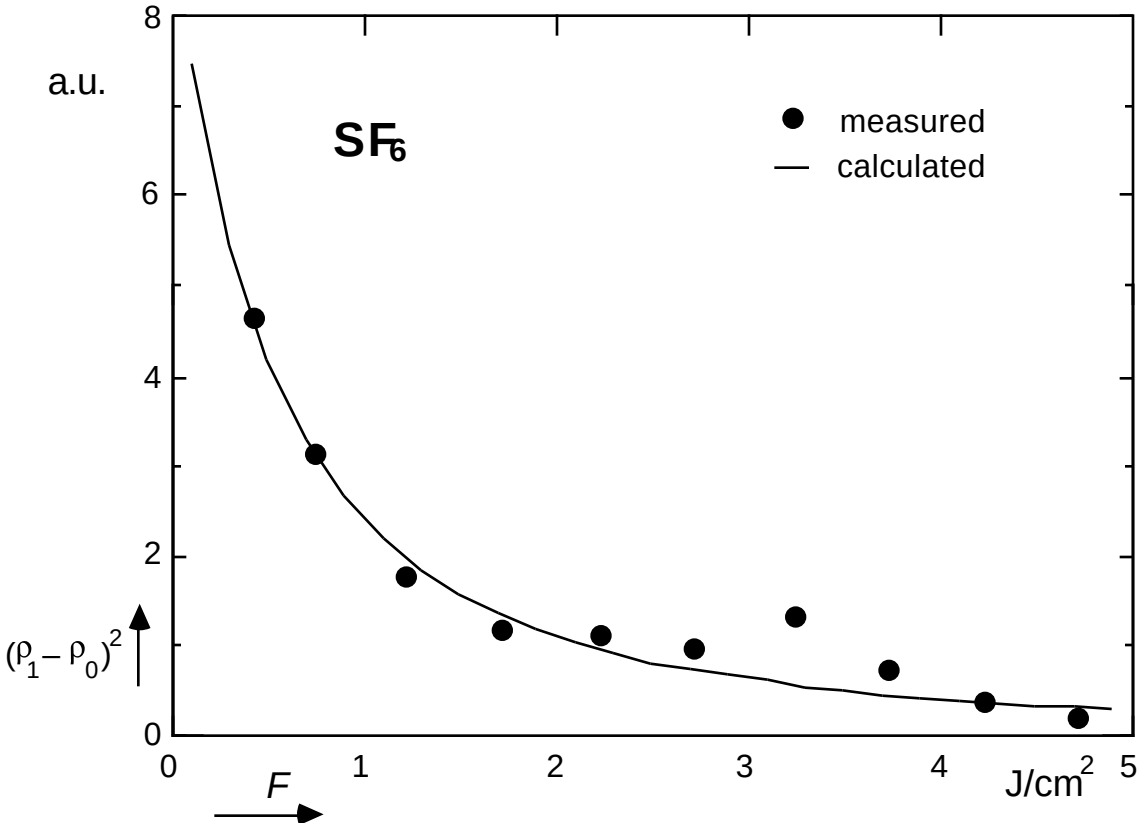

Fig. 7.6. Comparison of the measured and calculated square of the population difference between the vibrational ground and first excited state of the ν_1 mode of SF_6, $(\rho_1 - \rho_0)^2$.

2) Instead of a low pressure bulk sample, a molecular beam machine will be used. Because of the supersonic expansion, the sample molecules are cooled, so that the distribution of the initial states can be greatly narrowed.

With these improvements, it will be possible to further our understanding of intramolecular dynamic processes, not only for infrared multiphoton excitation, but also for a broad range of other physical and chemical phenomena.

References

1 Y.R. Shen, *The Principles of Nonlinear Optics* (John Wiley & sons, New York, 1984)

2 M.D. Levenson, *Introduction to Nonlinear Laser Spectroscopy* (Academic Press, New York, 1982)

3 J. W. Nibler and G. V. Knighten, Coherent anti-Stokes Raman spectroscopy, in *Raman Spectroscopy of Gases and Liquids* (A. Weber, ed.) Springer Verlag, Berlin, 1978.

4 Topics in current physics, *Coherent Nonlinear Optics*, M.S. Feld, V.S. Letokhov. Eds. (Springer Verlag, Berlin, 1980)

5 N. Bloembergen, Nonlinear Optics (W.A. Benjamin Inc., Massachusetts, 1977)

6 Michael G. Littman, Applied Optics, **23**, 24 (1984)

7 Charles A. Bradley, Jr., Phys. Rev. **40**, 908 (1932)

8 T. Shimanouchi, J. Phys. Chem. Ref. Data **6**, 993 (1977)

9 V.N. Bagratashvili, Yu.G. Vainer, V.S. Doljikov, V.S. Letokhov, A.A. Makarov, L.P. Malyavkin, E.A. Ryabov, and E.G. Sil'kis, Opt. Lett. **6**, 148 (1981)

CHAPTER 8

CONCLUSIONS

In this thesis, the intramolecular vibrational energy distribution of infrared multiphoton excited molecules is studied by time-resolved Raman spectroscopy. This chapter presents a summary of the results and conclusions.

In chapter 2 relations between the intensity of the Raman signals and the mode energy were derived. According to these relations, I_{norm}, the normalized Raman intensity, is a direct measure the average vibrational quanta in the Raman mode. Since I_{norm} is independent of the Raman cross-section of the modes, this quantity can be used to compare the energy in different Raman modes and to obtain the intramolecular vibrational energy distribution.

Experimental results for SF_6, CF_2Cl_2, CH_3CHF_2 and CF_2HCl are presented in chapters 4 and 5. The Raman scattering intensity was measured as a function of various parameters, such as time delay, infrared fluence, infrared intensity, infrared frequency and sample gas pressure. From the observed linear pressure dependence of the Raman signal it followed that the measurements are free from collisional effects. In other words, the data obtained in the experiment result solely from the interaction between the infrared radiation and single, isolated molecules, not from the collisions between molecules.

For SF_6, the energy in the Raman mode was compared with the total energy in the molecule, obtained from photoacoustic experiments. Assuming an equilibrium energy distribution, it was shown that the total energy calculated from the Raman data exactly matches the one obtained in the photoacoustic experiments. The assumption of an equilibrium energy distribution is further supported by the fact that there is no collisional relaxation of the Raman signals for SF_6. If the energy distribution were not equilibrium, collisions would change the energy in the Raman mode, and the Raman signals would not remain constant.

The linear infrared fluence dependence and small intensity dependence of the Raman signals of SF_6 agree with the quasicontinuum model, as well as with the results from photoacoustic and multiphoton-dissociation measurements. This is what one would expect for an equilibrium intramolecular energy distribution, since in that case the Raman mode energy is proportional to the total energy. The intensity dependence of the Raman signals is most significant at low pump energy. This indicates that in this region the coherence of the excitation is not completely lost.

The infrared pumping frequency dependence has a profile similar to the small-signal linear absorption, except that it is displaced toward the low frequency side due to the anharmonicity of the mode. Since the total profile is the convolution of the profile for each individual absorption step, it should be narrower than the linear absorption profile. However, this expected narrowing effect seems to be compensated by power broadening and anharmonicity shifts. The frequency dependence profile agrees with the infrared multiphoton absorption profile as well as the frequency dependence of the infrared multiphoton dissociation probability reported in the literature. This indicates that the anti-Stokes Raman signal is proportional to the total vibrational energy stored in the molecule

for *all* the CO_2-lines within the absorption profile, and not only for the center frequency. Therefore the intramolecular vibrational energy equilibrium appears to be established for infrared multiphoton excitation at all frequencies that lie within the absorption profile of SF_6.

In contrast to SF_6, measurements on CF_2Cl_2, CH_3CHF_2 and CF_2HCl show highly nonequilibrium intramolecular energy distributions. In CF_2Cl_2, where two modes can be pumped by the CO_2 laser, the pump mode always contains most energy after excitation. Since the observed nonequilibrium energy distribution does not depend on pumping fluence, it cannot be the result of averaging one highly excited equilibrium ensemble and one "bottlenecked" nonequilibrium ensemble at low excitation, because the relative fractions of these two ensembles change with the pumping fluence. As buffer gas is added to the sample, the nonequilibrium distribution relaxes back to equilibrium because of collisional relaxation. The time dependence of the nonequilibrium energy distribution shows that collisional relaxation occurs on a much longer time scale (μs) than intramolecular energy transfer (ps).

As we have seen, in the spontaneous Raman experiment both cases of intramolecular equilibrium below the dissociation threshold, as well as cases of nonequilibrium close to dissociation were found. This shows that the well-established intramolecular equilibrium in infrared multiphoton *dissociation* experiments cannot be generally extended to infrared multiphoton excitation. From the point of view of classical nonlinear dynamics, as the energy increase, mode couplings will gradually break down the regularity of the phase space trajectory. For a completely irregular (stochastic or chaotic) trajectory the energy distribution is equilibrium, while for the regular, quasiperiodic trajectories the energy is localized. Depending on how the regular, quasiperiodic

trajectories are perturbed by the intermode couplings, equilibrium can be established among all the vibrational modes or among only a subset of the modes.

The KAM theorem states that at low energy, mode couplings will not render the phase space trajectory irregular unless the commensurate frequencies condition (1.1) is satisfied. This provides us a way to explain the difference between the observation for SF_6 and CF_2Cl_2. From the KAM theorem, one would expect that the more often condition (1.1) is satisfied, the more likely the distribution will be equilibrium. In chapter 1 for both SF_6 and CF_2Cl_2, the number of times condition (1.1) is satisfied as a function of the energy involved was calculated. The result of this calculation shows that the experimental results agree with what one would expect from the KAM theorem.

Although the KAM theorem was originally derived to explain how a system can become ergodic, it can be applied to the infrared multiphoton excitation and provide insights on how nonresonant modes participate in the excitation process. In particular, our study shows that in addition to the density of states, which increases rapidly with the size of the molecule, condition (1.1) is also an important factor for the intramolecular energy distribution.

APPENDIX A

PROGRAMS FOR THE KAM THEOREM

A.1 Program for CF_2Cl_2

```
#include <stdio.h>
#define NMODE 9
#define ZERO 20
#define BOUND 10000
#define UNIT 1000

int lamda[NMODE] = {1098, 667, 457, 261, 322, 1167, 446, 923, 433};
int cindex[NMODE];
float count[100];

main()
{
extern int lamda[];
extern int cindex[];
extern float count[];
FILE *log, *fopen();
register int i;

if((log = fopen("sfrf.log", "w")) == NULL)
exit(1);

charm(NMODE-1, BOUND);
fprintf(log, "energy          count\n\n");
printf("energy      count\n\n");
for(i=0; i<BOUND/UNIT; i++){
fprintf(log, "%d    %.3g\n", i, count[i]);
printf("%d          %.3g\n", i, count[i]);
}
}
```

```
charm(ith_mode, bound)
int ith_mode, bound;
{
extern int cindex[];
extern int lamda[];
extern float count[];
register int left, com, i;

if (ith_mode == 0){
for(cindex[ith_mode] = -bound/lamda[ith_mode];
cindex[ith_mode] <= bound/lamda[ith_mode]; cindex[ith_mode]++){

left = bound - abs(cindex[ith_mode])*lamda[ith_mode];

com = 0;
for(i=0; i<NMODE; i++)
com += cindex[i]*lamda[i];

if(abs(com) < ZERO){
count[(BOUND-left)/UNIT] += 1.0;
}
}
}
else{
for(cindex[ith_mode] = -bound/lamda[ith_mode];
cindex[ith_mode] <= bound/lamda[ith_mode]; cindex[ith_mode]++){

charm(ith_mode-1, bound - abs(cindex[ith_mode])*lamda[ith_mode]);
}
}
}
```

A.2 Program for SF_6

```
#include <stdio.h>
#define NMODE 15
#define ZERO 20
#define BOUND 10000
#define UNIT 1000

int lamda[NMODE] = {775, 644, 644, 965, 965, 965, 617, 617, 617, 524, 524, 524, 363, 363, 363};
int cindex[NMODE];
float count[100];

main()
{
extern int lamda[];
extern int cindex[];
extern float count[];
FILE *log, *fopen();
register int i;

if((log = fopen("sfrf.log", "w")) == NULL)
exit(1);

charm(NMODE-1, BOUND);
fprintf(log, "energy          count\n\n");
printf("energy      count\n\n");
for(i=0; i<BOUND/UNIT; i++){
fprintf(log, "%d     %.3g\n", i, count[i]);
printf("%d          %.3g\n", i, count[i]);
}
}


charm(ith_mode, bound)
int ith_mode, bound;
{
extern int cindex[];
extern int lamda[];
extern float count[];
register int left, com, i;

if (ith_mode == 0){
for(cindex[ith_mode] = -bound/lamda[ith_mode];
cindex[ith_mode] <= bound/lamda[ith_mode]; cindex[ith_mode]++){

left = bound - abs(cindex[ith_mode])*lamda[ith_mode];

com = 0;
for(i=0; i<NMODE; i++)
com += cindex[i]*lamda[i];

if(abs(com) < ZERO){
count[(BOUND-left)/UNIT] += 1.0;
```

```
}
}
}
else{
for(cindex[ith_mode] = -bound/lamda[ith_mode];
cindex[ith_mode] <= bound/lamda[ith_mode]; cindex[ith_mode]++){

charm(ith_mode-1, bound - abs(cindex[ith_mode])*lamda[ith_mode]);
}
}
}
```

APPENDIX B

DATA ANALYSIS PROGRAMS

B.1 Data analysis programs

fanalyze.c

```
#include<math.h>
#include<stdio.h>
#include<signal.h>
#include<sys/types.h>
#include<sys/stat.h>
#include<sgtty.h>
#include"constant.h"
#include"data.h"
#include"plot.h"


int         restric, rstrmin, rstrmax, functiontype, pipe_pid, job, tmpfile,
            file, shotnum, channum;
char        termtype[TCL], dname[60], sname[15];
double      fitparam[MAXTERMS];

main (argc, argv)
int     argc;
char   *argv[];

{
   extern int  job, tmpfile;

   extern char termtype[], dname[];
```

```
 struct sgttyb   fbuf;
 struct stat                    bufa, bufb;

 char    rbuf[80], df[100], tp[100], pf[100], *tplate, *mktemp();

int    fitflag;


 switch (argc) {
          case 1:
             dname[0] = '\0';
             break;
          case 3:
              sprintf (dname, "/usr/meas/output/%s/%s", argv[1], argv[2]);
             break;
          case 2:
             sprintf (dname, "%s", argv[1]);
                    if( strncmp( dname, "/usr/meas/output/", 17) == 0)
                    break;
          default:
             printf ("Usage: fanalyze [system file]\n");
             exit (-1);
}

 if (setterm () == -1)
          exit (0);
 if (strcmp (termtype, "pro") != 0 &&
             strcmp (termtype, "tek4014") != 0 &&
             strcmp (termtype, "vt100") != 0) {
          printf ("\07\nYou cannot plot on this terminal!\n");
          hitrtc ();
          exit (0);
}
 clearscreen ();
 dataname ();
 for (;;) {
          clearscreen ();
          printf ("\
                    fanalyze v%d.%d (%d-%d-19%d)    (c) Molecular Physics\n\n\n\
                              FANALYZE PROGRAM MAIN MENU:\n\n\n\
                              1) Information on %s\n", EDITION, VERSION,
                    DAY, MONTH, YEAR, dname),
             printf ("\
                              2) Analyze and plot\n\
                              3) Select another file\n\
                              4) Enter data manually\n");
          printf ("\
                              5) Invoke local shell\n\
                              6) Return to Main Menu\n\
                              7) Help\n\Select one:\n");
          qcursor();
          job = getnum (1, 7);
          clearscreen ();
          switch (job) {
             case 1:
```

```
                sprintf(tp, "expose %s", dname);
                system(tp);
                break;
        case 2:
                if( file != 0 )
                        close(file);
                if( dataname() == -1)
                break;
        if ((file = open (dname, 0)) == -1) {
                printf ("\n\07Fail to open %s.\n", dname);
                hitrtc ();
                localsh("FANALYZE");
                break;
        }
                getinfo ();
                tplate = "dplotXXXXXX";
                mktemp(tplate);
                sprintf( df, "/usr/meas/tmp/%s", tplate);
                for(;;){
                if ((tmpfile = creat(df, 0644)) == -1){
                   printf ("Can't open tmpfile %s\
Hit carriage return to enter shell.                ", df);
                   ioctl (0, TIOCFLUSH, &fbuf);
                   read (0, rbuf, 80);
                        localsh("FANALYZE");
                }
                else
                        break;
                }
                for(;;){
                system("vi +14 /usr/meas/src/getdots.c");
                stat("/usr/meas/src/getdots.c", &bufa);
                stat("/usr/meas/src/getdots", &bufb);
                if( bufa.st_mtime < bufb.st_mtime )
                break;
                if( system("cc -o /usr/meas/src/getdots \
/usr/meas/src/getdots.c -lm") == 0 )
                break;
                else
                hitrtc();
                }
                getdata ();
                close (tmpfile);
                printf ("\n\nFit a function to the data points?\n");
                qcursor();
                fitflag = NO;
                if (getyn () == 'y') {
                   fitflag = YES;
                   sprintf(tp, "fit %s", df);
                   system(tp);
                }
                tplate = "plotXXXXXX";
                mktemp(tplate);
                sprintf( pf, "/usr/meas/tmp/%s", tplate);
                for(;;){
```

```
                        for(;;){
                    if ((tmpfile = creat(pf, 0644)) == -1){
                        printf ("Can't open tmpfile %s\
Hit carriage return to enter shell.                    ", pf);
                        ioctl (0, TIOCFLUSH, &fbuf);
                        read (0, rbuf, 80);
                            localsh("FANALYZE");
                    }
                    else
                            break;
                    }
                        close(tmpfile);
                        sprintf(tp,"plotit %s %s", df, pf);
                        system(tp);
                        saveplot (df, pf);
                        if (fitflag == YES)
                            printf ("Another fit to the same points?\n");
                        else
                            printf ("Fit a function to these datapoints?\n");
                        qcursor();
                        if (getyn () == 'y') {
                            fitflag = YES;
                            sprintf(tp,"fit %s", df);
                            system(tp);
                          }
                        else
                            break;
                    }
                    unlink(df);
                    break;
                case 3:
                    if( file != 0 )
                            close(file);
                    dname[0]='\0';
                    dataname ();
                    break;
                case 4:
                    system ("enterdata");
                    break;
                case 5:
                    localsh("FANALYZE");
                    break;
                case 6:
                    if( pipe_pid != 0 )
                    kill(pipe_pid, SIGKILL);
                    exit (0);
                    break;
                case 7:
                    system ("more /usr/meas/help/analyze");
                    help ();
                    hitrtc ();
            }
    }
}
```

```
dataname () {

    extern char dname[], sname[];
    struct stat stbuf;
   int     s;
    char    buf[50];

            for(;;){
            if (dname[0] == '\0') {
                clearscreen ();
                printf ("\n\n\nSystem:\n");
                qcursor();
                scanf ("%s", sname);

                printf ("\nFilename:\n");
                qcursor();
                scanf ("%s", buf);
                sprintf (dname, "/usr/meas/output/%s/%s", sname, buf);
            }
            s = stat (dname, &stbuf);
            if (s == -1) {
                printf ("The file '%s' does not exist!\n\n\
Do you want to create it and enter data manually?\n", dname);
                qcursor();
                if (getyn () == 'y') {
                        sprintf (buf, "enterdata %s", dname);
                        system (buf);
                        break;
                   }
                else
                        {
                        dname[0] = '\0';
                        return (-1);
                        }
            }
            else
                        break;
   }
    return (0);
}

getinfo () {
    externint  file, shotnum, channum;
    long    lseek();

    lseek (file, PSHOTNUM, 0);
    read (file, &shotnum, 2);

    lseek (file, PCHANNUM, 0);
    read (file, &channum, 2);
}

saveplot (df, pf)
char *pf, *df;
```

```
{
    char dataname[60], plotname[60];
    extern char termtype[];
    struct stat stbuf;
   int     i, dump;
    char    cmd[100], *lf, *savelog();

   dump = NO;
    printf ("Save this plot?\n");
    qcursor();
   if (getyn () == 'y') {
   for (i = 1;; i++) {
            sprintf (plotname, "%s_p%d", dname, i);
            if (stat (plotname, &stbuf) == -1) {
               break;
            }
   }
            link(pf, plotname);
            unlink(pf);
            sprintf (dataname, "%s_d%d", dname, i);
            sprintf (cmd, "cp %s %s", df, dataname);
            system(cmd);
            lf = savelog(plotname, dataname);
            chgename(dataname, plotname, plotname);
            sprintf(cmd, "grep -h -v '+++' /usr/meas/src/getdots.c >> %s", lf);
            system(cmd);
   }
   else
            {
            dump = YES;
            unlink(pf);
            }
   if (strcmp (termtype, "pro") == 0) {
            printf ("Print this plot?\n");
            qcursor();
            if (getyn () == 'y') {
                        if( dump == YES){
                        lf = "tmpplot.log";
    sprintf(cmd, "grep -h -v '+++' /usr/meas/src/getdots.c >> %s", lf);
    system(cmd);
                        system ("lscreen;lscreen -bic\
                              /usr/meas/tmp/clr_name;\
                               pplot /usr/meas/tmp/name_tmp;pscreen");
                        }
                  else {
                              sprintf(cmd, "/usr/bin/pplot %s", plotname);
                              system (cmd);
                              cursorhome();
                              system ("pscreen");
                        }
                        sprintf(cmd, "lpr -n %s", lf);
                        printf("\07\07\n\nPlease rewind the paper on printer to \
print additional information...\n");
                        hitrtc();
                        system(cmd);
```

```
                clearscreen ();
               }
   }
if(dump == YES)
unlink(lf);
}

char *savelog(plotname, dataname)
char *plotname, *dataname;
{
        extern int          restric, rstrmin, rstrmax, functiontype;
        extern double       fitparam[];
        static char         log[100];
        int                 i, tmp, fd;
        FILE                *fp, *fopen();

        sprintf(log, "%s.log", plotname);
                for(;;){
                if ((tmp = creat(log, 0644)) == -1){
                   printf ("Can't open tmpfile %s\
Hit carriage return to enter shell.                ", log);
                        hitrtc();
                        localsh("FANALYZE");
                }
                else
                        break;
                }
        if ( ( fp = fdopen(tmp, "w")) == NULL )
                {
                printf("\n\nFail to open %s\n", log);
                hitrtc();
                return(NULL);
                }
        for(;;){
        if( (fd = open(dataname, 0)) == -1){
        printf("\n\n\07Fail to open %s,\n\
Hit CR to enter shell.", dataname);
        hitrtc();
        localsh("FANALYZE");
        }
        else
                break;
        }
        switch( restric ){
        case 0:
                break;
        case 1:
        fprintf(fp, "\n\nReject shot# outside %d %d\n", rstrmin, rstrmax);
                break;
        case 2:
        fprintf(fp, "\n\nReject shot# between %d %d\n", rstrmin, rstrmax);
                break;
        }
        lseek(fd, PFTYPE, 0);
        read(fd, &functiontype, 2);
```

```
        for(i=0; i<MAXTERMS; i++){
        lseek(fd, PFITPAR(i), 0);
        read(fd, &fitparam[i], 8);
        }
        if( functiontype != 0){
        fprintf(fp,"\nFit Function : Type %d\n", functiontype);
        fprintf(fp,"        parameters : ");
        for(i=0; i<5; i++)
                fprintf(fp, "a[%d]=%.5g ", i, fitparam[i]);
        fprintf(fp, "\n                   ");
        for(i=5; i<10; i++)
                fprintf(fp, "a[%d]=%.5g ", i, fitparam[i]);
        }
        fprintf(fp, "\n\n");
        fclose(fp);
        close(fd);
        return(log);
}

openpipe(p, q)
int p[2], q[2];
{
        extern int pipe_pid;

        if( pipe(p) < 0 || pipe(q) < 0 )
        return(-1);
        if( ( pipe_pid = fork()) == 0 ){
        close(0);
        dup(p[0]);
        close(p[0]);
        close(1);
        dup(q[1]);
        close(q[1]);
        execl("/usr/meas/src/getdots", "getdots", 0);
        }
        if( pipe_pid == -1 )
                return(-1);
        return(0);
}

getdata()
{
        int     intnum, errorflag, p[2], q[2], c, dinfo[3],
                nplot;
        extern  int     restric, rstrmin, rstrmax, kplot, file, tmpfile,
                        channum, shotnum;
        float   ybegin, ylength, ymin, ymax,
                finfo[2], xbegin, xlength, getf(), xdata, ydata, splot;
        register int    i;
        long    lseek();
        char    xsym[10], ysym[10], xunit[10], yunit[10], buf[10];
        extern  char    sname[], dname[];
        struct {
                float   x;
                float   y;
```

```
                float       s;
                int         n;
                } transbuf;

        clearscreen();
        printf ("\nEnter the symbols and units:\n\n\
                                        Symbol Y-axis:\n");
        qcursor();
        scanf ("%s", ysym);
        printf ("\t\t\t\tUnit   Y-axis:\n");
        qcursor();
        scanf ("%s", buf);
        if (buf[0] == '.')
                sprintf (yunit, "a.u.");
        else
                sprintf (yunit, "%s", buf);
        printf ("\t\t\t\tSymbol X-axis:\n");
        qcursor();
        scanf ("%s", xsym);
        printf ("\t\t\t\tUnit   X-axis:\n");
        qcursor();
        scanf ("%s", buf);
        if (buf[0] == '.')
                sprintf (xunit, "a.u.");
        else
                sprintf (xunit, "%s", buf);

    lseek(tmpfile, SYSNAME, 0);
    write(tmpfile, sname, 15);
    lseek(tmpfile, PLOTNAME, 0);
    write(tmpfile, rindex(dname, '/') + 1, 15);
    lseek(tmpfile, XSYM, 0);
    write(tmpfile, xsym, 10);
    lseek(tmpfile, YSYM, 0);
    write(tmpfile, ysym, 10);
    lseek(tmpfile, XUNIT, 0);
    write(tmpfile, xunit, 10);
    lseek(tmpfile, YUNIT, 0);
    write(tmpfile, yunit, 10);

    clearscreen();
    printf ("\n\
Enter:                                                  X-origin: ");
    xbegin = getf ();
    printf ("\n\
                                                        X-full scale: ");
    xlength = getf () - xbegin;

        lseek (tmpfile, XBEGIN, 0);
        write (tmpfile, &xbegin, 4);
        lseek (tmpfile, XLENGTH, 0);
        write (tmpfile, &xlength, 4);

        printf ("\n\
Average Y-data in how many intervals?                           ");
```

```
            intnum = getnum (0, 200);

printf("\n\
Reject shot# ?                          Enter    0) don't reject\n\
                                                 1) reject outside\n\
                                                 2) reject between\n");
        qcursor();
        if( (restric = getnum(0,2)) != 0){
        printf("\n\
                                                 minimum = \n");
        qcursor();
        rstrmin = getnum(0, shotnum-1);
        printf("\n\
                                                 maximum = \n");
        qcursor();
        rstrmax = getnum(rstrmin, shotnum-1);
        }
            printf ("\n\
Plot with error bars?                                                    ");
            errorflag = NO;
            if (getyn () == 'y')
                    errorflag = YES;
            lseek (tmpfile, PFLAG, 0);
            write (tmpfile, &errorflag, 2);

        while( openpipe(p,q) == -1){
        printf("\nFail to open pipes, check if there are too many process\
runing....\n");
        hitrtc();
        localsh("FANALYZE");
        }
   printf("\n\n\n\n");
        switch(restric){
        case 0:
                dinfo[0] = shotnum;
                break;
        case 1:
                dinfo[0] = rstrmax - rstrmin + 1;
                break;
        case 2:
                dinfo[0] = shotnum - rstrmax + rstrmin + 1;
                break;
        }
        dinfo[1] = channum; dinfo[2] = intnum;
        write(p[1], dinfo, 6);
        read(q[0], &c, 2);
        finfo[0] = xbegin; finfo[1] = xlength/intnum;
        write(p[1], finfo, 8);
        read(q[0], &c, 2);

        turbo(restric, rstrmin, rstrmax, p, q);
        ymin = 1.0e37;
        ymax = -1*ymin;
        kplot = 0;
        read(q[0], &kplot, 2);
```

```
        write(p[1], &c, 2);
        for( i=0; i<kplot; i++){
                read(q[0], &transbuf, 14);
                write(p[1], &c, 2);
                xdata = transbuf.x;
                ydata = transbuf.y;
                splot = transbuf.s;
                nplot = transbuf.n;
                lseek (tmpfile, PXPLOT (i), 0);
                write (tmpfile, &xdata, 4);
                lseek (tmpfile, PYPLOT (i), 0);
                write (tmpfile, &ydata, 4);
                lseek (tmpfile, PSPLOT (i), 0);
                write (tmpfile, &splot, 4);
                lseek (tmpfile, PNPLOT (i), 0);
                write (tmpfile, &nplot, 2);
                if (ydata > ymax)
                   ymax = ydata;
                if (ydata < ymin)
                   ymin = ydata;
        }
        lseek (tmpfile, PKPLOT, 0);
        write (tmpfile, &kplot, 2);

   clearscreen();
   printf ("\n\
Y values:          min = %.4g          max = %.4g\n\n\
Enter:                                Y-origin: ", ymin, ymax);
   ybegin = getf ();
   printf ("\
                                Y-full scale: ");
   ylength = getf () - ybegin;

        lseek (tmpfile, YBEGIN, 0);
        write (tmpfile, &ybegin, 4);
        lseek (tmpfile, YLENGTH, 0);
        write (tmpfile, &ylength, 4);

        close(p[1]);
        close(q[0]);
}
```

getdots.c

```
#include<stdio.h>                                                    /*+++*/
#include<math.h>                                                     /*+++*/
#define     MAXCH       18                          /*+++*/
#define     OUTSIDE             1                    /*+++*/
#define     BETWEEN             2                    /*+++*/
                                                                     /*+++*/
transform(d, chnum, xp, yp, zp, file)                                /*+++*/
int     chnum;                                                       /*+++*/
float   d[], *xp, *yp, *zp;                                          /*+++*/
FILE    *file;                                                       /*+++*/
```

```
{                                                                       /*+++*/
int i;                                                                  /*+++*/
float x, y, z, plasma, red, flu, ir, F, tphc, uv, pmt, man, Iso, shot;  /*+++*/
float yaver;                                                            /*+++*/
float   rmax[MAXCH], rmin[MAXCH];                                       /*+++*/
static  int     rtyp[MAXCH];                                            /*+++*/
                                                                        /*+++*/
/***************** YOUR MANIFESTATION **********************/
plasma = d[0]; red = d[1]; flu = d[2]; ir = d[3]; tphc = d[4];
uv = d[5]; pmt = d[6]; man = d[7]; shot = d[8];
rtyp[0] = OUTSIDE; rmin[0] = 1000; rmax[0] = 5000;
rtyp[1] = OUTSIDE; rmin[1] = 600; rmax[1] = 5000;
rtyp[2] = OUTSIDE; rmin[2] = -200; rmax[2] = 200;
rtyp[3] = OUTSIDE; rmin[3] = 350; rmax[3] = 1379;
rtyp[4] = OUTSIDE; rmin[4] = 800; rmax[4] = 4000;
rtyp[5] = OUTSIDE; rmin[5] = 200; rmax[5] = 5000;
rtyp[6] = OUTSIDE; rmin[6] = -10; rmax[6] = 5000;
rtyp[7] = OUTSIDE; rmin[7] = 336.2; rmax[7] = 336.2;
if( checkshot (d, chnum, rtyp, rmax, rmin) == -1 ) return(-1);
        ir = (ir - 14.6)/7.15;
        uv = (uv + 3.26)/539;
        Iso = 22.3/3*2;
        tphc = tphc/1570 - 0.5;
        F = ir * .0393;
        x = F;
        y = pmt/uv/Iso;
        z = 1;

/***************** END OF YOUR WORK ***********************/          /*+++*/
                                                                        /*+++*/
        *xp = x; *yp = y; *zp = z;                                      /*+++*/
        return(0);                                                      /*+++*/
}                                                                       /*+++*/
                                                                        /*+++*/
checkshot (d, chnum, rtyp, rmax, rmin)                                  /*+++*/
float   d[], rmax[], rmin[];                                            /*+++*/
int     chnum, rtyp[];                                                  /*+++*/
{                                                                       /*+++*/
   int i;                                                               /*+++*/
                                                                        /*+++*/
   for (i = chnum; i >= 0; i--)                                         /*+++*/
        {                                                               /*+++*/
        if ( rtyp[i]==1 && (d[i] > rmax[i] ||                           /*+++*/
                d[i] < rmin[i]))                                        /*+++*/
                return (-1);                                            /*+++*/
        if ( rtyp[i]==2 && d[i] < rmax[i] && d[i] > rmin[i] )    /*+++*/
                return(-1);                                             /*+++*/
        }                                                               /*+++*/
   return (0);                                                          /*+++*/
}                                                                       /*+++*/
                                                                        /*+++*/
main()                                                                  /*+++*/
{                                                                       /*+++*/
        FILE    *file, *fopen();                                        /*+++*/
int     chnum, shnum, n[200], dinfo[3], i, j, c, intnum, kplot;  /*+++*/
```

```
float   x[200], y[200], s[200], intlen, xbegin, finfo[2],                   /*+++*/
        xval[200], yval[200], zval[200], y2val[200],            /*+++*/
        xdata, ydata, zdata, d[MAXCH];                          /*+++*/
        double  sqrt();                                                     /*+++*/
        struct  {                                                           /*+++*/
                float   x;                                                  /*+++*/
                float   y;                                                  /*+++*/
                float   s;                                                  /*+++*/
                int     n;                                                  /*+++*/
                } plotbuf;                                                  /*+++*/
                                                                            /*+++*/
        read(0, dinfo, 6);                                          /*+++*/
        write(1, &c, 2);                                            /*+++*/
        read(0, finfo, 8);                                          /*+++*/
        write(1, &c, 2);                                            /*+++*/
        shnum = dinfo[0]; chnum = dinfo[1]; intnum = dinfo[2];/*+++*/
        xbegin = finfo[0]; intlen = finfo[1];                       /*+++*/
        for (j = 0; j < intnum; j++) {                              /*+++*/
                n[j] = 0;                                           /*+++*/
                xval[j] = 0;                                                /*+++*/
                yval[j] = 0;                                                /*+++*/
                zval[j] = 0;                                                /*+++*/
                y2val[j] = 0;                                               /*+++*/
        }                                                                   /*+++*/
                                                                            /*+++*/
        file = fopen("/usr/meas/src/fanalog", "w");                 /*+++*/
  for (i = 0; i<shnum; i++){                                        /*+++*/
        read(0, d, 4*MAXCH);                                        /*+++*/
        write(1, &c, 2);                                            /*+++*/
        if(transform(d, chnum, &xdata, &ydata, &zdata, file) == -1)/*+++*/
                continue;                                                   /*+++*/
        for (j = 0; j < intnum; j++)                                /*+++*/
        if (xdata >= (xbegin + ((float) j ) * intlen)               /*+++*/
        && xdata < (xbegin + ((float) j + 1 ) * intlen)) {          /*+++*/
                  yval[j] = yval[j] + ydata;                        /*+++*/
                  xval[j] = xval[j] + xdata;                        /*+++*/
                  zval[j] = zval[j] + zdata;                        /*+++*/
                  y2val[j] = y2val[j] + ydata * ydata;              /*+++*/
                  n[j] = n[j] + 1;                                  /*+++*/
                        break;                                              /*+++*/
        }                                                                   /*+++*/
  }                                                                         /*+++*/
                                                                            /*+++*/
  kplot = 0;                                                                /*+++*/
  for(i = 0; i < intnum; i++){                                  /*+++*/
        if ( n[i] != 0) {                                               /*+++*/
/***************** YOUR MANIFESTATION **********************/             /*+++*/

                y[kplot] = yval[i] / zval[i];
                x[kplot] = xval[i] / n[i];
                if( n[i] > 1 )
s[kplot] = (float)sqrt((y2val[i] - n[i] * y[kplot] * y[kplot] ))*n[i]
                /(n[i] - 1)/zval[i];
                else
                        s[kplot] = 1.0e37;
```

```
/***************** END OF YOUR WORK ***********************/
                        n[kplot] = n[i];                                    /*+++*/
                        kplot++;                                            /*+++*/
            }                                                                       /*+++*/
    }                                                                               /*+++*/
            write(1, &kplot, 2);                                                    /*+++*/
            read(0, &c, 2);                                                 /*+++*/
     for(i = 0; i < kplot; i++){                                            /*+++*/
            plotbuf.x = x[i];                                               /*+++*/
            plotbuf.y = y[i];                                               /*+++*/
            plotbuf.s = s[i];                                               /*+++*/
            plotbuf.n = n[i];                                               /*+++*/
            write(1, &plotbuf, 14);                                         /*+++*/
            read(0, &c, 2);                                                 /*+++*/
    }                                                                               /*+++*/
}                                                                                   /*+++*/
```

turbo.c

```
#include"data.h"
#include"constant.h"
#include<stdio.h>

long        count;
int         file, channum, shotnum, call, shnum;

turbo(restric, rstrmin, rstrmax, p, q)
int restric, rstrmin, rstrmax, p[], q[];
{
            extern long         count;
            extern int          file, shotnum, channum, call, shnum;
            FILE *fp, *fdopen();
            int         i;

            while( ( fp = fdopen(file, "r")) == NULL ){
            printf("\n\n\07fail to open the stream...\n");
            hitrtc();
            localsh("TURBO");
            }
            count = 0L;
            switch( restric ){
            case 0:
                        shnum = shotnum;
                        fseek(fp, BDATA, 0);
                        call = 0;
                        for( i = 0; i<shotnum; i++ )
                        getashot(fp, p, q, i);
                        break;
            case 1:
                        shnum = rstrmax - rstrmin + 1;
                        fseek(fp, PDATA(0, rstrmin), 0);
                        call = 0;
                        for( i = rstrmin; i <= rstrmax; i++ )
```

```
                getashot(fp, p, q, i);
                break;
        case 2:
                shnum = shotnum - rstrmax + rstrmin +1;
                fseek(fp, BDATA, 0);
                call = 0;
                for( i = 0; i <= rstrmin; i++ )
                getashot(fp, p, q, i);

                fseek(fp, PDATA(0, rstrmax), 0);
                call = 0;
                for( i = rstrmax; i<shotnum; i++ )
                getashot(fp, p, q, i);
                break;
        }
}

getashot(fp, p, q, shot)
FILE *fp;
int p[], q[], shot;
{
        extern long     count;
        extern int      channum, shotnum, call, shnum;
        static float    buf[2058];
        static ints;
        int             deploy[4], co, ch, c;
        float   data[MAXCH];

        if( call == 0 ){
        s = 0;
        co = fread(buf, 4, 2048, fp);
        }
        data[channum] = shot;
        for( ch=0; ch<channum; ch++){
        data[ch] = buf[s];
        s++;
        if(s == co ){
                count = count + co;
                cursorup();
                printf("(%.0f%%) - processed %.0f Kb of %.0f Kb.\n",
                100.0*count/channum/shnum, 4.0*count/1000,
                4.0*shnum*channum/1000);
                s = 0;
                co = fread(buf, 4, 2048, fp);
                }
        }
        write(p[1], data, 4*MAXCH);
        read(q[0], &c, 2);
        call++;
}
```

energy.c

```
#include<math.h>
```

```
float w[9] = { 260, 320, 433, 455, 664, 877, 919, 1082, 1147 };
                                /* w is wave number of CF2Cl2 modes */
int   d[9] = { 1, 1, 1, 1, 1, 1, 1, 1, 1 };

/*          <n> = 1/( exp(hw/kt) - 1 )    */

float calcuT(Irel)
float Irel;
{
        float h, c, w, k, t, t0;
        double log(), exp();

        h = 6.625e-27;
        k = 1.38e-16;
        c = 3e10;
        w = 775;
        t0 = 293;

        t = h*c*w/k/log( (1 - exp(-1*h*c*w/k/t0))/Irel + 1 );
        return(t);
}

float calcuI(T, w)
float T, w;
{
        float h, c, k, I, t0;
        double log(), exp();

        h = 6.625e-27;
        k = 1.38e-16;
        c = 3e10;
        t0 = 293;

        I = (1 - exp(-1*h*c*w/k/t0)) / (exp(h*c*w/k/T) - 1);
        return(I);
}

float energyT(w, t)
float w, t;
{
        float h, c, k, out;
        double exp();

        h = 6.625e-27;
        k = 1.38e-16;
        c = 3e10;

        out = w/(exp(w*h*c/k/t) - 1)/933;
        return(out);
}

float total(t)
float t;
{
```

```
        int i;
        float total;
        extern  float   w[];
        extern  int     d[];

        total = 0;
        for(i=0; i<9; i++)
        total = total + d[i]*energyT(w[i], t);

        return(total);
}

float energyI(w, Irel)
float w, Irel;
{
        float h, c, k, n, t0;
        double log(), exp();

        h = 6.625e-27;
        k = 1.38e-16;
        c = 3e10;
        t0 = 293;

        n = (1 - exp(-1*h*c*w/k/t0))*Irel;
        return(n);
}
```

B.2 Interprocess communication routines

```
#include "mtool.h"

closmod(p, q, m, m_pid)
int p[], q[], m, m_pid;
{
        register int r, (*hstat)(), (*istat)(), (*qstat)();
        int status;

        switch(m){
                case 0: close(p[1]);
                        break;
                case 1: close(q[0]);
                        break;
                case 2: close(p[1]);
                        close(q[0]);
                        break;
        }
        istat = signal(SIGINT, SIG_IGN);
        qstat = signal(SIGQUIT, SIG_IGN);
        hstat = signal(SIGHUP, SIG_IGN);
        while((r = wait(&status)) != m_pid && r != -1 );
        if( r == -1)
                status = -1;
        signal(SIGINT, istat);
        signal(SIGQUIT, qstat);
        signal(SIGHUP, hstat);
        return(status);
}


#include "mtool.h"

execute(s)
char *s;
{
        int status, pid, r, i, c;
        register int (*istat)(), (*qstat)();
        char *argp[MARG], buf[MARG][ARGL];

        for(i=0; i<MARG; i++)
        argp[i] = &buf[i][0];
        c = splis(s, argp);
        argp[c] = 0;
        if((pid = fork()) == 0){
                execvp(argp[0], argp);
                _exit(127);
        }
        istat = signal(SIGINT, SIG_IGN);
        qstat = signal(SIGQUIT, SIG_IGN);
        while((r = wait(&status)) != pid && r != -1 );
```

```
        if( r == -1)
                status = -1;
        signal(SIGINT, istat);
        signal(SIGQUIT, qstat);
        return(status);
}


#include "mtool.h"

makemod(sfile, efile, compile, editor)
char *sfile, *efile, *compile, *editor;
{
        char cmd[CMDL], buf[80];
        struct stat bufa, bufb;

        sprintf(cmd, "%s %s", editor, sfile);
        for(;;){
        execute(cmd);
        stat(sfile, &bufa);
        stat(efile, &bufb);
        if( bufa.st_mtime < bufb.st_mtime )
        break;
        if( execute(compile) == 0)
        break;
        else
        read(0, buf, 80);
        }
}


#include "mtool.h"

openmod(s, p, q, m)
char *s;
int p[], q[], m;
{
        int m_pid, i, c;
        char *argp[MARG], buf[MARG][ARGL];

        for(i=0; i<MARG; i++)
        argp[i] = &buf[i][0];

        switch(m){
        case 0: if( pipe(p) == -1 )
                return(-1);
                break;
        case 1: if( pipe(q) == -1 )
                return(-1);
                break;
        case 2: if( pipe(p) == -1 || pipe(q) == -1 )
                return(-1);
                break;
        }
```

```
        if( ( m_pid = fork()) == 0 ){
        switch(m){
        case 0: close(p[1]);
                close(0);
                dup(p[0]);
                close(p[0]);
                break;
        case 1:  close(q[0]);
                close(1);
                dup(q[1]);
                close(q[1]);
                break;
        case 2:
                close(0);
                dup(p[0]);
                close(p[0]);
                close(1);
                dup(q[1]);
                close(q[1]);
                break;
        }
        c = splis(s, argp);
        argp[c] = 0;
        execvp(argp[0], argp);
        _exit(127);
        }

        switch(m){
                case 0: close(p[0]);
                        break;
                case 1: close(q[1]);
                        break;
                case 2: close(p[0]); close(q[1]);
                        break;
        }

        return(m_pid);
}

splis(s, argp)
char *s, *argp[];
{
        int i, j, k, blank;

        j = -1;
        blank = 1;
        k = 0;
        for(i=0; *(s + i) != '\0'; i++){
        switch(*(s+i)){
        case ' ':
        case '\t':
        case '\n':
                if( blank == 0 )
                *(argp[j] + k) = '\0';
                blank = 1;
```

```
                break;
        default:
                if( blank == 1 ){
                k = 0;
                j++;
                }
                blank = 0;
        *(argp[j] + k) = *(s+i);
        k++;
        break;
        }
        }
        if( blank == 0)
        *(argp[j] + k) = '\0';

        return(++j);
}
```